Role of endogenous retrovirus promoter activity in tumor suppression

---

Dissertation

for the award of the degree

"Doctor rerum naturalium" (Dr. rer. nat.)

of the Georg-August-Universität Göttingen

within the doctoral program

"Molecular Biology of Cells"

of the Georg-August University School of Science (GAUSS)

submitted by

Sonja Katharina Krönung

born in

Fulda, Germany

Göttingen 2015

Thesis Committee

Prof. Dr. Matthias Dobbelstein,

Institute of Molecular Oncology, Faculty of Medicine

Prof. Dr. Holger Reichardt,

Department of Cellular and Molecular Immunology, Faculty of Medicine

Prof. Dr. Michael Zeisberg,

Department of Nephrology and Rheumatology, Faculty of Medicine

Members of the Examination Board

Referee: Prof. Dr. Matthias Dobbelstein, Institute of Molecular Oncology

2nd Referee: Prof. Dr. Holger Reichardt, Dept. of Cellular and Molecular Immunology

Further members of the Examination Board

Prof. Dr. Michael Zeisberg, Department of Nephrology and Rheumatology

Prof. Dr. Heidi Hahn, Department of Human Genetics

Prof. Dr. Lutz Walter, Department of Primate Genetics

Prof. Dr. Ralph Kehlenbach, Department of Molecular Biology

Date of oral examination: **April 27, 2015**

Affidavit

Herewith I declare, that I prepared the PhD Thesis: "Role of endogenous retrovirus promoter activity in tumor suppression" on my own and with no other sources and aids than quoted.

Göttingen, _____ _____

(Sonja Katharina Krönung)

Dedicated to my parents.

TABLE OF CONTENTS

LIST OF FIGURES

LIST OF TABLES

ABBREVIATIONS

°C	Degree Celcius
µg	Microgram
µl	Microliter
µM	Micromolar
5hmC	5-hydroxymethylcytosine
5mC	5-methylcytosine
APOBEC3	Apolipoprotein B mRNA-editing enzyme 3
APOC1	Apolipoprotein C1
APS	Ammonium persulfate
bp	Base pair
BSA	Bovine serum albumine
cDNA	Complementary DANN
ChIP	Chromatin immunoprecipitation
ChIP-seq	ChIP-sequencing
conc.	Concentration
Ct	Cycle threshold
C-terminal	Carboxy terminus of a protein
DMEM	Dulbecco's Modified Eagle's Medium
DMSO	Dimethyl sulfoxide
DNA	Deoxyribonucleic acid
DNMT	DNA methyltransferase
dNTPs	Deoxyribonucleotide triphosphates
DR5	Death receptor 5
DTT	Dithiotreitol
ECL	Enhanced chemiluminescence immune detection
EDTA	Ethylene diamine tetraacetatic acid
EGTA	Ethylene glycol tetraacetic acid
endo-siRNA	Endogenous small interfering RNA
ERV	Endogenous retrovirus
et al.	Et alii
etc.	Et cetera
FC	Fold change
FCS	Fetal Calf Serum

FDA	US Food and Drug Administration
G	GM12878 cells
g	Gram
GBP5	Guanylate-binding protein 5
GTAp63	Germ cell-associated TAp63
H	HeLa-S3 cells
h	Hour
HAT	Histone acetyltransferase
HDAC	Histone deacetylase
HDACi	HDAC inhibitor
HERV	Human endogenous retrovirus
HP1	Heterochromatin protein 1
IAP	Intracisternal type A particle
IgG	Immunoglobulin G
IP	Immunoprecipitation
K	Lysine; K562 cells
KAP1	KRAB-associated protein 1
kDa	Kilodalton
KDM1A	Lysine (K)-specific demethylase 1A
KRAB-ZFPs	Krüppel-associated box domain-zinc finger proteins
LINE	Long interspersed elements
LTR	Long terminal repeat
M	Molar
MBD	Methyl-CpG-binding domain
MeCP2	Methyl-CpG-binding protein 2
mESC	Mouse embryonic stem cells
MetOH	Methanol
mg	Milligram
min	Minute
ml	Milliliter
mM	Millimolar
M-MuLV	Moloney murine leukemia virus
mRNA	Messenger RNA
n	Sample size
N_2	Nitrogen

NF-Y	Nuclear transcription factor Y
NF-YA	NF-Y subunit alpha
NF-YB	NF-Y subunit beta
NF-YC	NF-Y subunit gamma
ng	Nanogram
NGS	Next-generation sequencing
nm	Nanometer
nM	Nanomolar
NP-40	Nonidet P-40 substitute
N-terminal	Amino-terminus of a protein
NuRD	Nucleosome remodeling and histone deacetylase
PARP1	Poly-(ADP-ribose)-polymerase 1
PBS	Phosphate buffered saline
PCR	Polymerase chain reaction
PIC	Protease inhibitor cocktail
piRNA	PIWI-interacting RNA
PIWIL1	Piwi-like protein 1
qPCR	Quantitative real-time PCR
RACE	Rapid amplification of cDNA ends
RNA	Ribonucleic acid
rpm	Rounds per minute
RT	Room temperature; Reverse transcriptase
SAHA	Suberoylanilide hydroxamic acid
SD	Standard deviation
SDS	Sodium dodecyl sulfate
SDS-PAGE	Sodium dodecyl sulfate polyacrylamide gel electrophoresis
sec	Second
SETDB1	SET domain, bifurcated 1
shRNA	Small hairpin RNA
SINE	Short interspersed elements
siRNA	Small interfering RNA
SSC	Scrambled control siRNA
TA	Transactivation
TE	Transposable element
TEMED	Tetramethylethylenediamine

TET	Ten-eleven translocation
Tm	Melting temperature
TRAIL	TNF-related apoptosis-inducing ligand
Tris	Trisamine
TSA	Trichostatin A
tss	Transcription start site
U	Unit
UCSC	University of California Santa Cruz
UV	Ultraviolet
V	Volt
vs.	Versus

1 Abstract

Roughly 8% of the human genome consists of human endogenous retroviruses (HERVs). They are believed to be remnants of ancient retroviral infections of the germline that were passed on from one generation to the next over millions of years. While initially regarded as „junk DNA“, it has become increasingly clear that HERV elements exert defined functions in their hosts. In 2011, our group reported the discovery of an isoform of the tumor suppressor p63 that is expressed under the control of a long terminal repeat (LTR) of the endogenous retrovirus family 9 (termed LTR12). Due to its expression in the spermatogonia of the testis, this isoform was called Germ cell-associated TAp63 (GTAp63). Transcription of GTAp63 was found to be silenced in testicular cancer cells. However, it could be restored by treatment with histone deacetylase inhibitors (HDACi). Moreover, a recent approach identified a set of 17 cellular genes driven by an LTR12 whose transcription can be enhanced by HDACi treatment in testicular cancer cells. Among these genes was *TNFRSF10B*, which encodes for Death Receptor 5.

Following up on these previous findings, the main goals of this study were to verify *TNFRSF10B* as a novel candidate gene that is driven by an LTR12, to elucidate the functional implications of this regulation in tumor cells and to clarify the mechanisms behind the localized activation of these specific promoter sites.

We identified at least three LTR12-driven transcripts of *TNFRSF10B* whose expression is inducible by HDAC inhibitor treatment. Insertion of the solitary LTR12 upstream of the *TNFRSF10B* gene occurred roughly 18 million years ago. Combined treatment of HDAC inhibitor Trichostatin A (TSA) and TNFRSF10B’s ligand TRAIL resulted in an enhanced apoptotic response in testicular cancer cells. Moreover, we observed enhanced LTR12 promoter activity upon treatment with HDAC inhibitors in a variety of human cancer cell lines. Apart from TSA, induction of LTR12 promoter activity was also observed with the FDA-approved HDAC inhibitor SAHA as well as Entinostat and Mocetinostat, which are currently undergoing phase II clinical trials for cancer therapy. Regarding the mechanisms underlying the specific activation of LTR12-driven gene transcription, we identified increased binding of nuclear transcription factor Y at LTR12 genomic loci upon TSA treatment. The specific activation of LTR12-driven expression of putative tumor suppressor genes like *TP63* and *TNFRSF10B* suggests a novel mechanism of how inhibition of HDACs can exert anti-cancer effects.

Taken together, we present an example of how co-evolution of transposable elements with the host might have been beneficial for the host and therefore be rendered active in the human genome instead of being eliminated as “junk DNA”. Furthermore, LTR12 activation represents a plausible mechanism of how HDAC inhibitors exert anti-cancer activity in human cells.

2 Introduction

2.1 Endogenous retroviruses in the human genome

In the late 1960s researchers made an observation that seemed utterly impossible at the time – the existence of virus elements, which were not the result of a recent infection, but nonetheless resided within their host's genomes [1]. One of the first observations was the production of a viral *envelope* protein by normal, uninfected chicken cells and the inheritance of a group-specific antigen of the avian leucosis virus [1-3]. Since reverse transcriptase had not been discovered yet [4, 5], it took a few years before the existence of viruses "endogenously" residing in genomic DNA was widely accepted. However, it was only when the human genome was fully sequenced that the extent of virally inherited DNA was revealed. While protein-coding exons cover only about 1% of the human genome, endogenous retroviruses (ERVs) account for roughly 8% of it [6, 7].

2.1.1 Transposable elements and their activity

ERVs are classified as transposable elements (TE), i.e. DNA sequences that can change their position within the genome through excision and insertion events [8]. In total, TEs comprise at least 45% of the human genome [6]. A more recent evaluation in 2011 by de Koning *et al.* sets the number at 66-69% [9]. Transposable elements are roughly divided into class I, retrotransposons, and class II, DNA transposons. The main difference between these two classes is in their mechanism of transposition. Retrotransposons are first transcribed into RNA. This intermediate is reverse transcribed into cDNA by a reverse transcriptase and is then inserted into a new position in the genome. In each cycle of transposition, its content is copied. DNA transposons on the other hand are first "cut" from the DNA by various transposases and then inserted elsewhere. Additionally, rolling-circle DNA transposons (*helitrons*) and self-synthesizing DNA transposons (*polintons/mavericks*) have also been characterized [10, 11]. Among the retroelements, a further distinction is made based on the presence or absence of long terminal repeats. Long (LINE) and short (SINE) interspersed elements are examples of non-LTR retrotransposons [12]. On the other hand, human endogenous retroviruses are characterized as LTR transposons.

Mobility of genetic elements is of great interest, since insertion within or near a gene may alter its function and can cause diseases [13-15]. While DNA transposons seem to have been rendered completely inactive, a small number (<0.05%) of retrotransposons have retained the ability to mutate their host's genomes [6, 16, 17]. Among these mobile elements are subfamilies of SINE and LINE (*Alu,* LINE-1 and SVA elements), as well as HERV-K elements [16, 17]. Mills *et al.* described a set of 10,719 transposon insertions that are present only in the human or chimpanzee genome [16]. Since their last

common ancestor existed about six million years ago, the presence of these genetic elements in only one or the other genome suggests that they are the result of recent transposition events. Interestingly, these recent "endogenous" mutations are far more abundant in the human genome (72.5% of all identified insertions) than in the chimpanzee's [16].

2.1.2 Genomic organization of human endogenous retroviruses

A closer look at the genomic organization of LTR transposons provides further insight into their origins. During their replication cycle, retroviruses integrate as proviruses into the host's genome after reverse transcription of their RNA genome into DNA [18, 19]. Several million years ago, germ-line cells were infected by such exogenous retroviruses [3, 20]. Subsequently, the integrated viruses were passed on in a stable manner according to Mendelian Laws. Today's human endogenous retroviruses are believed to be "fossils" of these ancient infections [1, 18]. For a while, the "endogenized" retroviruses retained their ability to proliferate and spread– through both vertical and horizontal transmission. Therefore, multiple copies of a single founder virus arose at different chromosomal locations [20].

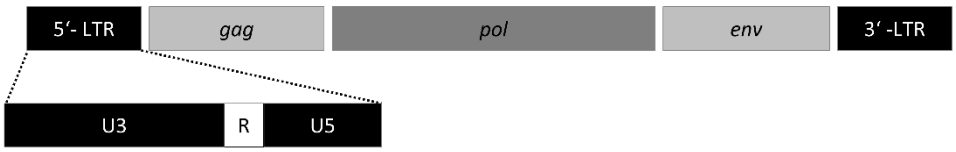

Figure 2-1. Exemplified genomic structure of a HERV

Three viral genes flanked by two long terminal repeats (LTR). The LTRs can act as promoters of RNA transcription. 3 major open reading frames are depicted: *gag* encoding structural proteins, *pol* encoding the viral enzymes and *env* encoding the retroviral envelope proteins. A magnified view of the 5'-LTR is shown. Both LTRs consist of U3, R and U5 regions and harbor promoter, enhancer and polyadenylation sequences. Transcription starts in the R region of the 5'-LTR. Adapted from Stoye, J. P. [18].

LTR transposons exist either as part of full-length endogenous retroviruses or as solitary LTRs. Full-length ERVs resemble the genome of exogenous retroviruses. They basically encode the retroviral *gag, pol* and *env* genes, flanked by two LTRs [18, 20, 21]. The *gag* gene encodes the structural proteins matrix, capsid and nucleocapsid. The *pol* gene encodes the viral enzymes protease, reverse transcriptase and integrase. The *env* gene encodes the proteins responsible for receptor binding and membrane fusion. However, *env* genes are only rarely present [12]. A possible explanation for the frequent loss of *env* genes is provided by Magiorkinis *et al.* who compared ERV sequences from 38

mammalian species and found enhanced spreading of the viral sequences within the genome upon *env* gene loss [22].

The flanking LTRs in an ERV are between 300 and 1,200 nucleotides in length [18]. They consist of U3, R and U5 regions and harbor promoter, enhancer and polyadenylation sequences [18, 20, 23]. Transcription starts in the R region of the 5'-LTR, and the polyadenylation signal is located at the end of the R region in the 3'-LTR [20].

Most ERV sequences are inactive due to accumulated mutations and deletions in their coding sequences [18]. However, some HERV still contain an intact open reading frame (ORF) and can be translated into protein. One of these functional genes is syncytin-1, the HERV-W *env* gene encoded by the ERVWE1 locus on chromosome 7 [20, 24]. Interestingly, syncytin-1 seems to have a physiological role during placenta morphogenesis, where it is implicated in the fusion of cytotrophoblast cells to form syncytiotrophoblasts [24]. Though such individual intact endogenous viral ORFs exist, viral particles are rarely observed in humans. So far only one subtype of HERV-K was shown to be able to produce viral particles [12, 25].

Solitary LTRs are the result of homologous recombination between two LTRs which results in the loss of the retroviral genes between them [12, 26]. Solitary LTRs in the human genome outnumber full-length ERVs by at least 10-fold [18]. Interestingly, key regulatory elements such as transcription factor binding sites, splice sites etc., are usually retained after such LTR-LTR recombinations [10]. Solitary LTRs have been shown to impact gene expression and can function as an alternative, or in some cases the primary promoter, of various cellular genes [27]. Regulation of gene expression by LTRs is an emerging field and we are only now beginning to appreciate the importance of these genetic elements in the regulation of cellular gene expression [10, 28]. The regulation of cellular genes by solitary LTRs is described in detail in section 2.3.

2.1.3 ERV classification and nomenclature

There are various approaches to name and classify ERVs. Traditionally, the letter referring to the amino acid specificity of the tRNA, which is predicted to prime reverse transcription of the viral mRNA, was used to name HERVs [3]. Members of the HERV-W group, for example, contain a primer binding site complementary to tryptophan-tRNA [21]. Aside from this, phylogenetic comparisons were conducted, comparing HERV sequences to the 7 known retroviral genera [19, 29]. A more recent approach categorized transposable elements based on their similarity to consensus sequences [30]. This nomenclature is used by the Repbase database (http://www.girinst.org/repbase/) for repetitive elements and was also applied in this study to name the respective HERV families and LTRs. The long

terminal repeats of the endogenous retrovirus HERV-9, which is a major focus of this work, are listed as “LTR12” in Repbase.

2.2 Silencing of endogenous retroviral elements in the human genome

As mentioned previously (see 2.1.1), the mobility of transposable elements can potentially be harmful to the host. Accordingly, various mechanisms evolved in order to restrict TE activity. These strategies include DNA methylation, small inhibitory RNAs and DNA-modifying proteins [31, 32].

2.2.1 Silencing of transposable elements by DNA methylation

One well-studied mechanism of TE silencing is through methylation of DNA. Herein DNA methyltransferases (DNMTs) catalyze the addition of a methyl group to the fifth carbon of a cytosine base [33]. This results in 5-methylcytosine (5mC). DNMTs either catalyze *de novo* methylation (DNMT3A and DNMT3B) or maintain existing patterns of methylation by recognizing hemi-methylated DNA (DNMT1) [34, 35]. Methylated DNA is recognized by specific proteins with a methyl-CpG-binding domain (MBD). Subsequently, these proteins, as for example methyl-CpG-binding protein 2 (MeCP2), can recruit co-repressor complexes which ultimately results in transcriptional silencing [36-38]. Moreover, methylation of DNA can directly interfere with transcription factor binding [39] and was once believed to have a long-term silencing effect. It was previously reported that DNA methylation and transcriptional silencing is initially established by *de novo* DNMTs during the blastocyst stage of embryonic development and maintained thereafter in differentiated cells [40-42]. However, more recent reports have shown that DNA methylation levels can also rapidly change, especially during DNA methylation reprogramming in early development [42, 43].

The recent discovery of Ten-eleven translocation (TET) enzymes has provided some mechanistic insight into the dynamics of DNA demethylation. TET1 was shown to catalyze the conversion of 5mC to 5-hydroxymethylcytosine (5hmC) in cultured cells [44]. Moreover, purified TET enzymes can catalyze further oxidation to 5-formylcytosine and 5-carboxylcytosine [45]. However, the consequences of these modifications are not yet fully understood. In a genome-wide screen of methylation patterns in mouse embryonic stem cells (mESC), 5hmC was found to be mostly associated with euchromatin and enriched at CpG islands [46]. There are different hypotheses on how oxidized 5mC might influence gene regulation and possibly DNA demethylation. 5hmC might be further converted to cytosine, resulting in a loss of DNA methylation at the respective site [45, 47]. Another possibility is the interference of 5hmC with DNMT1 activity [48]. This might result in the passive loss of DNA methylation

after multiple replication cycles. Moreover, MBD proteins, as for example MeCP2, are unable to bind to 5hmC [49], thereby abolishing their silencing effects. Aside from these activating functions, TET1 was also reported to mediate transcriptional repression by association with the SIN3A co-repressor complex [48].

Similar to other TE classes, silencing for HERV through epigenetic modification of DNA has previously been described whereas the removal of such modifications relieved this suppression. In germ cell tumors for example, hypomethylation of the HERV-K promoter results in overexpression of the HERV-K (HML-2) provirus [50, 51]. Furthermore, TET1 might be recruited by ERVs and promote their transcriptional derepression [52]. However, extensive studies in mESCs revealed that ERV transcription can remain silenced upon loss of DNMT1 [53] indicating the presence of DNA methylation-independent mechanisms of ERV silencing in undifferentiated cells [52, 53]. Further studies have implicated numerous histone-modifying enzymes in these silencing processes [43, 52].

2.2.2 Silencing of transposable elements by histone-modifying enzymes

Histones are proteins that take part in the higher organization of genomic DNA. 145-147 bp of DNA are wrapped around octamers consisting of two H2A, H2B, H3 and H4 subunits each [54, 55]. This basic unit of DNA packaging is called the nucleosome. The N-terminal tails of histones can be post-translationally modified [55]. The covalent addition of methyl, acetyl and phosphorylation groups, as well as ubiquitin or SUMO, allows for the tight regulation of gene expression [55, 56]. This occurs either through recruitment of factors that specifically recognize certain histone modifications or through changes in DNA dynamics [54]. For endogenous retroviral elements, silencing was proposed to arise through histone methylation or deacetylation in early mouse embryos [43, 52].

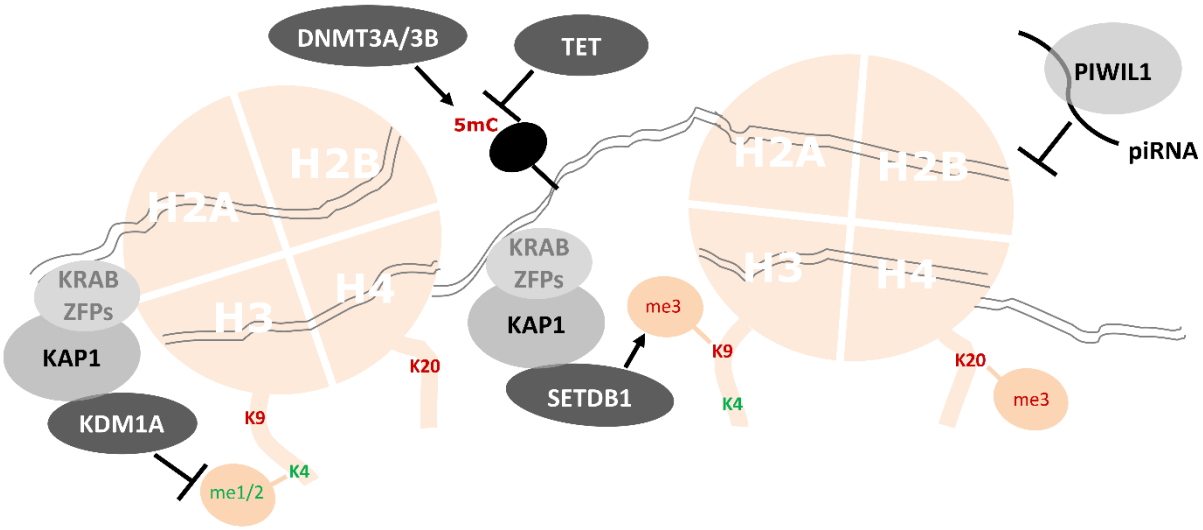

Figure 2-2. Histone-modifying enzymes and dynamic changes in DNA methylation involved in silencing of transposable elements

KRAB-associated protein 1 (KAP1) is recruited by KRAB-zinc finger transcription factors (KRAB ZFPs) and in turn scaffolds recruitment of silencing factors. These silencing factors include Lysine (K)-specific demethylase 1A (KDM1A) [which removes the active histone mark H3K4me1/me2] or histone methyltransferase SET domain, bifurcated 1 (SETDB1) [required for the establishment of inactive histone mark H3K9me3]. Depending on the ERV subfamily, they act alone or together to silence these endogenous retroviral sequences. Moreover, PIWIL1 might restrict ERV activity by demolishing transcripts of TEs through piRNAs. Another level of control is reached through the turnover of DNA methylation at proviral elements. ERVs might recruit Ten-eleven translocation (TET) proteins which process silencing 5mC marks on DNA. In turn these marks have to be reestablished by *de novo* DNA methyltransferases (DNMTs). Abbreviations: 5mC – 5-methylcytosine; K – lysine; me1 – methyl; me2, dimethyl; me3, trimethyl. Adapted from Leung, D. C. and Lorincz, M. C. [52] and Rowe, H. M. and Trono, D. [43].

One of the factors involved in this silencing is KRAB-associated protein 1 (KAP1). Upon recruitment by Krüppel-associated box domain-zinc finger proteins (KRAB-ZFPs), KAP1 can in turn act as a scaffold for the assembly of silencing complexes [57, 58]. These complexes can contain heterochromatin protein 1 (HP1), the NuRD histone deacetylase complex, Lysine (K)-specific demethylase 1A (KDM1A) or SET domain, bifurcated 1 (SETDB1) [43, 58]. SETDB1 adds one, two or three methyl groups to histone 3 lysine residue 9 (H3K9) [59]. H3K9me2 and H3K9me3 generally correlate with heterochromatin formation and gene silencing [60]. Depletion of SETDB1 was shown to result in an upregulation of ERVs and the loss of H3K9me3 in mESCs [61]. KDM1A, on the other hand, removes methyl groups from histone 3 K4. Methylation of H3K4 is generally correlated with active genes [60]. The expression of MERV-L elements has been shown to increase upon loss of KDM1A in mESCs [62]. This is accompanied by increased methylation of H3K4 and acetylation of H3K27 as well as decreased methylation of H3K9 [62].

Taken together, KAP1 confers chromatin silencing through the recruitment of factors that establish inhibiting marks or remove activating marks from histones. Depletion of KAP1 from murine blastocysts and embryos has been shown to result in a strong upregulation of intracisternal type A particle (IAP) LTR transposons [63]. Interestingly, KAP1 is the sole factor whose depletion was proven to exert an effect on ERV transcription in human cells [64]. For all other enzymes, data was predominantly obtained in mice.

2.2.3 Silencing of transposable elements by small RNAs

An increasing set of data indicates the involvement of small-RNAs, such as endogenous small interfering RNAs (endo-siRNAs) and PIWI-interacting RNAs (piRNAs), in the silencing of TEs [31, 43, 65]. Both, endo-siRNAs and piRNAs are defined by their short length of 21-35 nucleotides as well as their interaction with members of the Argonaute protein family [66]. Argonaute proteins are involved in the guidance of small RNAs to their targets. Endo-siRNAs were first detected in plants and *Caenorhabditis elegans* [67, 68]. They are selectively incorporated into Ago-class Argonaute-containing RNA-induced silencing complexes (RISC) [31, 66]. On the other hand, piRNAs were initially identified in *Drosophila melanogaster* [69]. They are mainly expressed in the germline and bind to PIWI-class Argonaute proteins [70, 71]. Upon transcription from TE-containing regions, the small RNAs mature in multiple processing steps [31]. Guided by Argonaute proteins, the single-stranded RNA can then bind complementary sequences in mRNA derived from TEs and lead to their degradation [31]. Herein, transcription of a TE locus can result in its own silencing.

While post-transcriptional control of TEs by piRNAs was first observed in *Drosophila*, PIWI homologues and corresponding TE silencing mechanisms have been identified in mammals. In mice, the loss of MILI (also known as PIWI-like protein 2) and MIWI2 (also known as PIWI-like protein 4) results in the decrease in piRNA expression. This led to changes in DNA methylation of regulatory elements of LINE-1 and IAP LTR transposons [72] which correlated with transcriptional activation of these TE in male germ cells [73]. The human homolog of Drosophila PIWI is HIWI (also known as PIWI-like RNA-mediated gene silencing 1 or short PIWIL1) [69]. However, its potential role in TE silencing remains unknown [74].

2.2.4 Silencing of transposable elements by cytosine deaminases and DNA repair factors

Aside from DNA methylation, histone modifications, and small RNAs, enzymes involved in DNA repair and metabolism can also influence TE activity. Members of the apolipoprotein B mRNA-editing enzyme 3 (APOBEC3) family convert cytidine to uridine (or deoxycytidine to deoxyuridine) [75].

Therein, deamination of cytosines in newly synthesized cDNA from LTR retrotransposons can result in either its degradation or deleterious mutations [31, 75, 76]. Moreover, DNA repair mechanisms have been shown to restrict retrotransposition. Overexpression of 3'-repair exonuclease 1 resulted in a reduced retrotransposition efficiency for LINE and murine IAP LTR transposons [77].

2.3 Effects of HERV elements on host genome function

Apart from the expression of viral proteins or deleterious transposition events, TEs may also function as promoters and enhancers for cellular genes [10, 27, 78]. Interestingly, about 31% of all transcription start sites (tss) were found to be located within sequences of transposable elements [79]. Thus, it comes as no surprise that the list of cellular genes whose expression is regulated by TEs is constantly increasing. Regarding human endogenous retroviruses in particular, the regulatory elements within LTRs can influence gene expression in multiple ways (see Figure 2-3) [19, 27]. Since LTRs harbor promoter, enhancer and polyadenylation sequences, they can influence gene transcription through the binding of specific transcription factors. Moreover, they can interfere with signaling of enhancer elements located further upstream or promote the formation of heterochromatin [10]. One transcription factor whose binding was shown to modulate the enhancing properties of an LTR is nuclear transcription factor Y (NF-Y). NF-Y is a trimeric transcription factor consisting of the three subunits alpha, beta and gamma. While NF-YA appears to confer sequence-specificity for the DNA motif CCAAT, NF-YB and NF-YC exert histone-like structural features [80, 81]. A solitary LTR of the endogenous retrovirus family 9 has been found to be inserted upstream of the beta-globin locus control region [82]. Further studies revealed that NF-Y bound to this LTR12 recruits GATA-2 and MZF1 in erythroid cells, assembling an active enhancer complex [83]. Moreover, mutations in the NF-Y DNA binding motif CCAAT were shown to reduce the enhancer activity and render the downstream globin promoter inaccessible [83].

Apart from this example, where a retroviral LTR serves as an enhancer for a nearby cellular gene, LTRs can also serve as alternative promoters. One example of an LTR serving as an alternate promoter for an adjacent gene is the HERV-E element upstream of apolipoprotein C1 (*APOC1*) on chromosome 19 [84]. APOC1 has a function in lipid metabolism and is mostly expressed in the liver, and transcription from the LTR shows the same tissue-specificity [27].

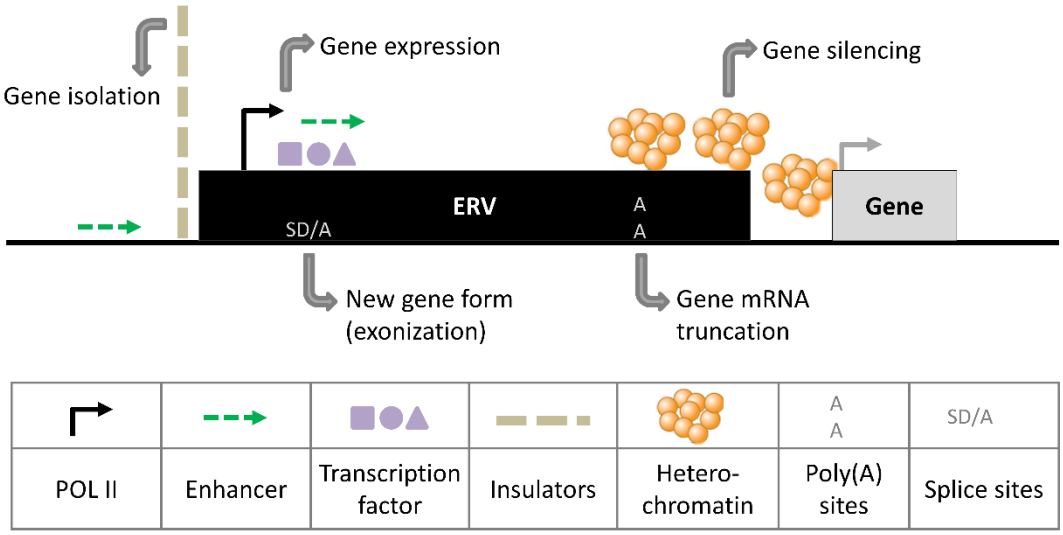

Figure 2-3. Regulatory sites of LTR retrotransposons and putative influences on host genes

Schematic of the genomic insertion of an endogenous retrovirus (ERV) upstream of a host gene and potential ways how the LTR can influence transcription of the adjacent gene. Rounded arrows represent putative consequences of LTR activity. Since LTRs harbor promoter, enhancer and polyadenylation sequences, they can influence gene transcription through binding of specific transcription factors. Moreover, they can interfere with signaling of enhancer elements located further upstream or promote the formation of heterochromatin. Alternative splice sites within the ERV sequences can further result in new or elongated exons (exonization) by influencing the splicing system. Adapted from Rebollo, R. *et al.* [10].

But aside from such LTRs with only minor effects on host genes, LTRs can also diversify or limit tissue specificity and, in some cases, even act as the primary promoter. One example for the latter is the host gene guanylate-binding protein 5 (*GBP5*). An LTR12 of the HERV-9 family, which is positioned upstream of this gene, functions as the primary promoter and is active primarily in endothelial cells and lymphocytes [27, 85].

Elements from the HERV-9 family were first identified by La Mantia *et al.* [86, 87]. Overall, LTR12 are significantly longer than other human LTR types and have a higher abundance of CpG [10, 19]. Moreover, these LTRs contain a variable copy number for tandemly repeated subelements of 41 and 72/80 bp [87, 88]. According to Repbase, about 5,817 regions in the human genome harbor an LTR12. Interestingly, LTR12s were shown to drive expression of a variety of human genes with no predominant tissue-specificity. Aside from *GBP5*, LTR12-driven gene expression has also been reported for *SEMA4D* and *DHRS2* in a variety of tissues, *ADH1C* in the liver, *ZNF80* in leukocytes, and *TP63* specifically in the testis (see next chapter) [27, 89-92].

2.3.1 An LTR12 serves as alternative promoter for *TP63*

In 2011, our group reported that the expression of the cellular gene *TP63* is controlled by an endogenous viral LTR [90]. The gene product p63 shows a high sequence and structural homology to p53 with all classical features of a transcription factor: An N-terminal transactivation domain, core DNA binding domain and a C-terminal oligomerisation domain [93, 94]. Two distinct transcription start sites had been known for *TP63*, resulting in a protein with or without a transactivation (TA) domain. Accordingly, the two protein products were termed TAp63 and deltaNp63 [93, 94]. The latter was known to be expressed in multilayered epithelia [95, 96]. For TAp63 a strong expression in mouse oocytes was shown, where it supposedly protects the female germ line by inducing apoptosis upon genotoxic stress [97]. Analysis of TAp63 expression in human cells led to the identification of a novel isoform of p63, Germ cell-associated TAp63 (GTAp63) [90]. Expression of this isoform is driven by an LTR12. Insertion of this LTR12 upstream of the *TP63* gene took place around 15 million years ago, resulting in its presence in the genomes of only humans, chimpanzees, gorillas and orangutans. Interestingly, transcription of GTAp63 was found to be largely confined to the human testis, whereas TAp63 is expressed in a broad variety of tissues [90]. Compared with normal human testis, GTAp63 mRNA transcription is strongly reduced in cell lines derived from human testicular cancers [90]. One possible mechanism for transcriptional silencing is deacetylation of histones (see also 2.2.2). Promoter regions of active genes usually display high levels of histone acetylation (see Figure 2-4) [60]. The enzymes involved in the addition and removal of acetyl groups to and from histones are histone acetyltransferases (HAT) and deacetlyases (HDACs) respectively [98]. Since HDACs were shown to remove acetyl groups from proteins other than histones, they are alternatively named Lys deacetylases [99, 100]. HDACs are divided into four classes. Class I (HDAC1, 2, 3 and 8), class IIa (HDAC4, 5, 7 and 9), class IIb (HDAC10 and 6) and class IV (HDAC11) have a common active site [98, 101, 102]. Their catalytic pocket is formed by a hydrophobic channel with a zinc atom (Zn^{2+}) at its end [101].

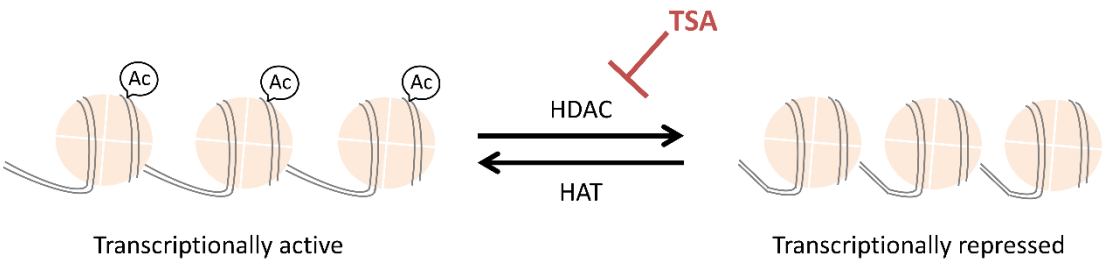

Figure 2-4. Influence of acetylation and deacetylation on chromatin structure and gene transcription

Simplified scheme of post-translational modification of histone tails and their influence on transcriptional activity. The chromatin structure of DNA wrapped around histones (light orange) can change between an open (left) and closed (right) conformation. While acetylation of histones by

histone acetyltransferases (HATs) is believed to relax the chromatin and render it more accessible to transcription machinery, deacetylation by histone deacetylases (HDACs) opposes these effects. Inhibitors of HDACs such as Trichostatin A (TSA) can inhibit HDAC activity. Abbreviations: Ac – acetyl group. Adapted from Johnstone, R. W. [103].

To shed further light on how LTR12-driven GTAp63 expression is silenced in testicular cancer cells, the involvement of HDACs in this process was assessed by treating cells with an HDAC inhibitor [90]. Inhibition of HDAC enzymes by treatment with Trichostatin A (TSA) restored GTAp63 expression in testicular cancer cell lines. Upon treatment with TSA, an over 1,000-fold increase in GTAp63 transcription was observed [90].

2.4 Comprehensive identification of genes driven by LTR12

In order to identify further human transcripts that originate from an LTR12 and are inducible by HDAC inhibition, two initial experiments were performed. First, testicular cancer cells were treated with the HDAC inhibitor TSA and total mRNA levels were compared to the transcriptome of untreated control cells by microarray analysis. Thereby, genes were identified which are upregulated by HDAC inhibition in a fashion similar to GTAp63. In a second approach, LTR12-containing transcripts were specifically identified by combining 3'-RACE and next-generation sequencing (NGS). As a first step, the transcriptome of normal testes tissue as well as testicular cancer cells after treatment with TSA, was reverse transcribed into cDNA using a modified Oligo(dT)-primer that introduces a SMART adaptor sequence (see Figure 2-5). Next, transcripts with LTR12 sequences at their 5'-end were specifically amplified in a RACE-PCR using a set of forward primers within the LTR12 and the reverse Universal Primer Mix, which recognizes the SMART adaptor. The resulting pool of PCR products was then analyzed by NGS. The 3'RACE, NGS and microarray experiment was designed and performed by Dr. Ulrike Beyer (Dept. of Molecular Oncology, UMG, Göttingen; currently MHH, Hannover).

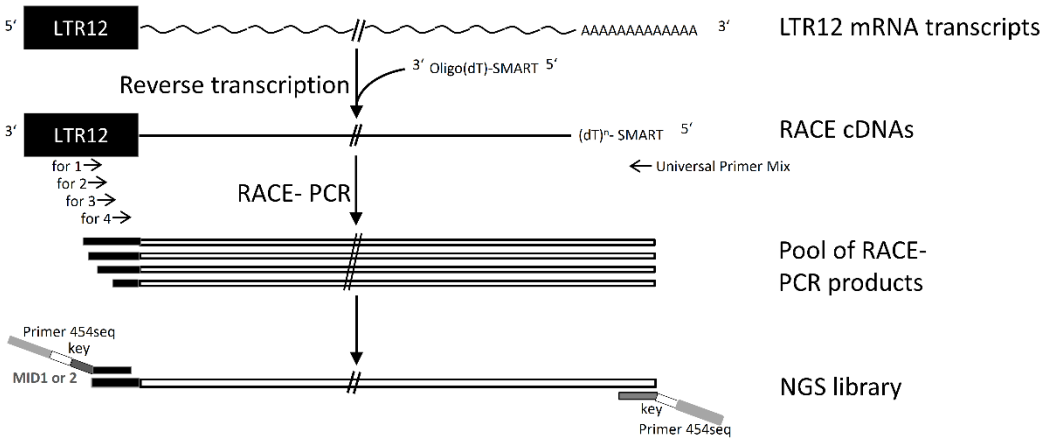

Figure 2-5. 3‘RACE to identify human transcripts that originate from a LTR12

First, the transcriptome was reverse transcribed into cDNA using a modified Oligo(dT)-primer which introduces a SMART adaptor sequence. Next, transcripts with LTR12 sequences at their 5‘-end were specifically amplified in a RACE-PCR using a set of forward primers within the LTR12 and the reverse Universal Primer Mix, which recognizes the SMART adaptor. The resulting pool of PCR products was then analyzed by next generation sequencing (NGS). Primers contained a Junior454-specific sequence (light grey box) and multiple identifier (MID) (dark grey box) to distinguish between RACE products from normal human testis (MID1) and TSA-treated testicular cancer cells (MID2). The experiment was designed and performed by Dr. Ulrike Beyer (Dept. of Molecular Oncology, UMG, Göttingen; currently MHH, Hannover).

The genes identified with both approaches are suitable candidates for being under the control of an LTR12 and reactivatable by HDAC inhibitor treatment. The 18 genes, whose expression was at least 5-fold upregulated in the microarray and which were found to contain an LTR12 sequence in their transcript by NGS, are shown in Table 2-I. Since we were especially interested in genes, whose altered expression might result in tumor cell death, we were intrigued to identify *TNFRSF10B* and *IER3* among these candidates. *TNFRSF10B* encodes for the protein death receptor 5 (DR5). Upon binding of its ligand TNF-related apoptosis-inducing ligand (TRAIL), the receptor undergoes trimerization [104]. Next, the adaptor molecule FAS-associated death domain protein is recruited, as well as pro-caspase-8 and/or pro-caspase-10. This so-called death-inducing signaling complex then results in apoptosis through cleavage of downstream caspases-3 and -7 [105-107].

Gene symbol	Gene name	Array FC>5	NGS normal testis	NGS tumor cells	Gene ontology
NR1H4	nuclear receptor subfamily 1, group H, member 4	274.4	2	4	transcription regulation; regulation of metabolic processes
C9orf53	chromosome 9 open reading frame 53	222.9	1118	1946	unknown
CPED1	Cadherin-like and PC-esterase domain-containing protein 1	106.9	2	2	endoplasmatic reticulum
C9orf85	chromosome 9 open reading frame 85				unknown
CCR4	chemokine (C-C motif) receptor 4	91.1	22	15	chemokine-mediated signaling; immune reponse
ACSBG1	acyl-CoA synthetase bubblegum family member 1	45.3	4	5	long-chain fatty acid metabolic process; ovarian follicle atresia
KCNN3	potassium intermediate/small conductance calcium-activated channel, subfamily N, member 3	40.0	407	377	synaptic transmission; potassium channel activity
CSF3	colony stimulating factor 3 (granulocyte)	31.1	53	38	cytokine-mediated signaling; immune response; cell proliferation
TMOD1	tropomodulin 1	15.2	7	2	formation of actin filament
SLC36A2	solute carrier family 36 (proton/amino acid symporter), member 2	14.8	4	37	amino acid transport; ion transport
IER3	immediate early response 3	14.3	12	2	apoptosis; regulation of DNA repair; regulation of inflammatory response
PIK3C2G	phosphoinositide-3-kinase, class 2, gamma polypeptide	10.6	19	90	chemotaxis; phosphatidyl-inositol-mediated signaling
TENM1	teneurin transmembrane protein 1	10.4	2	5	immune response; cell proliferation; regulation of MAP kinase activity
LINC01194	long intergenic non-protein coding RNA 1194	8.3	31	3	unknown
PTPN13	protein tyrosine phosphatase, non-receptor type 13 (APO-1/CD95 (Fas)-associated phosphatase)	7.3	16	2	protein dephosphorylation; regulation of apoptotic signaling
TP63	tumor protein p63	6.3	15	2	DNA damage response; apoptosis; regulation of DNA repair; cell aging
TNFRSF10B	tumor necrosis factor receptor superfamily, member 10b	5.7	7	119	apoptotic signaling
RADIL	Ras association and DIL domain	7.6	3	6	signal transduction; cell adhesion

Table 2-I. HDAC inhibitor-responsive LTR12-driven genes

2.5 Scope of the thesis

Endogenous retroviruses and their promoter elements are present in abundance in the human genome. However, their influence on gene expression remains to be fully understood. The discovery of LTR12-driven pro-apoptotic GTAp63 and its strong inducibility by HDAC inhibitor treatment in testicular cancer cells raised the possibility of inducing cancer cell death by targeting LTR12s. Furthermore, in a combined approach of RACE and microarray analysis, additional LTR12-driven genes were identified that are inducible in a similar fashion as GTAp63 in testicular cancer cells. Following up on these previous findings, the main goals of this study were to (1) verify *TNFRSF10B* as a novel candidate gene that is driven by an LTR12, (2) to elucidate the functional implications of this regulation in tumor cells, and (3) to clarify the mechanisms behind the localized activation of these specific promoter sites. Accordingly, we analyzed the presence of the LTR12 upstream *TNFRSF10B* in different species and narrowed the time of insertion down to about 18 million years ago. Furthermore, we tested the transcription of LTR12-driven *TNFRSF10B* upon treatment with HDAC inhibitors and verified their inducibility in testicular cancer cells. Moreover, we subjected testicular cancer cells to combined treatment with TNFRSF10B's ligand TRAIL and HDACi, asking whether the combination gives rise to enhanced cell death.

To clarify the mechanism behind the HDACi-mediated activation of LTR12 promoter activity, we tested a range of different HDACis, assessing whether enhanced transcription occurs upon treatment with HDACi from different chemical classes. Moreover, we applied HDACis to a panel of human cancer cell lines and quantified LTR12-driven gene transcription. Thereby, we investigated whether transcriptional activation of LTR12-driven gene expression upon HDACi treatment is limited to testicular cancer cells or whether it applies to tumor cells of different origin as well. We also tested the influence of various known factors involved in ERV silencing and performed an *in-silico* analysis of putative transcription factor binding sites within the LTR12 sequence. In particular, we asked if NF-Y represents a possible mediator of the localized activation of LTR12 promoters in the human genome. By chromatin immunoprecipitation (ChIP)-analysis with specific antibodies against NF-Y subunits alpha and beta we analyzed the association of NF-Y with LTR12s upon treatment with HDACi.

3 Materials

3.1 Human cell culture

3.1.1 Cell types

Cell line	Origin of cells	Culture media
GH	Testicular teratocarcinoma cell line	$DMEM^{full}$
H1299	Non-small cell lung carcinoma cell line	$DMEM^{full}$
HEK293	Embryonic kidney cell line	$DMEM^{full}$
HeLa	Cervical carcinoma cell line	$DMEM^{full}$
HH	Cutaneous T-cell lymphoma cell line	$RPMI^{full}$
HuT-78	Cutaneous T-cell lymphoma cell line	$RPMI^{full}$
K562	Leukemia/lymphoma cell line	$RPMI^{full}$
Ovcar-3	Ovarian carcinoma cell line	$RPMI^{full}$
U2OS	Osteosarcoma cell line	$DMEM^{full}$

Table 3-I. Human cell lines

Testicular tumor cell line was obtained from Roswitha Löwer, Paul-Ehrlich-Institut Erlangen/Frankfurt, Germany.

3.1.2 Culture media

Human cells were either cultivated in Dulbecco's Modified Eagle's Medium (DMEM) (see Table 3-XIII) enriched with 10% FCS, 50 U/ml Penicillin/Streptomycin and 200 µM L-Glutamine – referred to as $DMEM^{full}$. Alternatively, they were grown in RPMI 1640 medium enriched with 10% FCS, 50 U/ml Penicillin/Streptomycin and 200 µM L-Glutamine – referred to as $RPMI^{full}$. For transient transfections, DMEM was also used without any additions – referred to as $DMEM^{null}$.

For cryopreservation of human cells a freeze medium was used, consisting of FCS with 10% DMSO.

3.2 Nucleic acids

3.2.1 Oligonucleotides

3.2.1.1 Oligonucleotides for PCR for amplification of DNA fragments

Name	Sequence (5'→ 3')	
LTR12 upstream TNFRSF10B	for	GTGTCCCTGCACCNTTGCTAC
	rev	GAACATCAGAAGGAACAAACTCC
TNFRSF10B exon 5	for	GTA CNC CCT GGA GTG ACA TC
	rev	ATG ATG ATG CCT GAG ANN G

Table 3-II. Oligonucleotides for PCR

3.2.1.2 Oligonucleotides for quantitative real-time PCR (cDNA)

Name	**Sequence (5'→ 3')**	
RPLP0	for	GATTGGCTACCCAACTGTTG
	rev	CAGGGGCAGCAGCCACAAA
GTAp63	for	ATTCCGGACACCCTATCAGAG
	rev	CCCAGATATGCTGGAAAACCT
TAp63 total	for	GTTATTACCGATCCACCATGTCC
	rev	GCGGATACAGTCCATGCTAATC
TNFRSF10B LTR12 transcript 1	for	CGAGGCTTCATTCTTGAAGGCAG
	rev	CGGCGCGGCTGTACTTTCAC
TNFRSF10B LTR12 transcript 2	for	CCAAGTGCCTCCCTCAACTCA
	rev	CGGCGCGGCTGTACTTTCAC
TNFRSF10B LTR12 transcript 2+3	for	TTGCTACTGCTCACTCTTTGGGT
	rev	CGGAACTAACCTTCGCCCTG
TNFRSF10B total	for	TTCTGCTTGCGCTGCACCAGG
	rev	GTGCGGCACTTCCGGCACAT
KDM1A	for	TACAGCAGTGCGACAGGTTCG
	rev	TGCTGCTTCAGCACACCCAG
HDAC1	for	CCAGGAACTGGGGACCTAC
	rev	TCATCAATCCCGTCTCGGAG
HDAC2	for	GACAAACCAGAACACTCCAG
	rev	CTTCTCCATCTTCATCTCCAC
HDAC3	for	CTGACTCTCTGGGCTGTG
	rev	GAGGGATATTGAAGCTCTTG
HDAC4	for	CGAAGAAGCCGAGACGGTC
	rev	CAGGGGCGGCTCCTCTTC
HDAC5	for	GCTGTTGCTGGAGCAGGC
	rev	CTTGCCTACCGTCCGCATG
HDAC6	for	CAGGCAGCGAAGAAGTAGGC
	rev	GCTAGATTGGGGATAGAGCG
HDAC7	for	CGCATCCAGAGCATCTGGTC
	rev	CTCAGAGTGGACCGACTGC
HDAC8	for	CTCCAGAAGGTCAGCCAAG
	rev	TCCTATAGCTGCTGCATAGTC
HDAC9	for	GCCAACTGGAAGTGTTACTG
	rev	GAATTAGAATGCGTTGCTGTG
HDAC10	for	GCTCCTGTACCTCTTAGATGG
	rev	GCAGCAGAGGCTGGAGTG
HDAC11	for	CAGGCACCGACATCCTCGA
	rev	CACCATAAGGATGGGCACC
NF-YA	for	GGTACTGGAGCCAATCAGCG
	rev	CTGGAGATCCTAGAAGGCTGTG
NF-YB	for	GCCATACCTCAAACGGGAAAG
	rev	CTCTTGATGGCACCTTTCAC
NF-YC	for	CTGAAACCTCCAAAGCGTCAG
	rev	CCCTGGACTTGGACAGCGGTG
ADH1C total	for	CCACAAGTACTCACCAGCCTC
	rev	GAGGTGCAACCTCTACCTC
GBP5 total	for	CTGCTTGACACCGAGGGC
	rev	GAGTGCCAGTGCAAAGATC

SEMA4D LTR12	for	CACCGGGAGGAACGAACAA
	rev	CCATCAGTGTCGTCAAACATTTCA
DHRS2 LTR12	for	CACCAAGCGGTGAGACTATCAC
	rev	CGGGCAACTGCTGACAGCATAG
APOC1 HERV-E LTR	for	CAAGCCCTCCAGCAAGGATTCAG
	rev	GTGTGTTTCCAAACTCCTTCAG
GSDMB HERV-H LTR	for	CTGAAATTGGCTTCTGTTTCTGAG
	rev	CCAGAATTTGAAACTCAGCC
DNAJC15 HERV-H LTR	for	CCACCAAACAGGCTTTGT
	rev	CAGATCCGAAATGCGTAGCG
IL2RB MaLR LTR	for	ATGTGGAACCGGCTTCCTT
	rev	GCAGATGCCCAAGAGGTAGC
HERV-K envelope [108]	for	ATTGGCAACACCGTATTCTGCT
	rev	CAGTCAAAATATGGACGGATGGT
HERV-W envelope [109]	for	ATGGAGCCCAAGATGCAG
	rev	AGATCGTGGGCTAGCAG

Table 3-III. Oligonucleotides for qRT-PCR (cDNA)

3.2.1.3 Oligonucleotides for quantitative real-time PCR (ChIP)

Name	**Sequence (5'→ 3')**	
Myoglobin	for	CTCATGATGCCCCTTCTTCT
	rev	GAAGGCGTCTGAGGACTTAAA
CCNB1 [110]	for	CCCCGCCCCTCTCGAAC
	rev	TTAAACCCCGCACTGCTCCC
DHRS2 LTR12	for	GGACCAATCAGCTCTCC
	rev	GAACCAGAGCAGGTTGCTGC
PGPEP1L LTR12	for	CACCCACATCCTGCTGATT
	rev	TCCAGCTCCAGGATTGTAAAC
TNFRSF10B LTR12	for	CGCTGATTGGTGGTTTACAATC
	rev	GAATGCACCAATTGACACTC
GTAp63 LTR12	for	CAGACCACTCGGCTCTACCAATC
	rev	GTGTGCACCCAAAGAGTGAG

Table 3-IV. Oligonucleotides for qRT-PCR (ChIP DNA)

All oligonucleotides were purchased from Metabion.

3.2.2 Small interfering RNAs (siRNAs)

Target	**siRNA ID**	**Sequence**
Negative Control #1	4390843	undisclosed
Negative Control #2	4390846	undisclosed
HDAC1	s73	sense: CUAUGGUCUCUACCGAAAAtt antisense: UUUUCGGUAGAGACCAUAGtt
HDAC2	s6493	sense: GGGUUGUUUCAAUCUAACAtt

		antisense: UGUUAGAUUGAAACAACCCag
HDAC3	s16877	sense: CCAAGAGUCUUAAUGCCUUtt antisense: AAGGCAUUAAGACUCUUGGtg
HDAC8	s31698	sense: GGUCCCGGUUUAUAUCUAUtt antisense: AUAGAUAUAAACCGGGACCag
KDM1A#1	s617	sense: GGUCUUGGAGGGAAUCCUAtt antisense: UAGGAUUCCCUCCAAGACCtg
KDM1A#2	s618	sense: GAGCAAGAGUUUAACCGGUtt antisense: ACCGGUUAAACUCUUGCUCta
KDM1A#3	s619	sense: CUGCAGUUGUGGUUGGAUAtt antisense: UAUCCAACCACAACUGCAGtg
TNFRSF10B#1	s16756	sense: CUGAUAAAGUGGGUCAACATT antisense: UGUUGACCCACUUUAUCAGCA
TNFRSF10B#2	s225038	sense: UGCUGUUGGUCUCAGCUGATT antisense: UCAGCUGAGACCAACAGCAGG
NFYA#1	s9529	sense: AAACCAAGCCGAUGAAGAAtt antisense: UUCUUCAUCGGCUUGGUUUgg
NFYA#2	s9530	sense: GGAGCACAGAUUGUUCAAAtt antisense: UUUGAACAAUCUGUGCUCCtg
NFYB	s9531	sense: CAAUCAAUGGAGAAGAUAUtt antisense: AUAUCUUCUCCAUUGAUUGtt
NFYC#1	s9534	sense: GGAAUUUAACAGUGAAAGAtt antisense: UCUUUCACUGUUAAAUUCCgg
NFYC#2	s9535	sense: GGCUCGUAUUAAGAAGAUUtt antisense: AAUCUUCUUAAUACGAGCCag

Table 3-V. Small interfering RNAs

All siRNAs are “silencer select” and were purchased from Ambion® Life Technologies.

3.3 Proteins

3.3.1 Antibodies

Name	Source	Company (Cat.No.)
NF-YA	Mouse, monoclonal	Santa-Cruz (sc-17753)
NF-YB	Rabbit, polyclonal	Genespin (PAb001)
IgG, ChIP grade	Rabbit	Abcam, Cambridge, UK (ab46540)

Table 3-VI. Antibodies for ChIP

Name	MW [kDa]	Source	Dilution	Company (Cat.No.)
Hsc-70	70 kDa	Mouse		Santa-Cruz (sc-7298)
PARP	89, 116 kDa	Rabbit	1:1000	Cell Signaling (9542)
Caspase-3	17, 19, 35 kDa	Rabbit	1:1000	Cell Signaling (9662)
Cleaved Caspase-3	17, 19 kDa	Rabbit	1:500	Cell Signaling (9664)
Hsp90	84 kDa	Rabbit	1:1000	Chemicon (AB3468)
HDAC1	55 kDa	Rabbit	1:1000	Diagenode (pAB-053-050)
HDAC2	60 kDa	Mouse	1:1000	Cell Signaling (5113)

Table 3-VII. Primary antibodies for Western blot

Name	Dilution	Company (Cat.No.)
HRP-coupled AffiniPure F(ab')2 fragment, anti-mouse IgG (H+L)	1:15,000	Jackson Immunoresearch, Europe, Newmarket, UK; 711-036-152
HRP-coupled AffiniPure F(ab')2 fragment, anti-rabbit IgG (H+L)	1:15,000	Jackson Immunoresearch, Europe, Newmarket, UK; 715-036-150

Table 3-VIII. Secondary antibodies for Western blot

3.3.2 Enzymes and other proteins

Reagent	Company
M-MuLV Reverse transcriptase (RT)	New England Biolabs
Rnase inhibitor	New England Biolabs
Taq DNA polymerase (Taq) for PCR	Fermentas, Thermo Scientific
Taq DNA polymerase (Taq) for qPCR	Primetech LTD, Minsk, Belarus
TRAIL (in sterile H_2O)	Gibco

Table 3-IX. Enzymes and other proteins

3.4 Consumables

Product	Company
12-well plates for Celigo	Corning, Corning, NY, United States
96-well plates for qPCR	4titude, Wotton, United Kingdom
Cell culture flasks (25 cm², 75 cm²,125 cm²)	Greiner, Frickenhausen, Germany
Cell culture plates (6-well, 12-well)	Greiner
Cell scraper (16 cm, 25 cm)	Sarstedt
Cryo tubes *Cryoline*	Nunc, Thermo Scientific
Filter tips (10 µl)	Starlab, Hamburg, Germany
Filter tips (20 µl, 200 µl, 1,000 µl)	Sarstedt
Parafilm	Brand
Pipet tips (10 µl, 20-200 µl, 1,000 µl)	Greiner
Protran nitrocellulose transfer membrane	Whatman, Dassel, Germany
Reaction tube (0.2 ml)	Sarstedt
Reaction tube (0.5 ml, 1.5 ml, 2.0 ml)	Eppendorf

Reaction tube (15 ml, 50 ml)	Greiner
Safe-lock reaction tube (1.5 ml)	Eppendorf
Sterile filter	Millipore, Merck
Syringe	Henke-Sass, Wolf, Tuttlingen, Germany
Syringe canula (different sizes)	B.Braun, Melsungen, Germany
Transparent sealing foil for 96-well plate	Sarstedt
Whatman paper	Whatman

Table 3-X. Consumables

3.5 Kits

Name	Company
BCA Protein Assay Kit	Thermo Scientific
Immobilon Western HRP Substrate Peroxide Solution	Millipore, Merck
SuperSignal West Femto Maximum Sensitivity Substrate	Thermo Scientific
Mini Elute Kit	Qiagen

Table 3-XI. Kits

3.6 Chemicals and reagents

Substance	Company
Acetic acid	Roth, Karlsruhe, Germany
Acrylamide-bisacrylamide	Roth
Agarose	Roth
Albumin Fraction V (Bovine Serum Albumine, BSA)	Roth
Ammonium persulfate (APS)	Roth
Ammonium sulfate ($(NH_4)_2SO_4$)	Roth
Aprotinin	Applichem
Bromophenol blue	Sigma-Aldrich
Calcium chloride dihydrate ($CaCl_2$ x $2H_2O$)	Roth
Chloroform	Roth
Complete Mini, EDTA-free Protease Inhibitor Mix tablet	Roche
Deoxyribonucleotide triphosphates (dNTPs) in single tubes	Primetech
Dimethyl sulfoxide (DMSO)	AppliChem
Dithiotreitol (DTT)	Sigma-Aldrich
DNA stain clear G (39804)	Serva
DMEM, powder	Gibco, Life Technologies
DNA ladder	Fermentas, Thermo Scientific
Ethanol 99.8%	Roth

Ethylene diamine tetraacetatic acid (EDTA)	Roth
Ethylene glycol tetraacetic acid (EGTA)	Roth
Fetal Calf Serum (FCS)	Gibco, Life Technologies
Formaldehyde, 37% solution	Roth
Glycerol	Roth
Glycine	Roth
Glycogen	Fermentas, Thermo Scientific
Glycogen blue	Ambion, Life Technologies
HEPES	Roth
Hydrogen chloride (HCl)	Roth
Isoamyl alcohol	Roth
Isopropanol	Th. Geyer, Renningen, Germany
L-Glutamine	Gibco, Life Technologies
Leupeptin Hemisulfate	Applichem
Lithium chloride (LiCl)	Roth
Lipofectamine 2000	Invitrogen, Life Technologies
Magnesium chloride ($MgCl_2$) for PCR, 25 mM	Fermentas, Thermo Scientific
Magnesium chloride hexahydrate ($MgCl_2$ x $6H_2O$)	Roth
Methanol >99% (MetOH)	Roth
Milk powder	Roth
Nonidet P-40 substitute (NP-40)	Sigma Aldrich
Nuclease free water	Ambion, Life Technologies
PBS, tablets	Gibco, Life Technologies
Pefabloc SC	Roth
Penicillin/Streptomycin	Gibco, Life Technologies
Pepstatin A	Applichem
Ponceau S	Roth
Potassium chloride (KCl)	Roth
Potassium hydrogenphosphate (KH_2PO_4)	Roth
Prestained Protein Ladder	Fermentas, Thermo Scientific
Protein A/G PLUS-Agarose	Santa Cruz
RNase inhibitor	Fermentas, Thermo Scientific
RPMI Medium	Gibco, Life Technologies
Sodium acetate (NaAc)	Roth
Sodium bicarbonate ($NaHCO_3$)	Roth
Sodium chloride (NaCl)	Roth
Sodium deoxycholate (NaDOC)	Applichem
Sodium dodecyl sulfate (SDS)	Roth
Sodium hydrogenphosphate heptahydrate (Na_2HPO_4 x $7H_2O$)	Roth
Sodium hydroxide (NaOH)	Sigma-Aldrich
Sucrose	Sigma-Aldrich
SYBR® Green-containing qPCR mix for ChIP analysis	Thermo Scientific
SYBR® Green	Invitrogen, Life Technologies
Taq buffer + KCl, 10x	Fermentas, Thermo Scientific
Tetramethylethylenediamine (TEMED)	Roth
Trasylol	Bayer, Leverkusen, Germany

Trehalose	Sigma-Aldrich
Trisamine (Tris)	Roth
Triton X-100	Applichem
TRIzol®	Invitrogen, Life Technologies
Trypsin/EDTA	Gibco, Life Technologies
Tween-20	Applichem
β-Mercaptoethanol	Roth

Table 3-XII. Chemicals and reagents

3.7 Buffers and solutions

Buffer / Solution	Components
ChIP buffer A	0.1 M NaCl 1 mM EDTA, pH 8.0 0.5 mM EGTA, pH 8.0 50 mM HEPES, pH 7.6 dissolved in H_2O
ChIP buffer B	0.25% Triton X-100 10 mM EDTA, pH 8.0 0.5 mM EGTA, pH 8.0 20 mM HEPES, pH 7.6 dissolved in H_2O
ChIP buffer C	0.15 M NaCl 1 mM EDTA, pH 8.0 0.5 mM EGTA, pH 8.0 50 mM HEPES, pH 7.6 dissolved in H_2O
ChIP washbuffer 1	0.1% SDS 0.1% NaDOC 1% Triton X-100 0.15 M NaCl 1 mM EDTA, pH 8.0 0.5 mM EGTA, pH 8.0 20 mM HEPES, pH 7.6 dissolved in H_2O
ChIP washbuffer 2	0.1% SDS 0.1% NaDOC 1% Triton X-100 0.5 M NaCl 1 mM EDTA, pH 8.0 0.5 mM EGTA, pH 8.0 20 mM HEPES, pH 7.6 dissolved in H_2O
ChIP washbuffer 3	0.25 M LiCl 0.5% NaDOC 0.5% NP-40 1 mM EDTA, pH 8.0 0.5 mM EGTA, pH 8.0 20 mM HEPES, pH 7.6

	dissolved in H_2O
ChIP washbuffer 4, 10x	10 mM EDTA, pH 8.0 5 mM EGTA, pH 8.0 200 mM HEPES, pH 7.6 dissolved in H_2O
ChIP elution buffer	1% SDS 0.1 M $NaHCO_3$ dissolved in H_2O
ChIP incubation buffer with SDS, 5x	0.75% SDS 5% Triton X-100 0.75 M NaCl 5 mM EDTA, pH 8.0 2.5 mM EGTA, pH 8.0 100 mM HEPES, pH 7.6 dissolved in H_2O
ChIP incubation buffer without SDS, 5x	5% Triton X-100 0.75 M NaCl 5 mM EDTA, pH 8.0 2.5 mM EGTA, pH 8.0 100 mM HEPES, pH 7.6 dissolved in H_2O
DNA gel loading buffer	40% Sucrose 10% Glycerin 0.25% Bromphenol blue Dissolved in H_2O
Dulbecco's Modified Eagle's Medium	10 g/l DMEM, powder 3.7 g/l NaHCO3 5.96 g/l HEPES dissolved in H_2O
Formaldehyde-mix	0.5 ml 37% formaldehyde 1.18 ml buffer A 15 ml PBS
Laemmli buffer, 6x	0.35 M Tris, pH 6.8 30% Glycerin 10% SDS 9.3% DTT 0.02% Bromphenol blue dissolved in H_2O
PBS, pH 7.4	24 mM NaCl 0.27 mM KCl 0.81 mM Na_2HPO_4 x $7H_2O$ 0.15 mM KH_2PO_4 dissolved in H_2O
PBS/T, pH 7.4	24 mM NaCl 0.27 mM KCl 0.81 mM Na_2HPO_4 x $7H_2O$ 0.15 mM KH_2PO_4 0.1% Tween-20 dissolved in H2O
PIC, 25x	1 tablet complete Protease Inhibitor Mix dissolved in 2 ml H_2O

Ponceau S solution	0.5% Ponceau S 1.0% Acetic acid dissolved in H_2O
qRT-PCR reaction buffer, 10x	750 mM Tris-HCl, pH 8.5 200 mM $(NH_4)_2SO_4$ 0.1% Tween-20 dissolved in H_2O
RIPA lysis buffer, pH 7.5	1% Triton X-100 1% Na deoxycholat 0.1% SDS 150 mM NaCl 10 mM EDTA 20 mM Tris, pH 7.5 50.000 KIU Trasylol dissolved in H_2O
SDS running buffer	25 mM Tris 86.1 mM Glycine 3.5 mM SDS dissolved in H_2O
SYBR® Green-containing qPCR mix	1x qRT-PCR reaction buffer 10x 3 mM $MgCl_2$ 1:75.000 SYBR® Green 0.2 mM dNTPs 20 U/ml Taq polymerase 0.25% Triton X-100 300 mM Trehalose in 10mM Tris, pH 8.5 dissolved in H_2O
TAE buffer	40 mM Tris 20 mM Acetic acid 2 mM EDTA dissolved in H_2O
Western blot blocking solution	5% milk powder dissolved in PBS/T
Western salts, pH 8.3	0.25 M Tris, pH 8.3 0.19 M Glycine 0.02% SDS dissolved in H_2O
Western blot transfer buffer	1x Western salts 10x 20% MeOH dissolved in H_2O

Table 3-XIII. Buffers and solutions

3.8 Pharmacological inhibitors

Chemical	Stock	Solvent	Company
Trichostatin A (TSA)	6 mM	DMSO	Sigma-Aldrich
Suberoylanilide hydroxamic acid (SAHA)	10 mM	DMSO	Selleckchem
Mocetinostat	5 mM	DMSO	Selleckchem
Entinostat	5 mM	DMSO	Selleckchem
PCI-34051	5 mM	DMSO	Selleckchem
Droxinostat	6 mM	DMSO	Selleckchem
Tubastatin A hydrochloride	5 mM	DMSO	Selleckchem

Table 3-XIV. Pharmacological inhibitors

3.9 Technical devices

Device	Company
Blotting chamber	Biozym, Hessisch Oldendorf, Germany
Cell counting chamber *Neubauer improved*	Brand, Wertheim, Germany
Centrifuge *5415R*	Eppendorf, Hamburg, Germany
Centrifuge *5810R*	Eppendorf
Centrifuge Megafuge *1.0R*	Heraeus, Thermo Scientific, Waltham, MA, United States
Chemiluminescence imager *Chemocam HR 16 3200*	Intas Science Imaging Instruments, Göttingen, Germany
Cytometer *Celigo*	Cyntellect, San Diego, CA, United States
DNA gel chamber	Biotech Service Blu, Schauenburg, Germany
Electrophoresis system, for SDS-PAGE	Amersham Biosciences, GE Healthcare, Little Chalfont, United Kingdom
FACS machine Guava PCA-96 Base System	Millipore, Merck, Darmstadt, Germany
Foil swelding machine *Vacupack plus*	Krups, Groupe SEB, Lyon, France
Freezer -20°C	Liebherr, Bulle, Switzerland
Freezer -80°C	Heraeus, Thermo Scientific
Gel Jet Imager	Intas Science Imaging Instruments
Heating Block	Grant Instruments, Hillsborough, NJ, United States
Heating Block *HLC*	HLC Biotech, Ditabis, Pforzheim, Germany
Ice-machine *B100*	Ziegra, Isernhagen, Germany
Laminar flow cabinet *Hera Safe*	Heraeus, Thermo Scientific
Liquid nitrogen tank *LS 4800*	Taylor-Wharton, Theodore, AL, United States
Magnetic stirrer *MR Hei-Standard*	Heidolph, Schwabach, Germany
Magnetic stirrer *MR3001*	Heidolph
Microscope *Axovert 40C*	Zeiss, Oberkochen, Germany
Microscope, Axioscope 2 Plus	Zeiss
Microwave	Cinex, Lippstadt, Germany

Mini Centrifuge *MCF-2360*	LMS, Tokyo, Japan
PCR machine for qRT-PCR *Chromo4*	Bio-Rad Laboratories
PCR machine *Thermocycler T personal*	Biometra, Göttingen, Germany
pH-meter *WTW-720*	WTW, Weilheim, Germany
Pipet *Multipette*	Eppendorf
Pipet, electric *Portable-XP*	Drummond, Broomal, PA, United States
Pipets Eppendorf Research Series 2100 (0.1-2.5 µl; 0.5-10 µl; 10-100 µl; 100-1000 µl)	Eppendorf
Pipette, multichannel *Research Plus*	Eppendorf
Power supply unit *Powerpack P25T*	Biometra
Refrigerator 4°C	Liebherr
Roller RM5 V-30	CAT, Staufen, Germany
Rotator *PTR 300*	Grant Instruments
Scales *Acculab ALC-6100.1*	Sartorius, Göttingen, Germany
Scales *LE623S*	Sartorius
Scanner *CanoScan 8600F*	Canon, Tokyo, Japan
Sequencer, automated *ABI 3100*	Applied Biosystems, Life Technologies
Shaker *PROMAX 2020*	Heidolph
Sonication device *Bioruptor®*	Diagenode, Liège, Belgium
Spectrophotometer *NanoDrop ND-1000*	PeqLab, Erlangen, Germany
Thermomixer *comfort*	Eppendorf
Vacuum pump	IBS Integra Biosciences, Fernwald, Germany
Vortex *Genie 2*	Scientific Industries, Bohemia, NY, United States
Water bath *TW 20*	Julabo Labortechnik, Seelbach, Germany

Table 3-XV. Technical devices

3.10 Software and databases

3.10.1 Software

Name	**Company**
Adobe Photoshop CS5	Adobe Systems, San Jose, CA, United States
BioEdit v.7.0.5.	Tom Hall, Ibis Therapeutics, Isis Pharmaceuticals, Carlsbad, CA, United States
CFX Manager Software for qPCR cycler	Bio-Rad
Excel	Microsoft, Redmond, WA, United States
INTAS lab ID	Intas Science Imaging Instruments
NanoDrop Software	Peqlab
Office Picture Manager	Microsoft, Redmond, WA, United States
UV imager software	Intas Science Imaging Instruments

Table 3-XVI. Software

3.10.2 Databases and online tools

Database	Web adress
ClustalW2	http://www.ebi.ac.uk/Tools/msa/clustalw2/
Ensembl Genome Browser	http://www.ensembl.org/index.html
Galaxy/Cistrome	http://cistrome.org/ap/root
Gene Expression Omnibus (GEO)	http://www.ncbi.nlm.nih.gov/geo/
IDT OligoAnalyzer 3.1	https://eu.idtdna.com/calc/analyzer
In-Silico PCR tool by UCSC	http://genome-euro.ucsc.edu/cgi-bin/hgPcr?hgsid=201706450_nHXcVWrMGyrI7f8PZ95EjikMtMNu
Primer-BLAST tool by NCBI	http://www.ncbi.nlm.nih.gov/tools/primer-blast/
PROMO MultiSiteSearch	http://alggen.lsi.upc.es/cgi-bin/promo_v3/promo/promoinit.cgi?dirDB=TF_8.3
Repbase CENSOR	http://www.girinst.org/censor/
Repbase Update	http://www.girinst.org/repbase/update/browse.php
SnapGene Viewer 2.6.2	http://www.snapgene.com/products/snapgene_viewer/
UCSC genome browser	genome.ucsc.edu

Table 3-XVII. Databases and tools

4 Methods

4.1 Cell biology

All cell culture work was performed under sterile conditions. The used solutions and media were pre-heated at 37°C before usage.

4.1.1 Culturing of human cells

After thawing, adherent and suspension cells were cultivated at 37°C, 5% CO_2 in coated cell culture dishes or flasks, respectively -covered with either $DMEM^{full}$ or $RPMI^{full}$ (see Table 3-I). Culture media was renewed every 3-4 days and cells were subcultured to avoid hyperconfluent growth. For subcultivation of adherent cells, first the culture medium was removed. Cells were washed once with pre-warmed 1x PBS and then incubated with trypsin/EDTA until detachment from the dish became visible. Then fresh culture medium was added for inactivation of trypsin and a fraction of the cells was transferred to a new dish, medium volume was filled-up with fresh culture medium and incubation continued at 37°C, 5% CO_2. For subcultivation of suspension cells, the cell suspension was transferred to 15 ml falcon tubes, spun down at 1,000 g for 5 min, supernatant was removed and cells re-suspended in fresh culture medium. Accordingly, a fraction of the cells was then transferred to a new flask under addition of fresh culture medium. Cells were subcultured for a maximum of 30 passages.

Depending on the given objections, specific cell numbers had to be seeded in 6-, 12- or 24-Well dishes. For this purpose cells of about 70-80% confluency were subjected to the same steps as for subcultivation. However, instead of transferring a cell fraction to a new dish, the cell suspension was transferred to a falcon tube and counted in a Neubauer counting chamber. The amount of cells x in one of the outer squares gives the cell concentration as $x \cdot 10^4$ cells/ml. Accordingly, the needed cell amount can be subtracted from the cell suspension and be seeded.

4.1.2 Freezing and thawing of cells

For cryopreservation, a 10 cm-dish with about 80% confluent cells was washed once with PBS and then incubated with 1.5 ml trypsin/EDTA until detachment from the dish. Then 8.5 ml fresh culture medium was added and the cell suspension was transferred to a 15 ml falcon tube. Then the cells were separated from the medium by centrifugation at 1,000 g for 5 min, the supernatant was removed and cells were resuspended in 3 ml freeze medium. The cell suspension was then evenly distributed to 3 cryotubes and stored at -80°C for 2 days before being transferred to liquid N_2 for long-term storage.

For thawing of the cells, an aliquot was rapidly warmed and transferred to a 15 ml falcon tube with 5 ml culture medium. Cells were centrifuged to separate the DMSO-containing supernatant at 1,000 g for 5 min. Then the cell pellet was resuspended in fresh culture medium and transferred to a coated cell culture dish. The following day, medium was changed to remove dead cells.

4.1.3 Transient transfection of human cells with siRNAs

To deplete specific proteins, cells were transiently transfected with siRNA. For preparation of a siRNA solution, Lipofectamine 2000 was mixed with $DMEM^{null}$ by vortexing – depending on the experimental set-up different amounts were used (see Table 4-I). For depletion of different HDAC isoforms or NF-Y subunits, the used siRNA mix consisted of 3 different siRNAs per Well. The total siRNA concentration was kept constant by adding the respective amount of scrambled control siRNAs (SSC). For HDAC depletion the total siRNA concentration was 15 nM per Well (5 nM of each siRNA). For NF-Y depletion the total siRNA concentration was 45 nM per Well (15 nM of each siRNA).

The mix was incubated for 5 min at RT for micelles to be formed. Next the lipofectamine mix was added to siRNA suspended in $DMEM^{null}$ and mixed gently. Subsequently, this siRNA-lipofectamine solution was incubated for 20 min at RT for the siRNA to be incorporated into the pre-formed micelles. In the meantime, a suspension of the target cells was prepared in $DMEM^{full}$. Then the siRNA-lipofectamine solution was distributed into 6- or 12-Well plates. Next, the respective amount of cells was added. Depending on the used cell line, different cell amounts were seeded. For the transient transfection with siRNAs targeting histone deacetylases (HDAC), $1.8 \cdot 10^5$ U2OS cells/Well were seeded in 6-Well dishes. For transient transfection with siRNAs targeting either *NF-Y* subunits alpha, beta or gamma, *TNFRSF10B* or *KDM1A* transcripts $1 \cdot 10^5$ GH cells/Well were seeded in 12-Well dishes. The cells were then incubated at 37°C, 5% CO_2 for 24 h. After this incubation period, the transfection medium was replaced by fresh $DMEM^{full}$ and incubation was continued for another 24 h.

For depletion of HDAC isoforms, NF-Y subunits and KDM1A all transfection steps were repeated 48 h after the initial transfection. During this transfection, the siRNA-lipofectamine solution was added directly onto the adherent cells. The second transfection was necessary to maintain a constant siRNA/cell ratio in the dividing cells. 24 h after this second transfection, the transfection medium was replaced again and cells were harvested for subsequent analysis 96 h after initial transfection.

Reagent	**per 6-Well** *HDACs*	**per 12-Well** *NF-Y subunits*	**per 12-Well** *TNFRSF10B, KDM1A*
Lipofectamine 2000	5 µl	2.5 µl	2.5 µl
DMEM^{null} (for mix with Lipofectamine 2000)	250 µl	125 µl	125 µl
siRNA (Stock: 50 µM)	0.75 µl	0.9 µl	0.3 µl
DMEM^{null} (for suspension of siRNA)	250 µl	125 µl	125 µl
Volume of cell suspension	2 ml	750 µl	750 µl
Total volume per Well	2,500 µl	1,000 µl	1,000 µl

Table 4-I. Volumes for transient transfection with siRNAs

The used siRNA sequences are listed in Table 3-V.

4.1.4 Treatment with chemicals

Depending on the used cell line, different cell densities were seeded in either 6- or 12-Well dishes (see 4.1.1). Cells were incubated for 18-24 h at 37°C, 5% CO_2 to allow adherent cells to settle. Then the drug was either added directly or the culture medium was replaced by fresh culture medium containing the respective amount of chemical. Then incubation was continued for 10-18 h depending on the experimental setup. To identify unspecific effects, at least one set of cells was treated with the solvent of the used drug alone.

4.1.5 Confluency measurement

Using the Celigo® Imaging Cytometer microscopic bright field pictures were taken 24, 48, 72, 96 and 120 h after initial transfection of GH cells with siRNA targeting either *TNFRSF10B* transcripts or scrambled controls. These pictures were analyzed regarding the confluency of the cells in each Well with the Celigo® software. The confluency was then plotted over the 5 day time course to visualize the growth rate.

4.2 Molecular biology

4.2.1 Extraction of RNA using TRIzol®

To extract full RNA from adherent human cells, the culture medium was replaced by 1 ml/6-Well or 0.5 ml/12-Well TRIzol®. For extraction of RNA from suspension cells, they were spun down at 1,000 g for 5 min and the supernatant was replaced by the respective amount of TRIzol®. Next, the samples were pipetted up and down several times to enhance cell lysis, transferred to 1.5 ml reaction tubes and incubated for 10 min at RT. Then 200 µl chloroform/1 ml TRIzol® was added and mixed thoroughly

by vigorous shaking. After 3 min incubation at RT, the suspension was subjected to phase separation by centrifugation at 12,000 g for 30 min at 4°C. The aqueous upper phase, containing the RNA, was carefully transferred to a fresh 1.5 ml reaction tube. Purification was achieved by precipitation with 500 µl isopropanol/1 ml TRIzol®. Therefore, the mix was shaken, incubated at RT for 15 min and centrifugated at 12,000 g for 60-90 min at 4°C. Subsequently, the RNA-containing pellet was washed twice with 70% Ethanol and then air-dried for 30 min. Depending on the size of the pellet it was then resuspended in 20-50 µl nuclease-free water and heated to 55°C for 5 min. Subsequently, RNA was stored at -80°C until further analysis.

4.2.2 Determination of nucleic acid concentrations

The concentration and purity of RNA was determined using the NanoDrop spectrophotometer. At a wavelength of 260 nm the concentration was measured. To identify DNA or protein contaminations, the 260/230 nm and 260/280 nm ratios were analyzed and considered favorable when above 1.80.

4.2.3 Reverse transcription of RNA

For further analysis of the transcriptome, messenger RNA was reversely transcribed into cDNA. Therefore, 1 µg of RNA was mixed with 2 µl of a primer mix consisting of (15 µM) random nonamer primers and (50 µM) anchored oligo-dT primers $dT_{23}VN$. Further 0.5 µl dNTP mix (20 mM of each deoxyribonucleotide triphosphate) was added. The mix was filled-up with water to a total volume of 16 µl and heated at 70°C for 5 min to demolish secondary structures. Subsequently, 4 µl of a master mix was added per reaction (see Table 4-II).

Reagent	**Volume**
Reaction buffer 10x	2 µl
RNase inhibitor	0.25 µl
M-MuLV Reverse Transcriptase	0.125 µl
RNase-free water	1.625 µl

Table 4-II. Master mix for reverse transcription of RNA

Each sample was prepared in duplicates – one where the enzyme reverse transcriptase, derived from moloney murine leukemia virus (M-MuLV), was added and one mock with water added instead. The latter serves to exclude contaminations with genomic DNA. The samples were incubated at 42°C for 1 h. Then the enzyme was deactivated by incubation at 95°C for 5 min. Afterwards, the cDNA was diluted by addition of 30 µl nuclease-free water and stored at -20°C until further analysis.

4.2.4 Primer design

Genomic sequences of the respective genes or genomic regions were retrieved from the UCSC Genome Browser. Transcript sequences were retrieved from the Ensembl database. All primers were designed manually and checked for the likelihood of hairpin secondary structures and dimer formation using the OligoAnalyzer 3.1 tool provided by Integrated DNA Technologies (IDT). Primer sequences were only considered with a ΔG of more than -10 kcal/mole. Subsequently, their specificity was checked using the Primer-BLAST tool provided by National Center for Biotechnology Information (NCBI) and the *In-silico* PCR tool provided by University of California Santa Cruz (UCSC).

Oligonucleotides to be used for quantitative real-time PCR for amplification of cDNA were preferentially placed in different exons with a product size of 300 base pairs at most. This allows to distinguish between cDNA and genomic DNA since the latter contains introns. All primer sizes must not exceed 24 nucleobases and a GC content of 60%. Melting temperatures were preferentially about 60°C.

4.2.5 *In-silico* transcription factor binding site prediction

First, sequences of LTR12 upstream of the cellular genes were retrieved from UCSC Genome Browser (see Table 4-III). These LTR12 were either previously described to drive expression of the adjacent gene [27] or were identified as candidates to drive gene expression in our recent approach (Table 2-I). Identification of each LTR12 was conducted by the CENSOR software tool [111] and complementing information was retrieved from the Repbase Update database [112]. Next, the LTR12 sequences were analyzed by PROMO, which uses the 8.3 version of TRANSFAC, for common transcription factor binding sites [113, 114]. Factor's and site's species was defined as human only. Dissimilarity margin was set to be equal as or less than 5%.

Gene name	Gene position (hg19)	location of LTR12 (hg19)
ADH1C	chr4:100,257,649-100,273,917	chr4:100274696-100275434
GBP5	chr1:89,724,634-89,738,544	chr1:89738137-89739573
SEMA4D	chr9:91,992,152-92,094,611	chr9:92094404-92095897
TNFRSF10B	chr8:22,877,648-22,926,700	chr8:22927451-22928865
TP63	chr3:189,507,449-189,615,068	chr3:189313733-189314949
DHRS2	chr14:24,105,573-24,114,848	chr14:24104837-24105861 chr14:24106921-24107605
NR1H4	chr12:100,897,138-100,957,645	chr12:100823898-100825322
C9orf53	chr9:21,967,138-21,967,753	chr9:21959077-21960418
CPED1	chr7:120,628,751-120,937,498	chr7:120699844-120701243
C9orf85	chr9:74,526,423-74,588,371	chr9:74578275-74579651
CCR4	chr3:32,993,066-32,996,403	chr3:32980994-32982647
ACSBG1	chr15:78,473,097-78,527,049	chr15:78537615-78539044
KCNN3	chr1:154,669,942-154,842,754	chr1:154650332-154651788
CSF3	chr17:38,171,614-38,174,066	chr17:38167005-38169009
TMOD1	chr9:100,263,462-100,364,025	chr9:100336320-100337735
SLC36A2	chr5:150,694,539-150,727,151	chr5:150786356-150787204
IER3	chr6:30,710,976-30,712,327	chr6:30774508-30775782
PIK3C2G	chr12:18,414,474-18,801,352	chr12:18652900-18654112
TENM1	chrX:123,509,756-124,097,666	chrX:124390314-124390725
CT49/ LINC01194	chr5:12,574,969-12,805,295	chr5:12661848-12663161 chr5:12796289-12796978
PTPN13	chr4:87,515,468-87,736,328	chr4:87468293-87469596
RADIL	chr7:4,836,687-4,923,335	chr7:4832980-4834366

Table 4-III. LTR12 locations in the human genome (hg19)

4.2.6 Polymerase chain reaction (PCR)

4.2.6.1 PCR for amplification of DNA fragments

To determine the existence of LTR12 sequences upstream of *TNFRSF10B* in difference species, a specific forward primer within LTR12 and a reverse primer upstream exon 1 of *TNFRSF10B* were used (see Table 3-II). If the LTR12 was present, amplification occurred which could be detected through subsequent DNA gel electrophoresis (see 4.2.7).

Reagent (Stock conc.)	Final concentration	1x
10x Taq buffer + KCl	1xl	5 µl
$MgCl_2$ stock (25 mM)	3 mM	6 µl
dNTP mix (20 mM each)	0,2 mM each	0.5 µl
Taq DNA-Polymerase	1,25 units	0.25 µl
water		36.95 µl
Primer (100 µM)	300 nM each	0.15 µl each
Genomic DNA (100ng/µl)	100 ng	1 µl

Table 4-IV. Volumes for PCR reactions

95°C	3 min		*Denaturation*
95°C	20 sec	32 cycles	*Denaturation*
56°C	25 sec		*Annealing*
72°C	25 sec		*Elongation*
72°C	5 min		
8°C	∞		

Table 4-V. PCR protocol

4.2.6.2 Quantitative real-time PCR for amplification of cDNA

To determine relative gene expression [115], quantitative real-time PCR was performed in a 96-Well-scale using SYBR® Green. The total volume per Well was 25 µl. The reaction mix consisted of 14 µl SYBR® Green-containing qPCR mix (see Table 3-XIII), 0.3 µM forward primer, 0.3 µM reverse primer, 2 µl cDNA (as described in 4.2.3), filled *ad* 25 µl with water. After pipetting on ice, the plate was sealed with plastic foil, shortly spun down at 800 g for 1 min and analyzed immediately. To diminish the influence of technical impreciseness, each sample was measured in triplicates. For each primer combination, samples without reverse transcriptase and samples with H_2O instead of cDNA served as negative controls. Moreover, the reference gene *RPLP0* was always measured in parallel, to allow for samples from different plates to be comparable.

95°C	2 min		*Denaturation*
95°C	15 sec	40 cycles	*Denaturation*
60°C	1 min		*Annealing & Elongation*
Plate read			
Melting curve 60°C to 95°C, every 0.5°C, hold 1 sec			

Table 4-VI. qRT-PCR protocol

Relative gene expression was calculated using a variation of the ΔΔCt-method [116]. Herein the ΔCt-value was calculated by normalizing the cycle threshold (Ct)-value of the gene of interest to the reference gene by subtraction. Since the amount of DNA is assumed to double in every cycle, Ct-values represent logarithmic values to the base of 2. Accordingly, $2^{-\Delta Ct\text{-value}}$ characterizes the relative normalized expression ratio for each sample. Two samples, e.g. an inhibitor-treated sample and a control sample, can further be compared by calculating their ratio (=fold change).

For all shown figures, biological replicas from at least 3 independently performed experiments were subjected to quantification.

4.2.6.3 Quantitative real-time PCR to analyze ChIP samples

To analyze DNA sequences, which were bound to specifically immunoprecipitated proteins (see 4.3.3), quantitative real-time PCR was conducted. Hereby, protein-DNA interactions can be identified and quantified as well as changes thereof. First a series of input dilutions was prepared (1:10 – 1:1000). This dilution series was then used to test all primer before measuring the ChIP samples. In disparity to the amplification of cDNA (see 4.2.6.2), a commercially available SYBR® Green-containing qPCR mix was used (Thermo Scientific) and 5 µl DNA template. This qPCR mix contains a Maxima Hot Start Taq DNA Polymerase which is inactive at RT. Upon incubation at 95°C for at least 4 min, its activity is restored (see Table 4-VII).

95°C	10 min		*Denaturation*
95°C	15 sec	40 cycles	*Denaturation*
60°C	1 min		*Annealing & Elongation*
Plate read			
72°C	5 min		
Melting curve 50°C to 95°C, every 0.5°C, hold 1 sec			

Table 4-VII. qRT-PCR ChIP protocol

Due to the limited availability of template DNA, samples were measured in duplicates instead of triplicates. For each primer combination, samples with H_2O instead of template DNA served as negative controls. Moreover, 1:10-diluted input samples were always measured in parallel. All ChIP samples of one experiment (input, IgG-ChIP, NF-YA-ChIP, NF-YB-ChIP) were always analyzed on the same plate to eliminate errors in the analysis due to varying PCR conditions.

Samples were analyzed as percentage of input chromatin, which characterizes the recovery. First the cycle threshold (Ct)-value of an IP sample was normalized to the corresponding input sample by subtraction ("ΔCt-value"). Corresponding to chapter 4.2.6.2, the $2^{-\Delta Ct\text{-value}}$ was calculated. Next, this normalized value was divided by a dilution factor of 100. This dilution factor takes into account the 1:10-less concentrated input sample (12 µl input chromatin versus 120 µl chromatin subjected to specific IP) and the 1:10 dilution of the input sample with water prior to the PCR. To obtain a value in percentage, last the value was multiplied by 100.

$$\Delta Ct\text{-value} = Ct_{IP\ sample} - Ct_{Input\ sample}$$

$$\text{Recovery (\% of input)} = 2^{-\Delta Ct\text{-value}}/100 * 100$$

For all shown figures, biological replicas from at least 3 independently performed experiments were subjected to quantification.

4.2.7 DNA gel electrophoresis

To visualize DNA fragments, agarose gels were used. Therefore, 0.6 g agarose was mixed with 60 ml TAE buffer for a 1% gel and boiled until a homogenous solution resulted. Then 3 µl DNA stain clear G was added to the liquid gel and casted in a casting chamber with a plastic comb. After incubation for 30 min at RT the gel polymerized. DNA samples were mixed with 1:6 DNA gel loading buffer and 10 µl was loaded per pocket. Agarose gel electrophoresis was performed at 100 Volt for 30-40 min. Finally, DNA fragments were visualized on a Gel Jet Imager by UV light.

4.3 Protein Biochemistry

4.3.1 Cell lysates for SDS-PAGE analysis

For analysis of protein expression, cells were lysed. Therefore, cells were scraped directly in the culture medium with a rubber spatula on ice. Then the cell suspension was homogenized by pipetting up and down several times and transferred to a 1.5 ml reaction tube. Next the supernatant was separated from the cells by centrifugation at 1,000 g for 5 min at 4°C. Supernatant was removed and cells were lysed by addition of 100 µl RIPA lysis buffer and incubated on ice for 30 min. Every 10 min the cell lysate was thoroughly mixed. After 30 min, the cell lysate was subjected to sonication using the *Bioruptor®* at high power (30 sec on; 30 sec off) for 5 min. Then samples were stored at -80°C until further analysis.

4.3.2 Separation of proteins by SDS-PAGE and Immunoblot analysis

4.3.2.1 SDS-PAGE

To separate proteins according to their molecular mass, sodium dodecyl sulfate polyacrylamide gel electrophoresis (SDS-PAGE) was used [117, 118]. Herein, SDS confers an overall negative charge to the proteins, resulting in their movement towards the anode upon applying an electric field. Their electrophoretic mobility is proportional to their molecular weight, resulting in a separation according to it. First, samples of lysed human cells (see 4.3.1) were thawed on ice and 20 µl Laemmli sample buffer was being added, containing the reducing agent dithiothreitol. Samples were heated to 95°C for 5 min, followed by mixing and brief centrifugation. To estimate protein sizes, 7 µl of a standard protein marker was loaded in parallel. The used polyacrylamide gels had an acrylamide/bisacrylamide

concentration of 12% (resolving gel) and 5% (stacking gel). Gel electrophoresis was performed at constant voltage initially at 100 Volt for 15 min, followed by 150 Volt for 2 h.

Reagent (Stock conc.)	Stacking gel	Resolving gel
Acrylamide-bisacrylamide	500 µl	4 ml
0.5 M Tris-HCl, pH 6.8	380 µl	
1.5 M Tris-HCl, pH 8.8		2.5 ml
10% SDS	30 µl	100 µl
10% APS	30 µl	100 µl
TEMED	3 µl	4 µl
water	2.1 ml	3.3 ml

Table 4-VIII. Composition of gels for SDS-PAGE

4.3.2.2 Immunoblotting

To visualize specific proteins, those separated by their molecular masses by electrophoresis were transferred from the polyacrylamide gel to a membrane. The transfer of the proteins, called blotting, was conducted by assembling a tight contact between the polyacrylamide gel and a nitrocellulose membrane with a pore size of 0.2 µm within a plastic carrier. This so called "tank-blot technique" was introduced by Bittner *et al.* [119]. Excessive space is filled with 3 sponges and 6 Whatman paper, which were equilibrated in transfer buffer before usage. Upon applying an electric field, the proteins then travel towards the anode due to their overall negative charge resulting from the SDS. Accordingly, the nitrocellulose membrane was placed on the anode side, resulting in protein transfer from the gel onto the membrane.

Blotting occurred on ice in the cold room in transfer buffer at 90 Volt for 100 min. The completeness of the protein transfer was monitored by staining of the membrane with ponceau S solution. To saturate unspecific binding sites, the membrane was incubated for 2 h in blocking solution.

4.3.2.3 Immunostaining

After blotting onto a membrane, specific antibodies can bind to the proteins and be visualized. Primary antibodies (see Table 3-VII) were diluted in 5 ml blocking solution and the membrane was incubated with the antibody solution over-night in a rolling 50 ml falcon tube in the cold room.

The following day, the membrane was washed three times with blocking solution for 10 min each. Then the membrane was incubated with a secondary antibody (see Table 3-VIII) diluted in blocking solution for 2 h at RT in a rolling 50 ml falcon. Next, the membrane was washed three more times with PBS/T for 10 min each. Afterwards, binding of antibodies was detected using enhanced

chemiluminescence immune detection (ECL). ECL-advanced solution was prepared freshly and the membrane was incubated with it for 1 min. The secondary antibody was linked to a horseradish peroxidase, which oxidizes the luminol in the ECL-solution. When luminol falls back to its unexcited state, electromagnetic waves are being emitted, which can be visualized by camera. The light signal indicates the position and quantity of the protein of interest on the membrane [120]. The exposition times varied between 10 sec and 10 min, depending on the signal intensity.

4.3.3 Chromatin harvest and chromatin immunoprecipitation

Interactions of proteins with specific target sites in the genome can be fathomed by immunoprecipitation (IP) of target proteins with specific antibodies. Following, the precipitated DNA, which had been bound to the protein, can be analyzed by qRT-PCR. The protocol used for chromatin harvest and the IP was modified after Denissov *et al.* [121].

4.3.3.1 Chromatin harvest for ChIP

At about 80% confluency, cells were washed once with PBS. Supernatant was removed completely. Cells from one 15 cm plate were cross-linked for 20 min by addition of 2.5 ml formaldehyde-mix. Next, cross-linking was stopped by addition of 250 µl 1.25 M glycine and a 5 min incubation time. From now on all steps were performed on ice and all centrifugations were carried out at 4°C. All liquid was removed and fixed cells were washed twice with pre-cooled PBS. Next, 2 ml cold buffer B was added to lyse the cells, followed by an incubation at 4°C for 10 min. Cells were scraped in buffer B and spun down at 2000 rpm for 5 min. This was followed by washing of the pellet with 4 ml cold buffer C and centrifugation at 2000 rpm for 10 min. After discarding the supernatant, cells were resuspended in about 700 µl 1x incubation buffer with SDS for sonication. The stock buffer was diluted with water and 1x PIC and 22.5 µl/ml 10% SDS were added prior to usage. Then chromatin was subjected to sonication using the *Bioruptor®* at high power (30 sec on; 30 sec off) for 10 min, 10 min and finally 5 min to shear the chromatin. Before each step, the cold water was replaced and a handful ice was added. After sonication, the suspension was spun down at 13,000 rpm for 5 min to pellet remaining unsheared chromatin. The supernatant was aliquoted and stored at -80°C until immunoprecipitation.

Before further usage of the chromatin, its quality was tested. 40 µl of the chromatin was mixed with 40 µl water and 2 µl 5 M NaCl. The solution was boiled at 99°C for 15 min. After cooling on ice, 1 µl 10 mg/ml RNase A was added and samples were incubated at 37°C for 10 min. Next, DNA was purified by phenol-chloroform purification. Therefore, 80 µl Phenol was mixed to the solution and then centrifuged at 13,000 rpm for 1 min. The colorless DNA-containing upper phase was transferred to a

fresh reaction tube and 80 µl chloroform was added to it. The mix was vortexed and then centrifuged at 13,000 rpm for 1 min. The upper phase was transferred to another fresh reaction tube and mixed with 8 µl 60% Glycol solution for further gel analysis (see 4.2.7). If the resulting fragments are between 50 and 300 bp in length, the sheared chromatin was used further.

4.3.3.2 Chromatin immunoprecipitation

For the immunoprecipitation of specific target proteins, Protein A/G PLUS-Agarose with 1:5 IgG:IgA was used, referred to as "beads". First the beads were equilibrated by two washing steps with 1x incubation buffer without SDS, enriched with 40 µl/ml 5% BSA and centrifugated at 4000 rpm for 2 min. Per reaction 50 µl bead suspension was used. After the last washing step, supernatant was removed completely and beads were resuspended in 25 µl per reaction. Then the immunoprecipitation mix was prepared according to Table 4-X. For the mix it was important to pipette the beads first, followed by the master-mix (see Table 4-IX), then the chromatin and last the antibody.

Reagent (Stock conc.)	**1x**
5% BSA	6 µl
25x PIC	12 µl
5x incubation buffer without SDS	36 µl
Water	Ad 148 µl

Table 4-IX. Chromatin IP master mix

Reagent (Stock conc.)	**1x**
Chromatin IP master mix	148 µl
Equilibrated beads	30 µl
Chromatin	120 µl
Antibody (1 µg/µl)	2 µl

Table 4-X. Volumes for IP

The immunoprecipitation mix was then rotated over-night in the cold room at 4°C. In parallel another 12 µl of each chromatin was aliquoted and rotated with the IP mixes overnight. This sample represents the input sample, containing 1:10 of the chromatin that was subjected to the immunoprecipitation. Furthermore, for each chromatin sample an IP with an isotype IgG control antibody was performed in parallel.

The next morning, beads were centrifuged at 4000 rpm for 2 min at 4°C and the supernatant was discarded. Hereby, only the specifically immunoprecipitated proteins and their cross-linked DNA was

retained. Next, the beads were washed on ice with 400 µl of each wash buffer – two times with washbuffer 1, one time with washbuffer 2, one time with washbuffer 3 and two times with washbuffer 4 (diluted 1:10 with water). After addition of the respective wash buffer, samples were inverted 4x4 times with small breaks in between, allowing the beads to settle. Then the beads were centrifuged at 4000 rpm for 2 min at 4°C. After the last wash step, supernatant was removed completely and beads were resuspended in 200 µl elution buffer. In parallel the input samples were mixed with 188 µl elution buffer. IP and input samples were then rotated for 20 min at RT. Next, they were centrifuged at maximum speed for 1 min at RT and the supernatant was transferred to fresh reaction tubes.

Next, decross-linking of protein and DNA was initiated by addition of 8 µl 5 M NaCl, followed by incubation in a shaker at 65°C for 4 h. Last, the co-immunoprecipitated DNA was purified using the Mini Elute kit (Qiagen) according to the manufacture's protocol. Elution was performed with 100 µl 1:10 diluted EB buffer and samples were stored at 4°C until further analysis by qRT-PCR (see 4.2.6.3).

4.4 Bioinformatic analyses of ChIP-seq data

In order to identify NF-Y binding sites within LTR12 sequences, publicly available ChIP-sequencing (ChIP-seq) data was retrieved and analyzed. Data was obtained for genomic DNA extracted from chromatin immunoprecipitation with specific antibodies against either NF-Y subunit alpha or beta [122]. First, NARROWPEAK-files were downloaded from the Gene Expression Omnibus website [123]. An overview of the downloaded files is shown in Table 4-XI. Next, these files were uploaded to the Galaxy/Cistrome platform, which provides multiple bioinformatic tools to analyze ChIP-Seq data [124].

Cell line	File name
K562	GSM935433_hg19_wgEncodeSydhTfbsK562NfyaStdPk.narrowPeak
	GSM935429_hg19_wgEncodeSydhTfbsK562NfybStdPk.narrowPeak
HeLa-S3	GSM935508_hg19_wgEncodeSydhTfbsHelas3NfyaIggrabPk.narrowPeak
	GSM935408_hg19_wgEncodeSydhTfbsHelas3NfybIggrabPk.narrowPeak
GM12878	GSM935506_hg19_wgEncodeSydhTfbsGm12878NfyaIggmusPk.narrowPeak
	GSM935507_hg19_wgEncodeSydhTfbsGm12878NfybIggmusPk.narrowPeak

Table 4-XI. Overview ChIP-seq data files

The information contained in the NARROWPEAK-files was then reduced by cutting columns c1, c2 and c3 as delimited by tab spaces. Next a bed-file containing information about the locations of LTR12 of interest was uploaded to the same platform (see Table 4-III). This bed-file contained 6 columns with information about chromosome, sequence start position, end position, name of adjacent gene, a

fictive score and the strand orientation (+ or -). Next, a VENN diagram was created for each cell line to identify the overlap between NF-Y binding sites and LTR12 locations. The respective command on the Galaxy/Cistrome platform can be found within the section “Integrative Analysis” and further “CORRELATION”. Interval 1 was selected as LTR12 locations, Interval 2 the NF-YA binding sites and interval 3 the NF-YB binding sites. The VENN diagram, however, provides only information about the total overlap, but not the involved genomic loci. Therefore, the tool “Intersect” was used to obtain information about the overlapping locations.

4.5 Statistical analysis

Results were analyzed for their statistical significance by the unpaired, two-tailed student’s t-test as provided by *Microsoft Excel*. A *p*-value below 0.05 indicated a significant difference between two data sets, e.g. inhibitor-treated samples compared to samples treated with the solvent of the inhibitor alone. All data sets were obtained in at least 3 independently performed experiments. Error bars are depicted as standard deviation (SD). To visualize *p*-values, asterisks were used:

* $p<0.05$

** $p<0.01$

*** $p<0.001$

5 Results

5.1 *TNFRSF10B* has previously unknown LTR12-driven isoforms

As we were especially interested in LTR12-driven gene transcripts that might be involved in cell death and therefore potentially influence the survival of transformed cells, TNFRSF10B was an interesting candidate. *TNFRSF10B* encodes for the protein death receptor 5. The gene *TNFRSF10B* is located on the minus strand of chromosome 8. A long terminal repeat of the HERV-9 family is inserted 757 bp upstream of the transcription start site of exon 1.

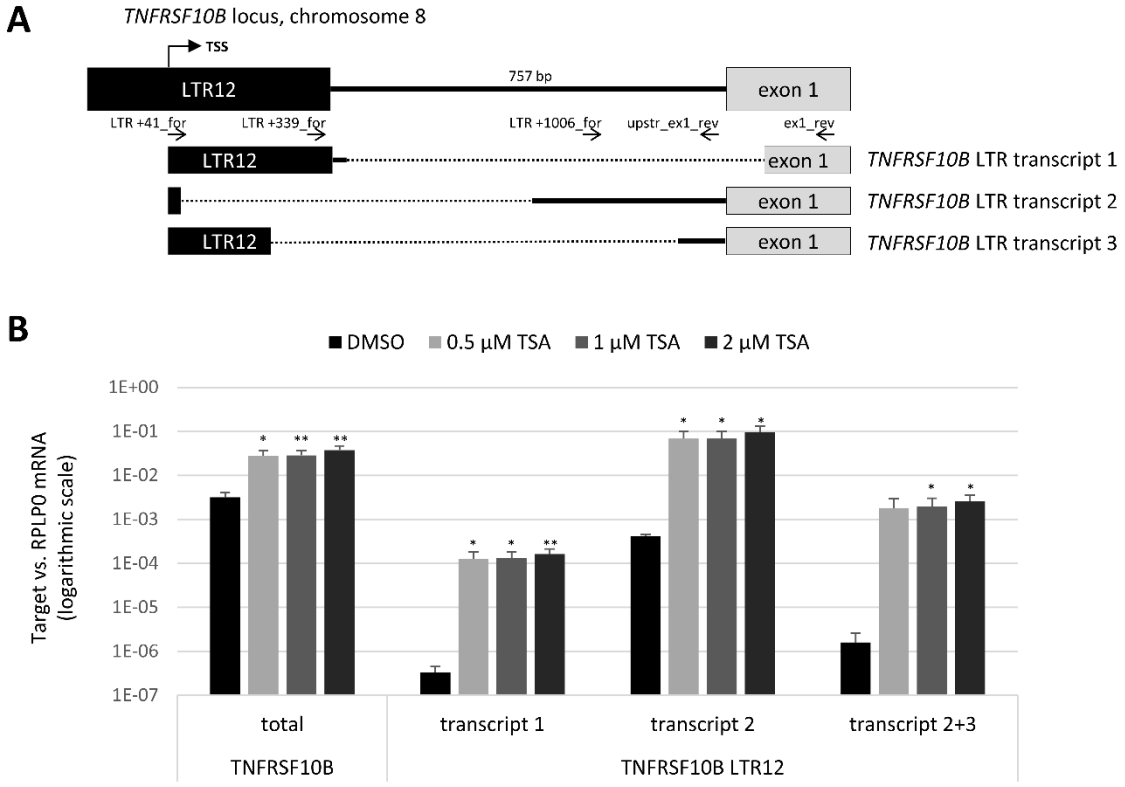

Figure 5-1. TNFRSF10B has previously unknown LTR12-driven isoforms

[A] Architecture of the TNFRSF10B gene locus on the reverse strand on chromosome 8. The newly identified LTR12 (black box) starts 757 bp upstream of the formerly known transcription start site of ENSEMBL transcript ENST00000276431 (light grey box). The transcription start site (TSS) within the LTR12 is shown with an arrow. Three transcripts originate from the LTR12 through alternative splicing (indicated by the dotted line). Primer locations of oligonucleotides to identify the different isoforms are shown. LTR transcript 1 is specifically amplified with LTR +339_for and ex1_rev; LTR transcript 2 with LTR +1006_for and ex1_rev; LTR transcripts 2+3 with LTR +41_for and upstr_ex1_rev. Translation of the newly identified transcripts results in the synthesis of the same protein as ENST00000276431. **[B]** GH cells (testicular cancer cell line) were treated with increasing concentrations of the HDAC inhibitor Trichostatin A (TSA) for 18 h followed by isolation of total RNA which was reverse transcribed into cDNA. Next, relative gene expression levels of the newly identified TNFRSF10B LTR transcripts were assessed by qRT-PCR. Treatment resulted in a significant increase for all three transcripts. mRNA levels were normalized to *RPLP0*. Control cells were treated with the TSA-solvent DMSO alone. Error bars represent SD (n=3). * = p<0.05, ** = p<0.01, *** = p<0.001; Transcripts were initially identified by Dr. Ulrike Beyer (Dept. of Molecular Oncology, UMG, Göttingen; currently MHH, Hannover). qPCR studies were conducted by Sonja Krönung (UMG, Göttingen).

5.1.1 Identification of three LTR-driven isoforms of *TNFRSF10B*

At least three different transcripts arise from the transcription start site within the LTR through alternative splicing (Figure 5-1A), as identified by RT-PCR. LTR transcript 1 is spliced from a splice donor site 31 bp downstream of the LTR12 onto an acceptor site 67 bp downstream of the previously known tss. The second LTR transcript is spliced 18 bp downstream of the LTR tss onto a second exon starting 373 bp upstream of the previously known tss. The third LTR transcript is spliced after 167 bp onto a second exon 92 bp upstream of the previously known tss. All three LTR transcripts contain the start codon ATG within exon 1 and result in translation of the same protein. The initial identification of the transcripts was done by Dr. Ulrike Beyer (Dept. of Molecular Oncology, UMG, Göttingen; currently MHH, Hannover). qPCR studies were conducted by Sonja Krönung (Dept. of Molecular Oncology, UMG, Göttingen).

5.1.2 Transcription of all three LTR-driven isoforms is induced by HDAC inhibitor treatment

TNFRSF10B transcription was previously shown to be upregulated in GH cells (testicular cancer cells) upon treatment with the HDAC inhibitor Trichostatin A (TSA) by microarray analysis (Table 2-I). Moreover, LTR-containing transcripts of *TNFRSF10B* were identified by 3'RACE followed by next generation sequencing (NGS) in TSA-treated GH cells and normal testis (Table 2-I). To verify these findings, GH cells were treated with increasing concentrations of TSA (0.5 µM, 1 µM and 2 µM) for 18 h after which total RNA was extracted and reverse transcribed into cDNA. Next, relative gene expression of the three newly identified TNFRSF10B LTR transcripts and TNFRSF10B total was analyzed by qRT-PCR (Figure 5-1B). For the assessment of the total level of TNFRSF10B transcription, primers were located in exon 3 and exon 4 of transcript ENST00000276431, thus including all known transcription start sites. Transcription of *TNFRSF10B* total was higher than of each LTR transcript in DMSO-treated cells. Treatment with TSA resulted in a significant increase in the level of total TNFRSF10B and all three LTR transcripts. However, the increase was more prominent for the LTR transcripts. Since transcription was overall highest for LTR transcript 2, it was representatively analyzed for *TNFRSF10B* LTR transcripts in the subsequent experiments.

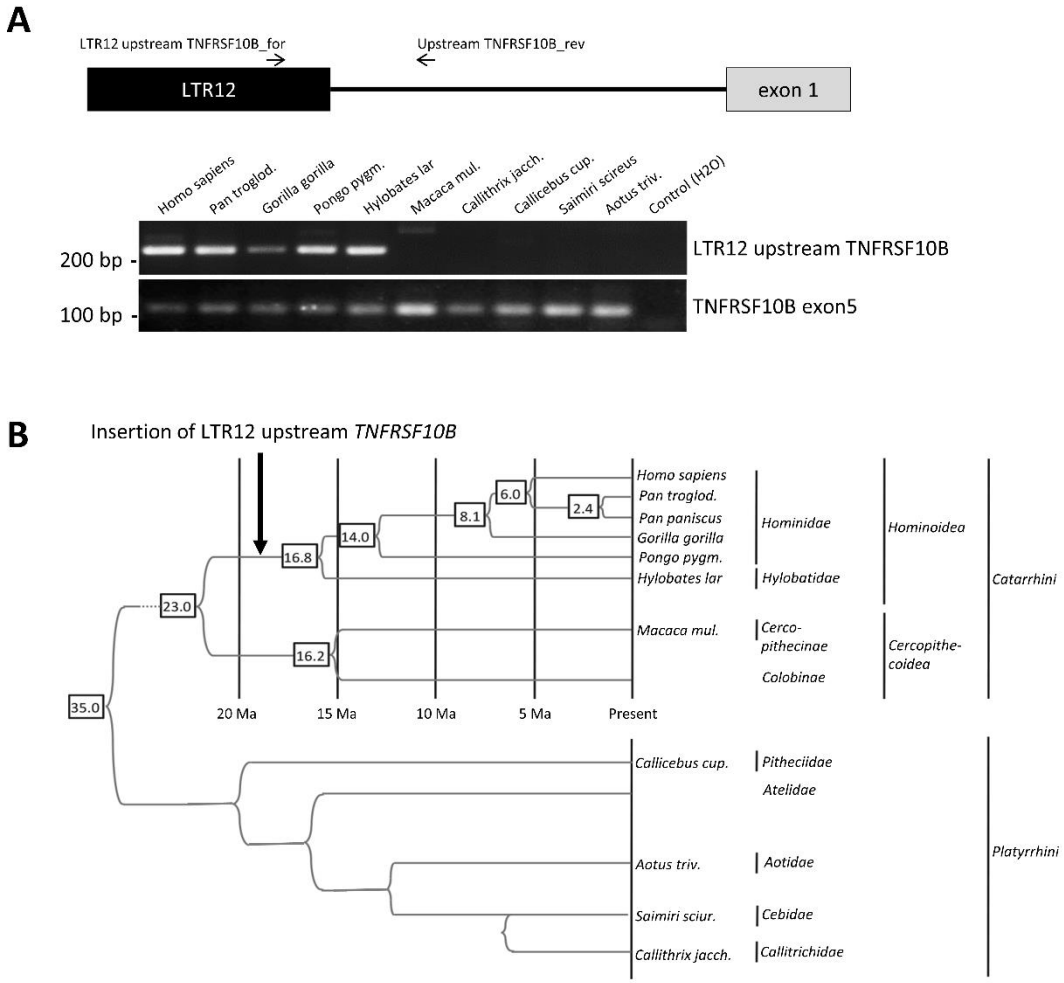

Figure 5-2. Insertion of LTR12 upstream TNFRSF10B occurred roughly 18 million years ago

[A] To determine the presence of LTR12 sequences upstream of TNFRSF10B in different species, a specific forward primer within LTR12 (LTR12 upstream TNFRSF10B_for) and a reverse primer upstream of exon 1 (Upstream TNFRSF10B_rev) were used. Genomic DNA from different species was subjected to PCR analysis. LTR12-containing transcripts were only amplified in genomic DNA from homo sapiens, pan troglodytes, gorilla gorilla, pongo pygmaeus and hylobates. **[B]** Insertion of the LTR12 upstream of TNFRSF10B occured in higher primates after the split of Hominoidea from Cercopithecoidea roughly 18 million years ago.

5.2 Insertion of LTR12 upstream *TNFRSF10B* occurred roughly 18 million years ago

To determine the presence of LTR12 sequences upstream of *TNFRSF10B*, a specific forward primer within LTR12 (LTR12 upstream TNFRSF10B_for) and a reverse primer upstream of exon 1 (Upstream TNFRSF10B_rev) were used. A schematic representation of the primer binding sites is shown in Figure 5-2A, upper panel. Primer sequences are given in Table 3-II. Genomic DNA from different primates was subjected to PCR analysis. Specifically amplified products were subsequently visualized by agarose gel electrophoresis. LTR12-containing transcripts were only amplified in genomic DNA from human *(homo sapiens),* chimpanzee *(pan troglodytes),* gorilla *(gorilla gorilla),* orangutan *(pongo pygmaeus)* and

gibbon *(hylobates)* (Figure 5-2A, lower panel). These results were also obtained upon aligning genomic sequences of various primate species using the Clustal algorithm (Figure 5-3), strongly indicating that insertion of the LTR12 upstream *TNFRSF10B* occurred in higher primates after the split of Hominoidea from Cercopithecoidea roughly 18 million years ago [125] (Figure 5-2B).

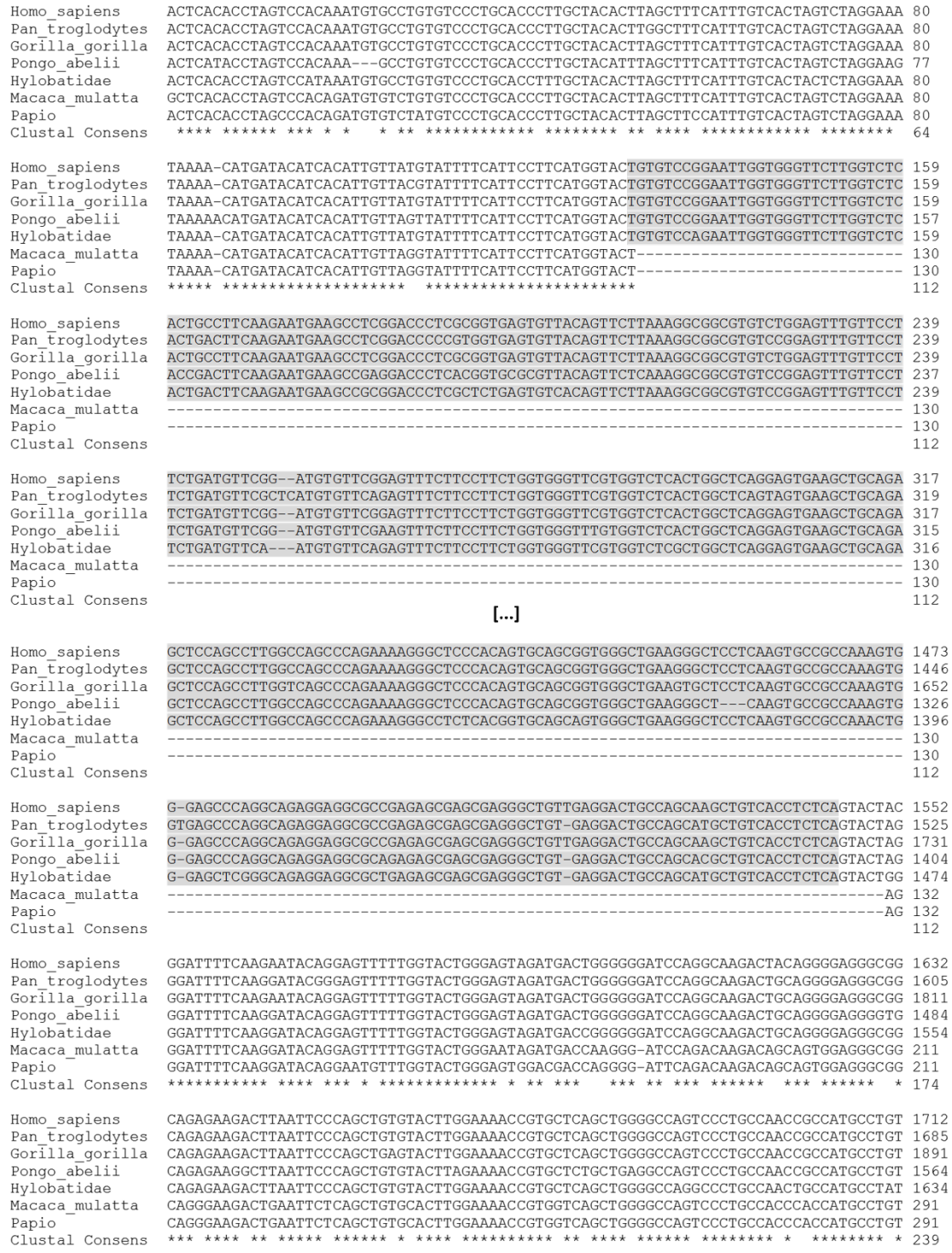

Figure 5-3. Insertion of LTR12 upstream *TNFRSF10B* in primates

Aligning genomic sequences of various primate species using the Clustal algorithm reveals the presence of LTR12 in homo sapiens to *hylobates*. The LTR12 sequence stained in light grey. However, it is not present in *macaca mulatta* and *papio*. Genomic sequences for all species were retrieved from the UCSC genome browser.

5.3 TNFRSF10B expression is high in testis and reduced in testicular cancer

5.3.1 TNFRSF10B transcripts are ubiquitously expressed in different human tissues, but differ in their use of transcription start sites

To gain insight into usage of the different transcription start sites for *TNFRSF10B,* we quantified its transcription in different human tissues. Therefore, a panel of RNA from normal human tissues (Ambion) was reverse transcribed to cDNA and analyzed by qRT-PCR. First, we quantified transcription of TNFRSF10B in total (Figure 5-4A) with primers located in exon 3 and 4. TNFRSF10B total mRNA was ubiquitously expressed in all tissues. Its transcription was highest in the small intestine. Next, we quantified transcription of TNFRSF10B LTR12 transcript 2 (Figure 5-4B). Transcription of the LTR-driven transcript was largely confined to the testicular tissue and the small intestine.

5.3.2 Protein levels of TNFRSF10B are reduced in testicular tumor cells in comparison to normal testis

Since GTAp63 is also specifically expressed in the human testis and its expression is lost in transformed testis tissue [90] (see 2.3.1), we were interested if a similar pattern existed for TNFRSF10B. We retrieved immunohistochemistry staining information from the Human Protein Atlas database. Staining intensities for TNFRSF10B were strong in normal testis tissues (Table 5-I). However, the staining intensity was consistently weaker in different testicular tumor cells. This indicates that protein levels of TNFRSF10B are indeed reduced upon transformation of testicular tissue.

Tissue, cell type	Patient ID	Age	Intensity	Quantity
Normal tissue, cells in seminiferous ducts	2254	26	Strong	>75%
Normal tissue, cells in seminiferous ducts	2435	46	Strong	>75%
Normal tissue, cells in seminiferous ducts	3355	56	Strong	>75%
Embryonal carcinoma, tumor cells	2071	26	Weak	<25%
Embryonal carcinoma, tumor cells	1740	36	Weak	>75%
Embryonal carcinoma, tumor cells	3627	25	Weak	25-75%
Seminoma, tumor cells	2721	22	Weak	<25%
Seminoma, tumor cells	2558	65	Weak	>75%
Seminoma, tumor cells	1700	41	Moderate	>75%
Seminoma, tumor cells	1777	43	Moderate	>75%
Seminoma, tumor cells	1818	71	Moderate	>75%
Mixed germ cell tumor, tumor cells	550	43	Negative	Negative
Mixed germ cell tumor, tumor cells	342	51	Weak	<25%

Table 5-I. TNFRSF10B protein expression is weaker in testicular cancer cells than in normal human testis

To compare the protein level of TNFRSF10B in normal and transformed tissue cells, staining intensities were obtained from the Human Protein Atlas database (www.proteinatlas.org). The immunohistochemistry stainings were classified as strong, moderate, weak or negative. The fraction of positive cells is given in the last column as „quantity“.

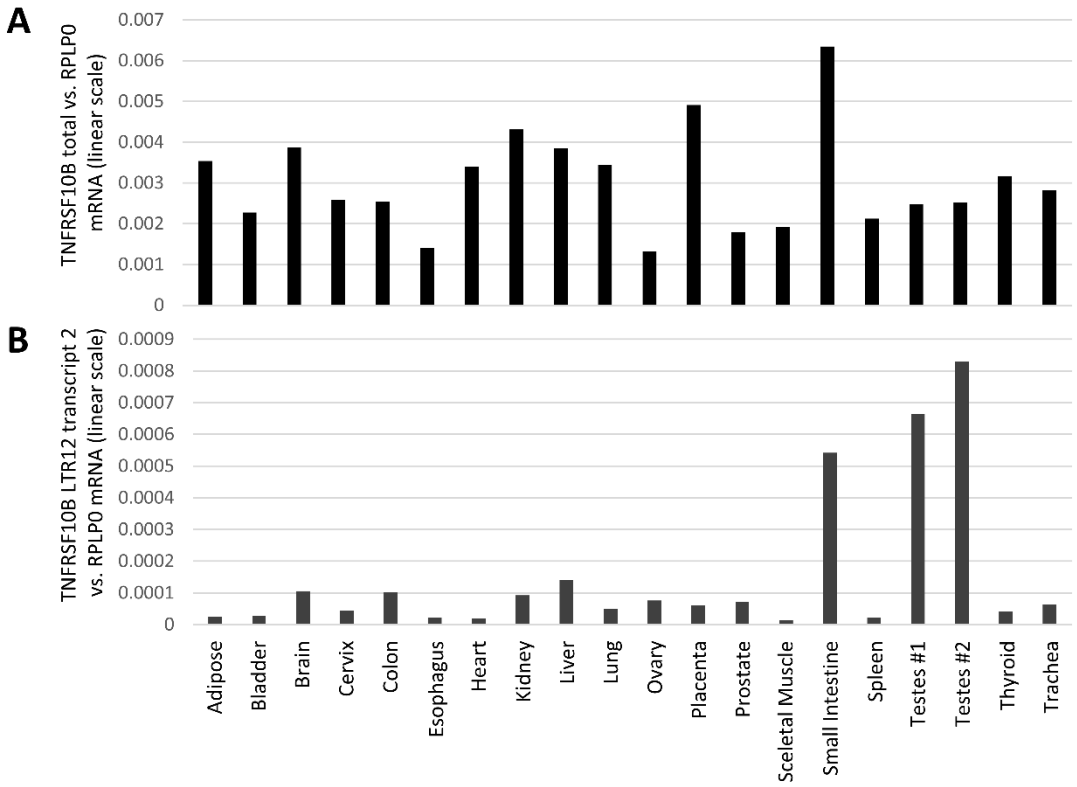

Figure 5-4. Examination of TNFRSF10B expression in normal human tissues

Transcription of TNFRSF10B was quantified in a panel of RNA samples from normal human tissues (Ambion) by qRT-PCR. Depicted is **[A]** the transcription of TNFRSF10B total and **[B]** transcription of TNFRSF10B LTR12 transcript 2. While total TNFRSF10B mRNA was ubiquitously expressed in all tissues, the LTR-driven transcript was largely confined to testicular tissue and the small intestine. mRNA levels were normalized to *RPLP0.*

5.4 Combinatorial treatment with TRAIL and TSA enhances apoptosis in testicular cancer cells

We next sought to determine whether the strong induction of LTR-driven TNFRSF10B expression influences the survival of transformed cells. We induced LTR12 transcription in GH cells by treatment with the HDAC inhibitor TSA. In parallel, we treated cells with TNFRSF10B's ligand TRAIL and combinations thereof. After treatment, the cells were harvested and total protein was isolated. In another set of experiments, the incubation was continued over five consecutive days and cell growth was assessed.

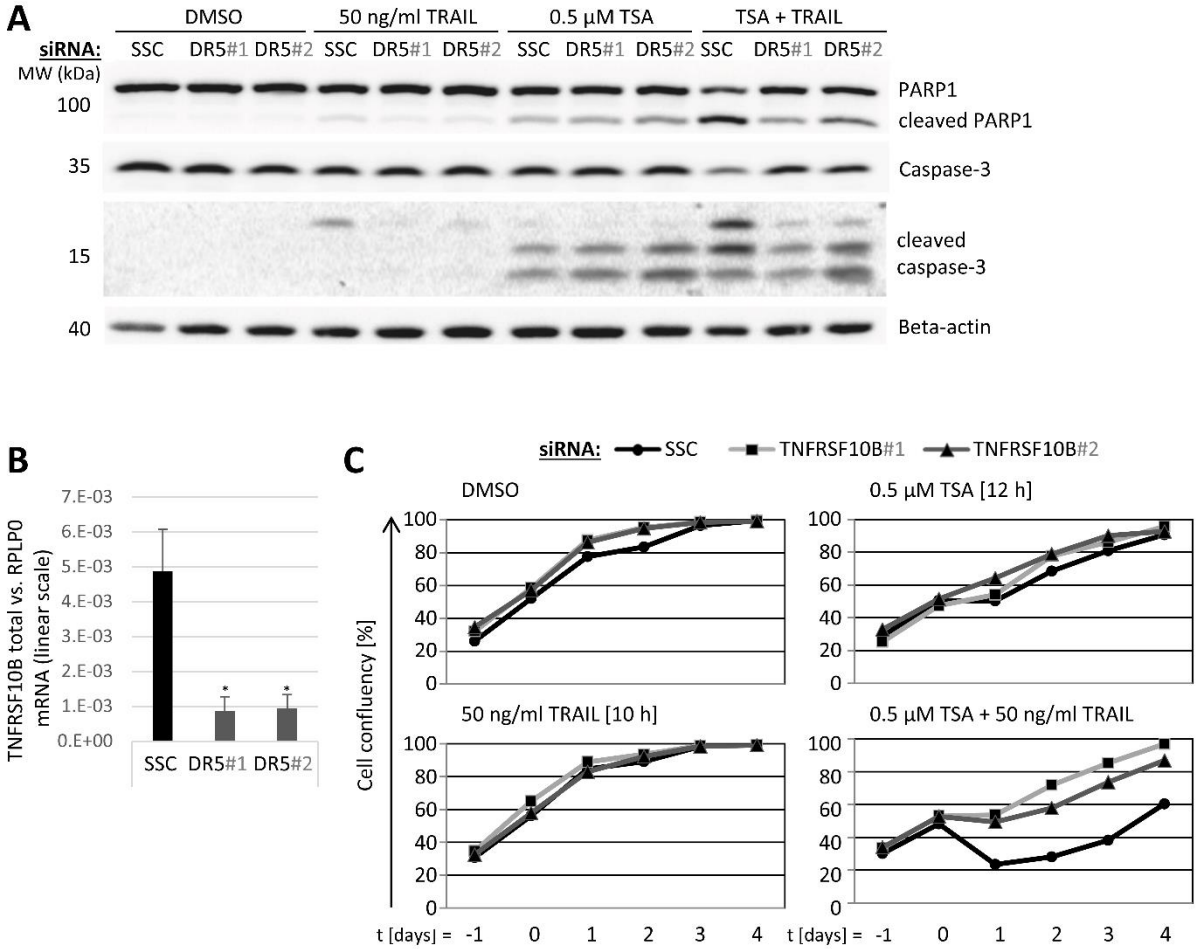

Figure 5-5. Combinatorial treatment with TRAIL and TSA enhances apoptosis in testicular cancer cells

GH cells were treated with either 0.5 µM TSA or 50 ng/ml TRAIL or a combination thereof for 12 h or 10 h. Cells treated with DMSO, the solvent of TSA, were used as controls. To assess the influence of Death Receptor 5 (TNFRSF10B) on cell viability, it was depleted by transfection with two different siRNAs (TNFRSF10B#1/DR5#1 and TNFRSF10B#2/DR5#2) 24 h prior to treatment. **[A]** + **[B]** After treatment, cells were harvested and **[A]** total protein was isolated and separated by SDS-PAGE followed by immunoblotting with specific antibodies against poly-(ADP-ribose)-polymerase 1 (PARP1), caspase-3, cleaved caspase-3 and beta-actin. Upon programmed cell death, caspase-3 is activated by cleavage and in turn cleaves various substrates including PARP1. Treatment with TRAIL or TSA alone results in cleaved caspase-3, however, the effects are stronger upon combinatorial treatment with both substances [lane 10]. Depletion of TNFRSF10B reduces this additive effect [lane 11 + 12]. **[B]** Total RNA was isolated and reverse transcribed into cDNA. Next relative gene expression of TNFRSF10B was assessed by qRT-PCR to monitor the efficiency of its depletion. mRNA levels were normalized to *RPLP0*. Error bars represent SD (n=3). * = p<0.05, ** = p<0.01, *** = p<0.001. **[C]** Treatment was terminated by replacing the culture medium and cell confluency was quantified (t=0). Then cell confluency was monitored consecutively for another 4 days. Prior to each measurement, culture medium was renewed to remove dead cells. Treatment with TRAIL alone did not affect cell growth. However, treatment with TSA alone led to a slight reduction in cell growth. Combinatorial treatment of cells transfected with scramble control siRNA, with TSA and TRAIL, resulted in strongly reduced growth. This growth defect was not observed in cells depleted of TNFRSF10B.

5.4.1 Combinatorial treatment with TRAIL and TSA diminishes cell growth by enhancing apoptosis in testicular cancer cells

After separation by SDS-PAGE, proteins were detected with specific antibodies against poly-(ADP-ribose)-polymerase 1 (PARP1), caspase-3, cleaved caspase-3 and beta-actin. Upon programmed cell death, caspase-3 is activated by cleavage and in turn cleaves various substrates including PARP1 [126, 127]. Treatment with DMSO alone did not result in apoptosis (Figure 5-5A, lane 1). Treatment with 50 ng/ml TRAIL for 10 h resulted in cleavage of caspase-3 and PARP1 (Figure 5-5A, lane 4). These effects were intensified upon treatment with 0.5 µM TSA for 12 h (Figure 5-5A, lane 7). However, combinatorial treatment with both substances enhanced apoptosis as indicated by diminished levels of unprocessed caspase-3 and PARP1 (Figure 5-5A, lane 10).

In addition to staining for apoptosis markers, cell growth was assessed by cell confluency measurements. Here, treatment with TSA and/or TRAIL was terminated by replacing the culture medium and cell confluency was quantified (t=0). Cell confluency was then monitored consecutively for another four days. Prior to each measurement, culture medium was renewed to remove dead cells. Upon treatment with DMSO, control cells reached 80% confluency one day after the treatment was ended (Figure 5-5C, upper left panel, black curve). The same effect was observed for treatment with 50 ng/ml TRAIL for 10 h (Figure 5-5C, lower left panel, black curve). Cells that were treated with 0.5 µM TSA for 12 h only reached 80% confluency after three days (Figure 5-5C, upper right panel, black curve). However, upon combined treatment with TSA and TRAIL, cells did not reach 80% confluency within the monitored time period (Figure 5-5C, lower right panel, black curve) indicating that the growth of these cells was severely defective.

In conclusion, the addition of TRAIL aggravates TSA-induced cell death. This at least suggests that TSA-induced DR5 may transmit the death signal from TRAIL.

5.4.2 Depletion of TNFRSF10B by siRNA rescues the detrimental effects of combined treatment with TSA and TRAIL on cell survival

To assess the influence of Death Receptor 5 (TNFRSF10B) on cell viability, it was depleted by transfection with two different siRNAs (TNFRSF10B#1/DR5#1 and TNFRSF10B#2/DR5#2) 24 h prior to treatment. Total RNA was isolated and reverse transcribed into cDNA. Next, relative gene expression of TNFRSF10B was assessed by qRT-PCR to monitor the efficiency of its depletion (Figure 5-5B). Depletion of TNFRSF10B reduced the additive effects of combined treatment with TSA and TRAIL (Figure 5-5A, lane 11+12).

Moreover, the growth defect upon treatment with TSA and TRAIL, observed in cells transfected with scramble control siRNA (5.4.1), was not observed in cells depleted of TNFRSF10B (Figure 5-5C, lower right panel, grey curves).

5.5 HDAC inhibitors from different chemical classes induce LTR12 transcription

All observations regarding the induction of LTR12-driven gene transcription so far were based on the use of TSA. This hydroxamate HDAC inhibitor binds Zn^{2+} which is an important cofactor for the eleven zinc-dependent HDACs. To examine if the observed effects are restricted to TSA, we tested a panel of HDAC inhibitors from different chemical classes for possible influences on LTR12 promoter activity (see Table 3-XIV).

5.5.1 Treatment with HDAC inhibitors from different chemical classes induces LTR12-driven gene expression in testicular cancer cells

GH cells were treated with increasing concentrations of HDAC inhibitors (0.5 µM, 2 µM, 8 µM) for 18 h. Next, total RNA was isolated and reverse transcribed into cDNA. Relative gene expression was then assessed by qRT-PCR. Aside from TSA, the hydroxamic acid histone deacetylase inhibitors Droxinostat and PCI-34051 were tested. Moreover, benzamide histone deacetylase inhibitors Entinostat, Mocetinostat and Tubastatin A hydrochloride were studied. Transcription of GTAp63 was significantly increased upon treatment with Trichostatin A, Entinostat, Mocetinostat and Tubastatin A (Figure 5-6A). The same observation was made for the LTR12-driven transcript of TNFRSF10B (Figure 5-6B). Entinostat and Mocetinostat are selective for HDAC1, HDAC2 and HDAC3. Tubastatin A is a selective inhibitor of HDAC6 (IC50 15 nM). However, Droxinostat that selectively inhibits HDAC3, 6 and also 8 does not show an increase in LTR12-driven gene transcription. Thus, inhibition of HDACs 1-3 appears to make the largest contribution to the activation of LTR12.

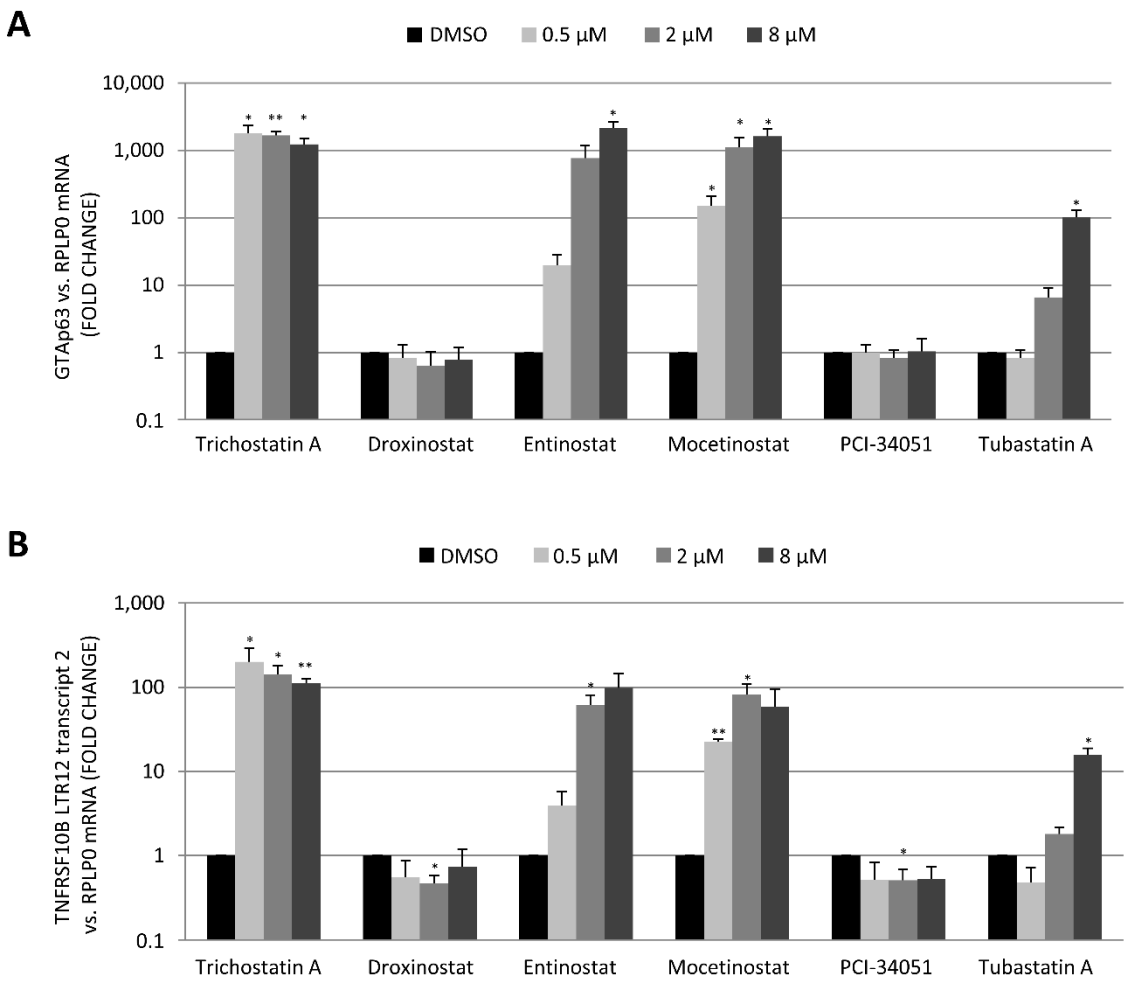

Figure 5-6. HDAC inhibitors from different chemical classes induce LTR12 transcription

GH cells were treated with HDAC inhibitors from different chemical classes. Cells were treated with increasing concentrations of each inhibitor (0.5 µM, 2 µM, 8 µM) for 18 h. After this incubation time, total RNA was isolated and reversely transcribed into cDNA. Next, relative gene expression was assessed by qRT-PCR. [A] The transcription of GTAp63 and [B] transcription of TNFRSF10B LTR transcript 2 is depicted. A significant increase in transcription of the LTR12-driven isoforms of TP63 and TNFRSF10B was observed upon treatment with Trichostatin A, Entinostat, Mocetinostat and Tubastatin A. mRNA levels were normalized to *RPLP0* and are shown as a fold change of DMSO-treated control cells. Error bars represent SD (n=3). * = $p<0.05$, ** = $p<0.01$, *** = $p<0.001$.

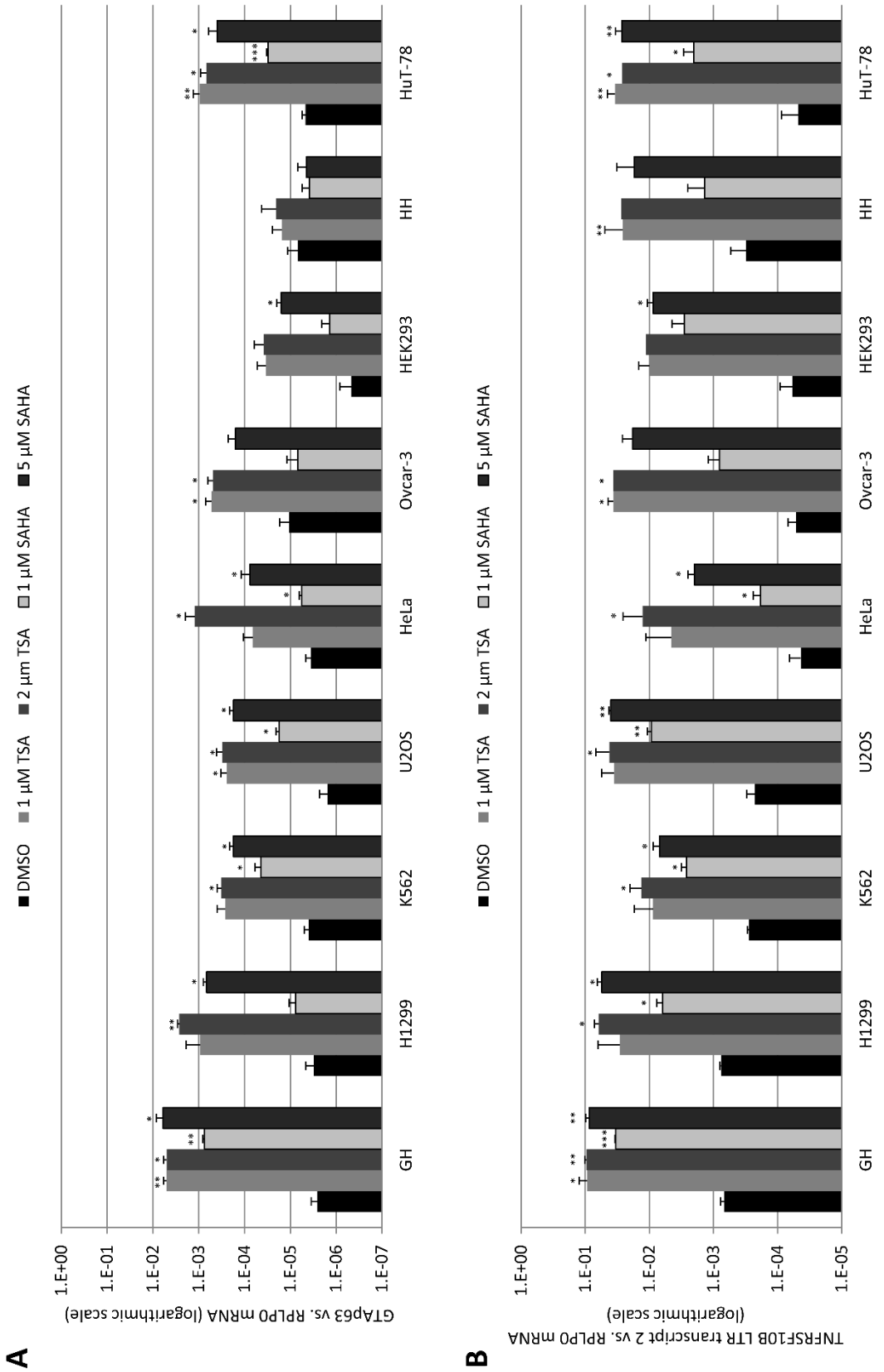

Figure 5-7. Treatment with HDAC inhibitors induces transcription of LTR12 in human cell lines derived from different tissues

Human cell lines derived from different tissues were treated with with HDAC inhibitors Trichostatin A (TSA) or suberoylanilide hydroxamic acid (SAHA). Cells were treated with increasing concentrations of

each inhibitor (1 µM, 2 µM for TSA and 1 µM, 5 µM for SAHA) for 18 h. After this incubation time, total RNA was isolated and reverse transcribed into cDNA. Next, relative gene expression was assessed by qRT-PCR. The transcription levels of LTR-driven isoforms of **[A]** GTAp63 and **[B]** TNFRSF10B LTR transcript 2 are depicted. Except for HH cells, a significant increase in transcription for both LTR-driven transcripts was observed in all tested cell lines. mRNA levels were normalized to *RPLP0*. Cells treated with DMSO were used as controls. The tested cell lines were GH (testicular cancer cell line), H1299 (lung carcinoma cell line), K562 (leukemia cell line), U2OS (osteosarcoma cell line), HeLa (cervical carcinoma cell line), Ovcar-3 (ovarian carcinoma cell line), HEK293 (embryonic kidney cell line), HH and HuT-78 (cutaneous T-cell lymphoma cell line). Error bars represent SD (n=3). * = $p<0.05$, ** = $p<0.01$, *** = $p<0.001$.

5.6 Treatment with HDAC inhibitors induces transcription of LTR12 in human cell lines derived from different tissues

As previously stated, we observed that LTR transcription is present in normal testis and is lost in testicular cancer cells [90]. However, treatment with HDAC inhibitors from different chemical classes can restore the transcription of LTR12-driven genes. This led us to hypothesize that the mechanism behind the de-repression of LTR12 transcription might also be accessible in cell lines derived from other tissues than testis.

Therefore, we treated a panel of human cell lines with HDAC inhibitors increasing concentrations of TSA (1 µM, 2 µM) and suberoylanilide hydroxamic acid (SAHA) (1 µM, 5 µM). After 18 h, total RNA was isolated and reverse transcribed into cDNA. Next relative gene expression was assessed by qRT-PCR. Except for HH cells, a significant increase in the transcription of both GTAp63 (Figure 5-7A) and LTR-driven *TNFRSF10B* (Figure 5-7B) was observed in all cell lines tested which includes H1299 (lung carcinoma cell line), K562 (leukemia cell line), U2OS (osteosarcoma cell line), HeLa (cervical carcinoma cell line), Ovcar-3 (ovarian carcinoma cell line), HEK293 (embryonic kidney cell line), and HuT-78 cells (cutaneous T-cell lymphoma cell line). In HH cells, which were derived from a cutaneous T-cell lymphoma, only LTR12-driven gene transcription of TNFRSF10B was significantly increased.

These results show that LTR12 promoter activity can be induced by treatment with HDAC inhibitors in cancer and non-cancerous cell lines derived from a broad variety of tissues.

5.7 HDAC inhibitors do not induce the transcription of all endogenous retroviral elements in the human genome

Since HDAC inhibitors can promote LTR12 promoter activity in cells derived from different tissues, we wanted to understand if this regulation was specific for the LTR12 promoter or a hallmark for all endogenous retroviral promoter elements in the human genome.

5.7.1 All tested LTR12-driven genes are responsive to HDAC inhibitor treatment

Initially, we designed primers for four cellular genes whose expression was shown to be partly regulated by an adjacent LTR12 (see 2.3) [27]. If possible, these primers were located exclusively in the LTR-driven isoforms. However, for *ADH1C* and *GBP5,* only total gene expression could be assessed.
GH cells and U2OS cells were then treated with increasing concentrations of TSA and SAHA. After 18 h, total RNA was extracted and reverse transcribed into cDNA. Next, gene expression of the four previously described LTR12-driven transcripts as well as GTAp63 and TNFRSF10B LTR12 transcript 2 was assessed by qRT-PCR. A significant increase for all six LTR12-driven transcripts was observed in GH cells (Figure 5-8A) and U2OS cells (Figure 5-9A). As compared to DMSO-treated control cells, the increase differed between the individual transcripts. Treatment of GH cells with 1 µM TSA increased ADH1C transcription 12-fold, GBP5 transcription 86-fold, LTR12-driven SEMA4D transcription 161-fold, TNFRSF10B 136-fold, GTAp63 2,050-fold, and DHRS2 up to 4,637-fold. Hence, LTR12 functions as a TSA-responsive promoter regardless of its integration site.

5.7.2 LTR-driven isoforms from different HERV families are not globally induced by HDAC inhibitor treatment

Next, we assessed the transcription of cellular genes driven by LTRs from ERV families other than HERV-9 and envelope genes of endogenous retroviruses HERV-K and HERV-W. Transcription of the MaLR-driven isoform of *IL2RB* and HERV-H LTR-driven *GSDMB* was increased upon treatment with TSA and SAHA in both cell lines, but less-than-tenfold (Figure 5-8B, Figure 5-9B). Transcription levels of the HERV-E LTR-driven isoform of *APOC1*, HERV-H LTR-driven isoform of *DNAJC15*, and also the HERV-K *envelope* transcript were decreased. Transcription of the HERV-W *envelope* was slightly increased in GH cells (up to 2.5-fold), and decreased in U2OS cells (down to 53% of transcription in DMSO-treated cells). Overall, endogenous retroviral promoter elements other than HERV-9 were not activated by HDAC inhibitor treatment to an extent that would be comparable to LTR12. We conclude that HDAC inhibitor treatment does not lead to a de-repression of ERV transcription in general.

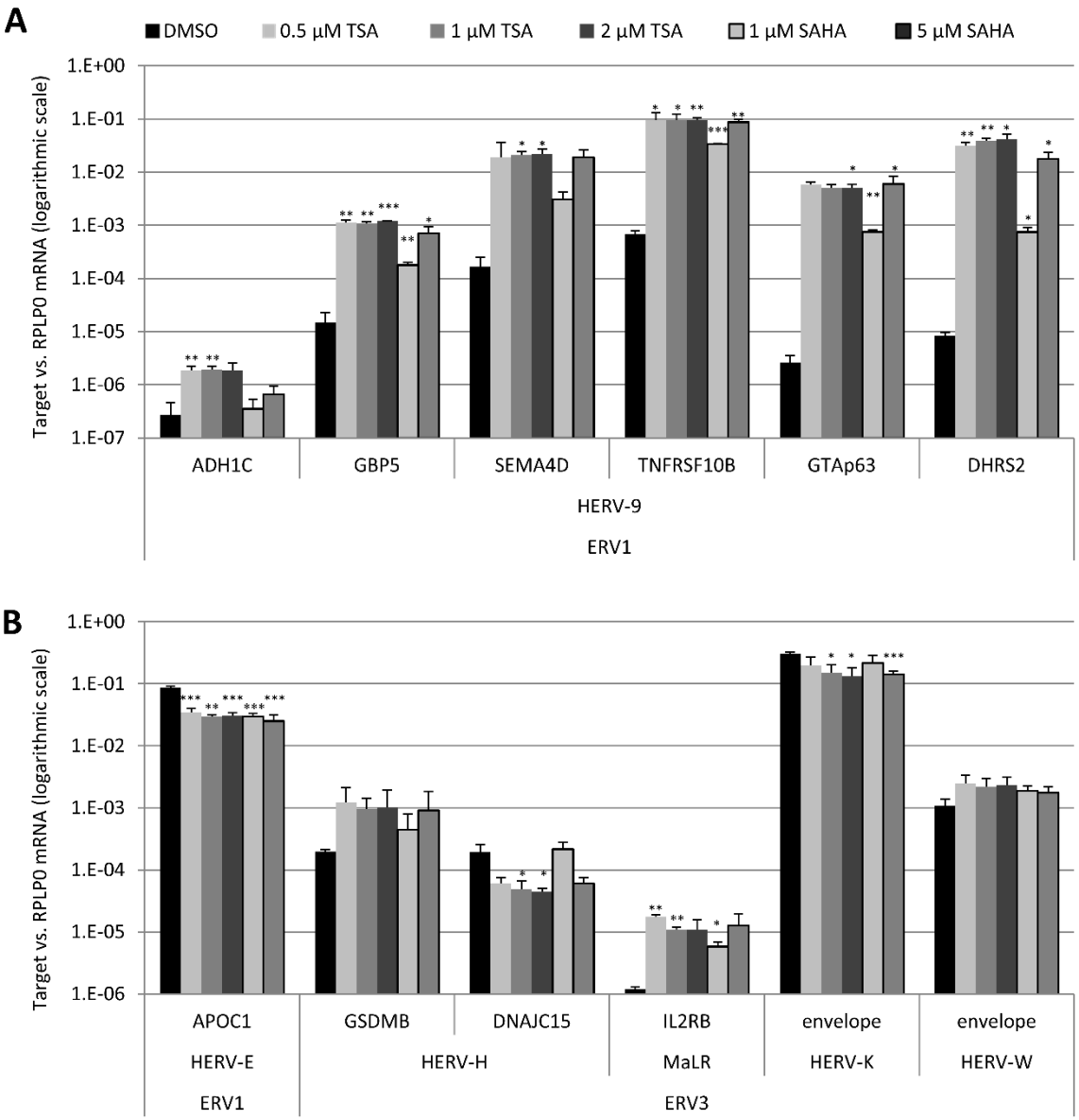

Figure 5-8. HDAC inhibitors do not induce the transcription of all endogenous retroviral elements

GH cells were treated with HDAC inhibitors Trichostatin A (TSA) or suberoylanilide hydroxamic acid (SAHA). Cells were treated with increasing concentrations of each inhibitor (0.5 µM, 1 µM, 2 µM for TSA and 1 µM, 5 µM for SAHA) for 18 h. After this incubation time, total RNA was isolated and reverse transcribed into cDNA. Next, relative gene expression was assessed by qRT-PCR. The transcription levels of **[A]** LTR12-driven isoforms of different cellular genes and, **[B]** cellular genes driven by LTRs from other ERV families and envelope genes of endogenous retroviruses HERV-K and HERV-W are depicted. A significant increase in the transcription of the LTR-driven isoforms was observed for all 6 cellular genes driven by an LTR12 (HERV-9 LTR). Transcription of the MaLR-driven isoform of IL2RB was also significantly increased upon treatment with TSA and SAHA. Transcription of the HERV-E LTR-driven isoform of APOC1, HERV-H LTR-driven isoform of DNAJC15 and also the HERV-K envelope transcript was significantly decreased. mRNA levels were normalized to *RPLP0*. Cells treated with DMSO, the solvent of TSA and SAHA, were used as controls. Error bars represent SD (n=3). * = $p<0.05$, ** = $p<0.01$, *** = $p<0.001$.

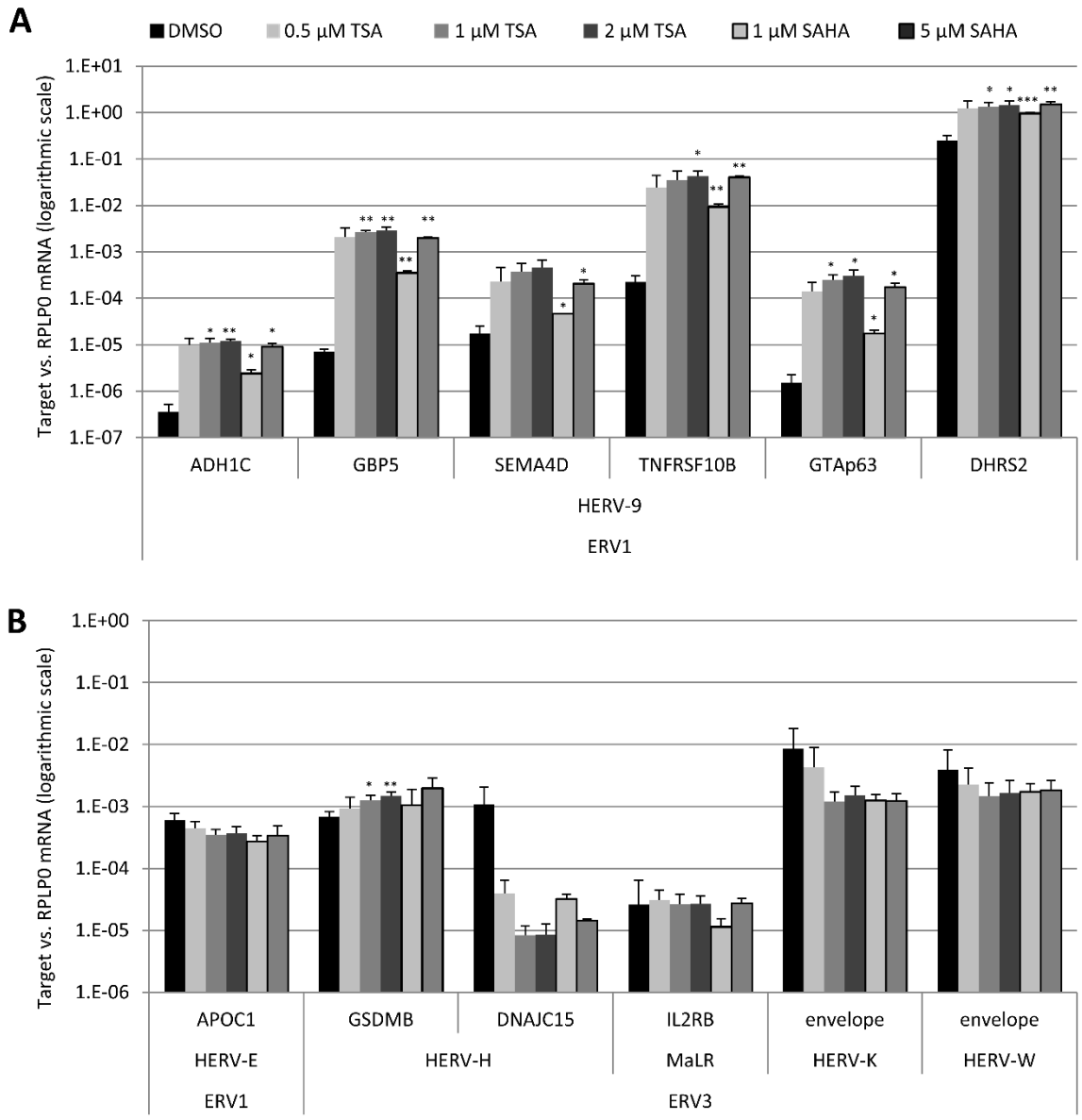

Figure 5-9. HDAC inhibitors do not induce the transcription of all endogenous retroviral elements

U2OS cells were treated with HDAC inhibitors Trichostatin A (TSA) or suberoylanilide hydroxamic acid (SAHA). Cells were treated with increasing concentrations of each inhibitor (0.5 µM, 1 µM, 2 µM for TSA and 1 µM, 5 µM for SAHA) for 18 h. After this incubation time, total RNA was isolated and reverse transcribed into cDNA. Next, relative gene expression was assessed by qRT-PCR. The transcription of [A] LTR12-driven isoforms of different cellular genes and [B] cellular genes driven by LTRs from other ERV families and envelope genes of endogenous retroviruses HERV-K and HERV-W is depicted. A significant increase in transcription of the LTR-driven isoforms was observed for all 6 cellular genes driven by an LTR12 (HERV-9 LTR). Transcription of the HERV-H-driven isoform of GSDMB was also significantly increased upon treatment with TSA. mRNA levels were normalized to *RPLP0.* Cells treated with DMSO, the solvent of TSA and SAHA, were used as controls. Error bars represent SD (n=3). * = $p<0.05$, ** = $p<0.01$, *** = $p<0.001$.

5.8 Depletion of various HDAC isoforms does not lead to a strong induction of LTR12 transcription

Since treatment with various HDAC inhibitors resulted in the activation of the LTR12 promoter, we sought to determine which HDAC isoform was primarily involved in this regulation. Since TSA inhibits only zinc-dependent HDAC isoforms, we focused on those.

5.8.1 HDAC isoforms 1, 2, 3 and 8 are most abundantly expressed in the cell lines used in this study

First, we determined the expression level of all eleven zinc-dependent HDAC isoforms in the cell lines we used. Total RNA from GH cells and U2OS cells was isolated, reverse transcribed into cDNA and then expression of all isoforms was quantified by qRT-PCR. In both cell lines, HDAC isoforms 1, 2 and 3 are most abundantly expressed, followed by HDAC8 (Figure 5-10A).

5.8.2 Depletion of the most abundantly expressed HDAC isoforms alone and in different combinations has only minor effects on LTR12 transcription

Aside from TSA, the HDAC inhibitors Entinostat and Mocetinostat led to the strongest increase in LTR12 transcription (Figure 5-6). Entinostat and Mocetinostat are rather selective inhibitors for HDAC isoforms 1, 2 and 3. In order to determine if HDAC1, HDAC2 and HDAC3 are the key enzymes for LTR12 regulation, we depleted them in U2OS cells by siRNA. Furthermore, combinations with HDAC8 were also tested. Total RNA and protein was isolated 96 h after the initial siRNA transfection (see 4.1.3). Massive cell loss was observed upon depletion of HDAC3. RNA was reverse transcribed into cDNA and relative gene expression was quantified by qRT-PCR. Transcription of GTAp63 was increased up to 4-fold upon combinatorial depletion of HDAC1+2, up to 3-fold upon depletion of HDAC1+2+3 and over 6-fold upon depletion of HDAC1+2+8 (Figure 5-10B, upper left panel). Transcription of the LTR12-driven TNFRSF10B isoform was not induced in a similar pattern. Depletion of HDAC3 alone and in combination with HDAC1 led to a 3-fold increase in transcriptional activity. Combined depletion of HDAC2+3, HDAC1+2+3 and HDAC1+2+8 also resulted in a slight induction (Figure 5-10B, upper right panel). Efficient silencing was shown at the mRNA level (Figure 5-10B, lower panel) as well as protein level for HDAC1+2 (Figure 5-10C). While treatment with HDAC inhibitors resulted in an over 200-fold increase in transcription of LTR12-driven *TP63* (GTAP63) and *TNFRSF10B* (Figure 5-6), depletion of the most abundantly expressed HDAC isoforms did not mimic these effects (Figure 5-10B).

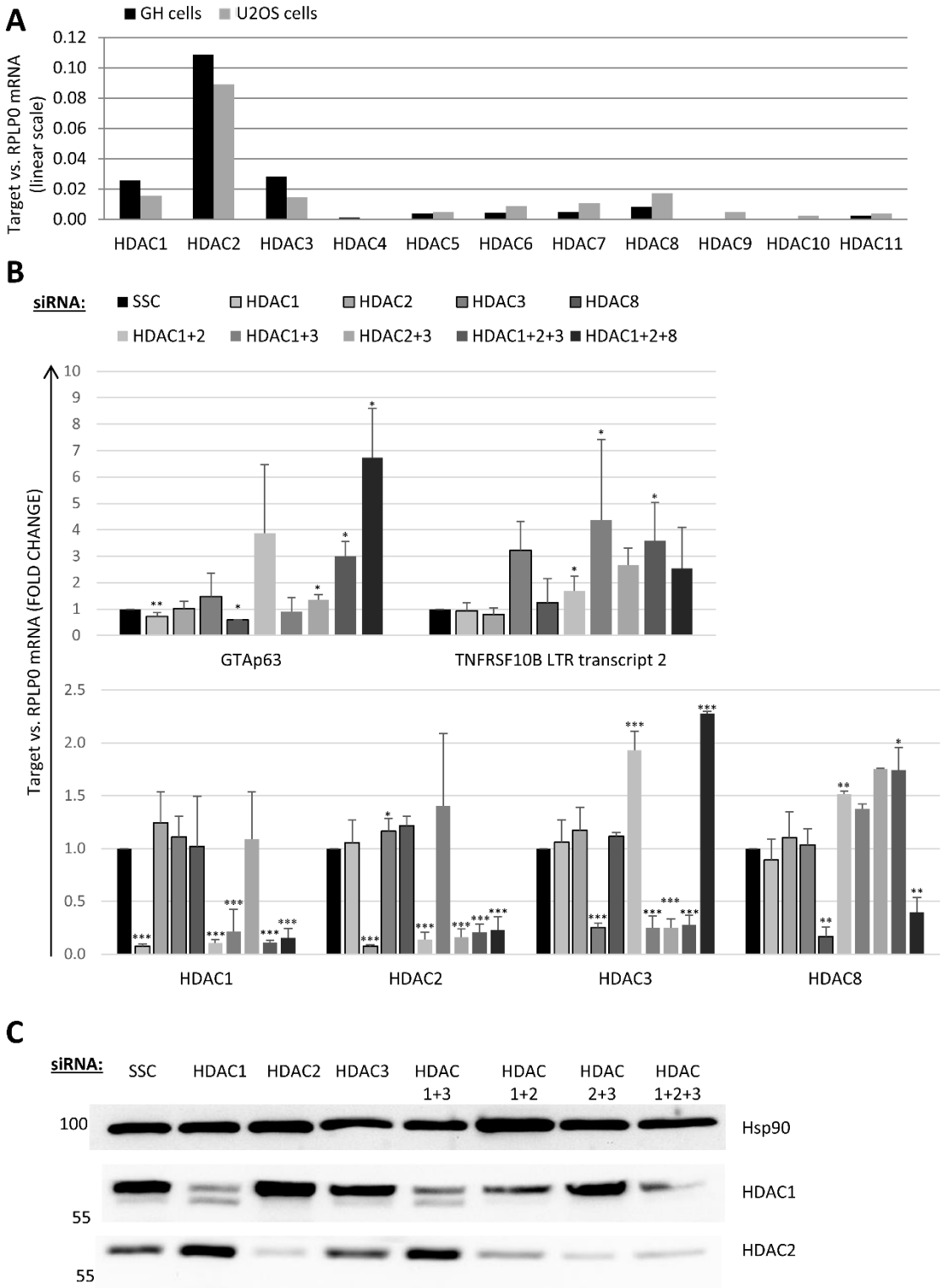

Figure 5-10. Depletion of various HDAC isoforms does not lead to a strong induction of LTR12 transcription

[A] Total RNA from GH cells and U2OS cells was isolated, reverse transcribed into cDNA and expression of the 11 zinc-finger-dependent HDAC isoforms quantified by qRT-PCR. In the cell lines used, HDAC isoforms 1, 2 and 3 are the most abundantly expressed while HDAC8 also shows robust expression. **[B]** In U2OS cells, HDAC isoforms 1, 2, 3 + 8 were depleted alone or in combinations by transfection with siRNAs. Cells were harvested 96 hours after initial transfection and total RNA was isolated and reverse transcribed into cDNA. Next, relative gene expression of GTAp63, TNFRSF10B LTR transcript 2 (upper panel) as well as the different HDAC isoforms (lower panel) was assessed by qRT-PCR. mRNA levels

were normalized to *RPLP0* and are shown as a fold change compared to control cells which were transfected with scrambled control siRNA. Depletion of these 4 isoforms did not result in a comparable induction of LTR12 transcription as observed upon treatment with HDAC inhibitors. Error bars represent SD (n=3). * = p<0.05, ** = p<0.01, *** = p<0.001; **[C]** In parallel total protein was isolated and separated by SDS-PAGE followed by immunoblotting with specific antibodies against HDAC1, HDAC2 and Hsp90 to demonstrate efficient protein depletion.

5.9 Assessment of different known ERV-regulating proteins in LTR12 regulation

In order to understand the underlying mechanism of HDAC inhibitor induced activation of LTR12-driven transcripts, we tested the influence of various ERV-regulating factors (see 2.2). First, we verified the expression of the respective factors in our cell lines. Next, we depleted each factor by siRNA transfection and analyzed if its absence influenced LTR12 transcription *per se* or its activation through HDAC inhibition. However, depletion of neither KRAB-associated protein-1 (KAP1), Piwi-like protein 1 (PIWIL1) nor ten-eleven translocation protein 1 (TET1) had any significant effect on LTR12 transcription (data not shown).

5.9.1 Depletion of KDM1A results in a slight induction of LTR12 transcription

Another potential target was Lysine (K)-specific demethylase 1A. Transcription of *KDM1A* was silenced in GH cells by independent treatment with three different siRNAs over 96 h (see 4.1.3). 18 h prior to harvesting, cells were treated with 0.5 µM TSA or its solvent DMSO. Total RNA was isolated and reverse transcribed into cDNA. Next, relative gene expression was assessed by qRT-PCR. Depletion of KDM1A resulted in a slight induction of LTR12 transcription in DMSO-treated control cells (Figure 5-11A). This induction varied between 2- to 19- fold for GTAp63 and 2- to 6- fold for TNFRSF10B LTR transcript 2 for the three siRNAs and experiments. Treatment with TSA resulted in an increase in LTR12 transcription which was not obstructed or enhanced by depletion of KDM1A.

KDM1A transcription was significantly reduced by all three siRNAs used as determined by qRT-PCR (Figure 5-11B). Moreover, treatment with TSA resulted in a significant reduction of KDM1A transcription in control cells, an effect also observed in the previously mentioned microarray (see 2.4).

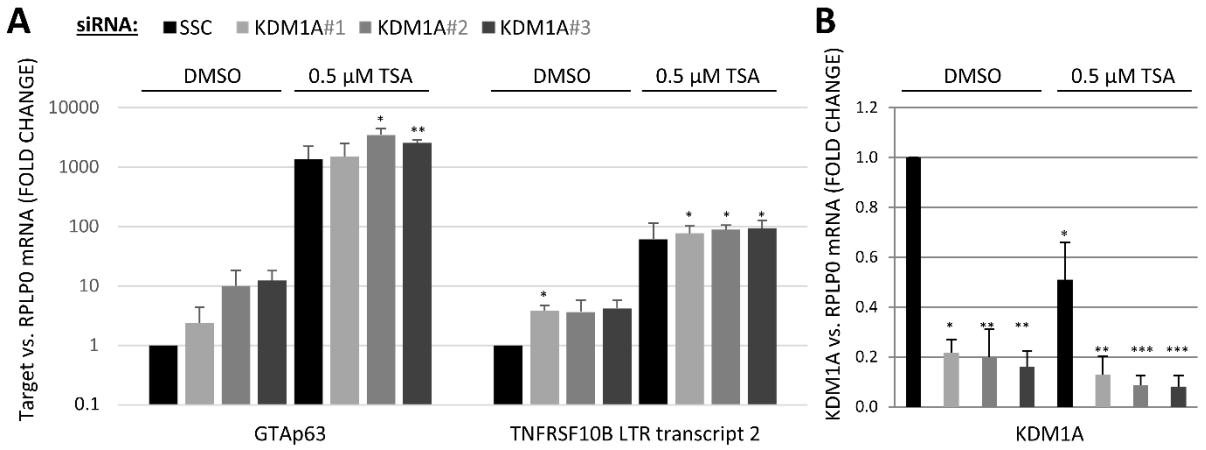

Figure 5-11. Depletion of KDM1A results in a slight induction of LTR12 transcription

Lysine (K)-specific demethylase 1A (KDM1A) was depleted in GH cells by independent transfection with 3 different siRNAs. Cells were incubated with either 0.5 µM Trichostatin A (TSA) or DMSO 18 h prior to harvesting. Cells were harvested 96 hours after initial transfection and total RNA was isolated and reverse transcribed into cDNA. Next, relative gene expression of [A] LTR12-transcripts GTAp63 and TNFRSF10B LTR transcript 2 as well as [B] KDM1A was assessed by qRT-PCR. mRNA levels were normalized to *RPLP0* and are shown as a fold change compared to control cells which were transfected with scrambled control siRNA. Depletion of KDM1A resulted in a slight induction of LTR12 transcription in DMSO-treated control cells. This induction varied between 2- to 19- fold for GTAp63 and 2- to 6-fold for TNFRSF10B LTR transcript 2 between the three siRNAs and experiments. Treatment with TSA resulted in a significant increase in LTR12 transcription. This induction was not obstructed by depletion of KDM1A. Transfection with siRNA resulted in a significant reduction in KDM1A transcription for all three siRNAs used. Treatment with TSA resulted in a significant reduction of KDM1A transcription in control cells. Error bars represent SD (n=3). * = $p<0.05$, ** = $p<0.01$, *** = $p<0.001$ relative to DMSO-treated SSC control cells.

5.10 Identification of specific LTR12-binding transcription factors

None of the previously described ERV-regulating factors showed a strong impact on LTR12 transcription (see 5.9). Moreover, we observed no broad strong transcriptional activation of ERV promoter elements upon treatment with HDAC inhibitors, but a rather restricted activation of ERV9 LTR transcription (Figure 5-8, Figure 5-9). Therefore, we sought to determine if a specific LTR12-binding transcription factor was involved in its regulation.

5.10.1 *In-silico* analysis of known and suggested LTR12-driven cellular genes reveals 13 transcription factors that might be involved in their regulation

To identify putative transcription factor binding sites involved in the HDAC activity-dependent activation of LTR12 transcription, we performed an *in-silico* analysis using the PROMO tool (see 4.2.5). Herein we compared the sequences of 24 ERV9 LTRs for shared binding sites. The analyzed sequences were either described previously to harbor alternative promoters for the transcription of adjacent

genes *(ADH1C, GBP5, SEMA4D* and *DHRS2)* or were identified as potential gene-regulating elements by us (Table 2-I). The LTR12 sequences adjacent to *TP63* and *TNFRSF10B* were also included in the analysis. Overall, the LTR12 sequences shared binding sites for 13 transcription factors (Table 5-II). Since we were especially interested to elucidate the mechanism behind HDAC inhibitor-induced LTR promoter activity, we performed a similar search with control LTR sequences. These sequences corresponded to the LTRs that were previously tested non- or only slightly responsive to HDAC inhibition (Figure 5-8 and Figure 5-9). Only factors that were predicted to bind in all LTR12, but not in the non-responsive LTR sequences (as indicated by "NO" in Table 5-II) were suitable candidates to be involved in the specific regulation. These factors were FOXP3 (forkhead box P3), GR (glucocorticoid receptor), PR A and PR B (progesterone receptors A and B), c-Ets-2 (cellular E-twenty-six) and NF-Y (nuclear transcription factor Y). Next, we sought to elucidate if one of these factors had been described in the regulation of endogenous retroviral elements before.

Gene Symbol	Consensus sequence	TRANSFAC ID	Control
C/EBP beta	TTGY	T00581	YES
STAT4	ATTTCC	T01577	YES
c-Ets-1	CTTCCTG	T00112	YES
GR-beta	AATXT	T01920	YES
YY1	CCAT	T00915	YES
TFIID	TXXAAAA	T00820	YES
FOXP3	XACAAC	T04280	**NO**
GR	CAAAAAX	T05076	**NO**
PR A	AACAGTX	T01661	**NO**
PR B	AACAGTX	T00696	**NO**
c-Ets-2	TAAGAGGAA	T00113	**NO**
RXR-alpha	TXAACCC	T01345	YES
NF-Y	ATTGGTCA	T00150	**NO**

Table 5-II. *In-silico* analysis of LTR12 sequences in different loci reveals a set of transcription factors possibly involved in LTR12 regulation

The sequences of 24 LTR12s in the human genome were analyzed for putative transcription factor binding sites by the PROMO MultiSearchSites tool. The LTR12 sequences were identified previously as candidates to drive the transcription of an adjacent cellular gene. The table sums up 13 transcription factors that might bind within the LTR12 sequences and be involved in their regulation. The consensus sequence of the binding motif is also given. As a control, a corresponding *in-silico* analysis was conducted with LTR sequences from different HERV families, that were tested in Figure 5-8 and Figure 5-9. If the respective transcription factor was also predicted to bind in these non-responsive sequences, it is indicated in the last column as "Yes". R: purine base; Y: pyrimidine base; X: either

5.10.2 NF-Y is frequently bound at LTR12 sequences in the human genome

In late 2013, John D. Fleming *et al.* reported that a bulk of NF-Y binding sites in human K562 cells overlapped with endogenous retroviral LTRs [122]. The majority of these LTRs were of the MLT1 and LTR12 type, which pointed towards a selective binding of NF-Y to these LTR families. We were intrigued by these findings and sought to determine, if NF-Y binding was also present on the LTR12 we studied.

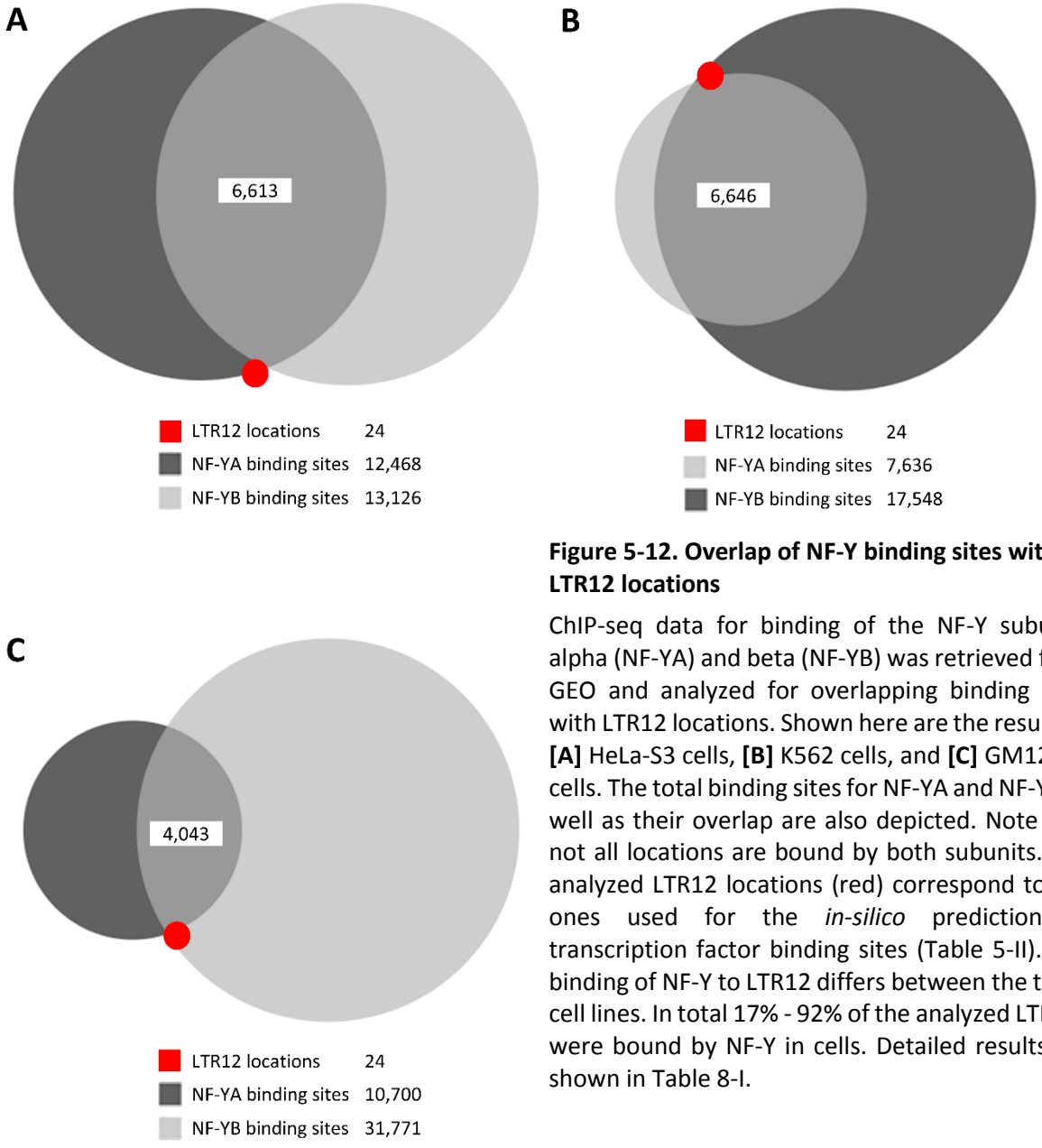

Figure 5-12. Overlap of NF-Y binding sites with LTR12 locations

ChIP-seq data for binding of the NF-Y subunits alpha (NF-YA) and beta (NF-YB) was retrieved from GEO and analyzed for overlapping binding sites with LTR12 locations. Shown here are the results in **[A]** HeLa-S3 cells, **[B]** K562 cells, and **[C]** GM12878 cells. The total binding sites for NF-YA and NF-YB as well as their overlap are also depicted. Note that not all locations are bound by both subunits. The analyzed LTR12 locations (red) correspond to the ones used for the *in-silico* prediction of transcription factor binding sites (Table 5-II). The binding of NF-Y to LTR12 differs between the three cell lines. In total 17% - 92% of the analyzed LTR12s were bound by NF-Y in cells. Detailed results are shown in Table 8-I.

5.10.3 NFY-binding sites overlap with LTR12 whose transcription is enhanced by HDAC inhibition

We retrieved information about NF-Y binding sites in HeLa-S3 cells (cervical carcinoma cell line), K562 cells (leukemia cell line), and GM12878 cells (lymphoblastoid cell line) from GEO (see 4.4) [122]. NF-Y is composed of three subunits – alpha, beta and gamma. Binding data was available for NF-Y alpha (NF-YA) and NF-Y beta (NF-YB). Next, we created a bed-file with the LTR12 locations, which we had previously subjected to an *in-silico* prediction of transcription factor binding sites (see 5.10.1). These LTR12s had in common, that they were proven or strongly suggested to drive transcription of adjacent cellular genes in an HDAC-dependent manner. Subsequently, we analyzed the overlap between NF-Y binding sites and LTR12 locations. In HeLa-S3 cells, 4 of the 24 LTR12s were bound by either NF-YA and/or NF-YB (Figure 5-12A). Table 8-I shows a summary of the respective LTR12s and subunits. Interestingly, 92% of the analyzed LTR12s showed NF-Y occupancy in K562 cells (Figure 10B) and in GM12878 cells 63% (Figure 5-12C). This showed that the predicted binding of NF-Y to LTR12s *in-silico* was actually present in cells.

5.10.4 NF-Y is expressed in our cell lines with levels differing between testis and testicular cancer cells

To determine, if NF-Y was also present in a testicular context, we assessed transcription of its three subunits. Therefore, total RNA from GH cells was isolated, that were either treated with 0.5 µM TSA for 18h or DMSO. Next, the RNA from GH cells and RNA from normal human testis tissue (Ambion) were reverse transcribed to cDNA and analyzed by qRT-PCR. Transcripts of all three subunits were present in normal testis tissue (Figure 5-13A, black bar). Interestingly, transcription was reduced in testicular cancer cells (Figure 5-13A, grey bars). Furthermore, transcription of subunits beta and gamma was further reduced upon treatment with TSA.

5.10.5 Knock-down of NF-Y results in moderate induction of LTR12-driven transcription

To determine whether the presence of NF-Y influences the promoter activity of LTR12 elements, we depleted NF-Y in GH cells by siRNA transfection. Cells were harvested 96 h after initial transfection and total RNA was isolated and reverse transcribed into cDNA. Relative gene expression of GTAp63n TNFRSF10B LTR transcript 2 as well as the three NF-Y subunits was assessed by qRT-PCR. Depletion of NF-YA and NF-YB resulted in a slight induction of GTAp63 (up to 5-fold) and LTR12-driven TNFRSF10B (Figure 5-13B, upper panel). Combined depletion of all three subunits increased these effects. However, large variations were observed between the different experiments. For example, induction of GTAp63 after depletion with siRNA combination NFYA#1 + NFYB + NFYC#2 varied between 13-fold

in experiment one, 6-fold in the second experiment and 18-fold in the third. Moreover, no efficient knock-down could be achieved at the transcriptional level for NF-YA nor NF-YB (Figure 5-13B, lower panel). We observed increased transcription of one subunit upon depletion of the other (single knock-downs data not shown). This effect was also observed for the NF-Y subunit gamma upon depletion of alpha and beta (Figure 5-13B, lower panel).

Overall, a slight tendency for LTR12 induction upon depletion of NF-Y subunits was observed, which was stronger than upon depletion of KDM1A (Figure 5-11A). However, further analysis must be conducted to confirm the significance of these results.

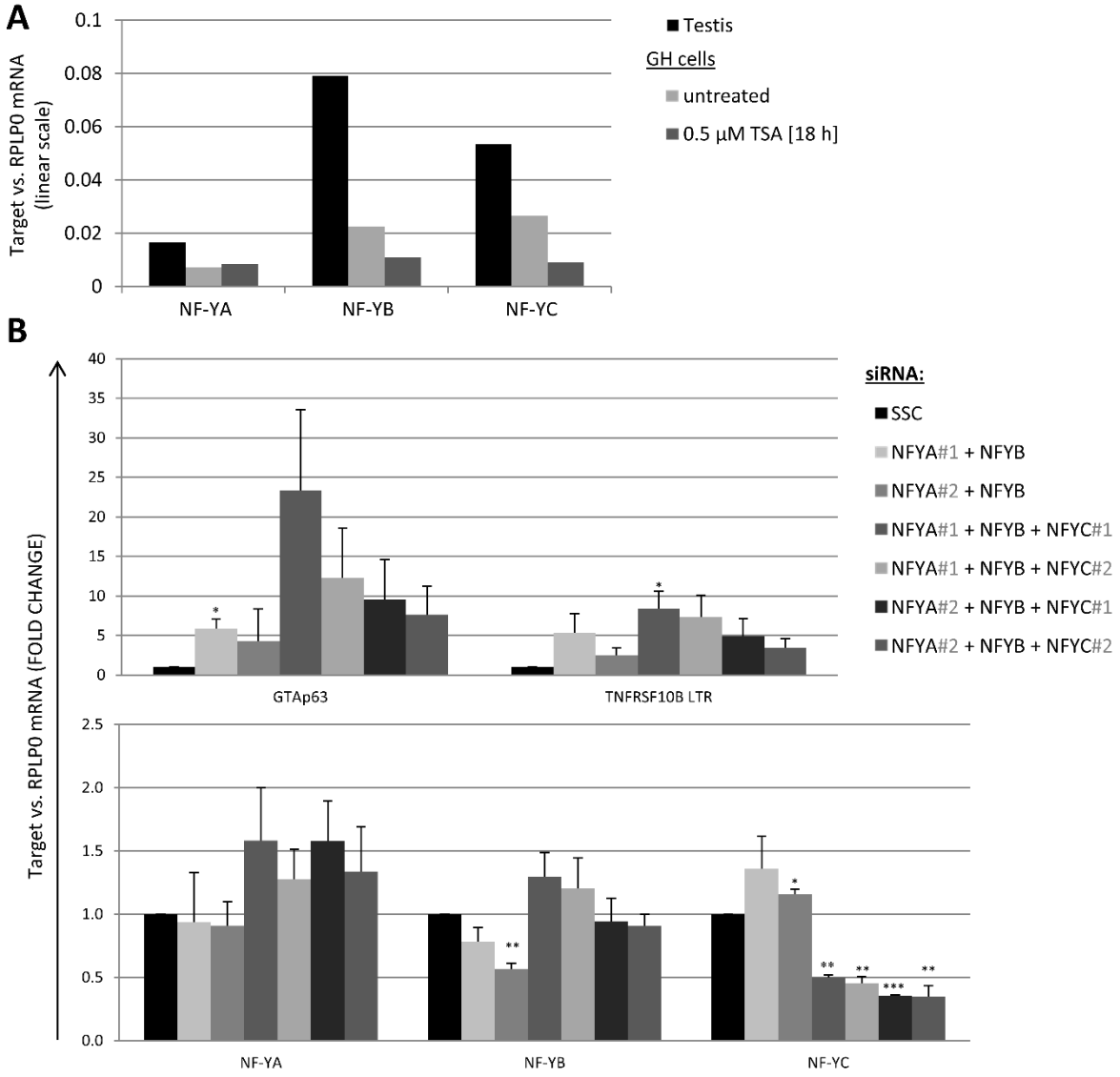

Figure 5-13. NF-Y expression pattern and possible involvement in LTR12 regulation

[A] Total RNA from GH cells was isolated, reverse transcribed into cDNA and expression of the three subunits of transcription factor NF-Y (alpha, beta, gamma) quantified by qRT-PCR. In parallel, an RNA sample from normal human tissue (Ambion) was analyzed. **[B]** In GH cells, NF-Y subunits alpha (NF-YA), beta (NF-YB) and gamma (NF-YC) were depleted in various combinations by transfection with siRNAs. Cells were harvested 96 hours after initial transfection and total RNA was isolated and reverse transcribed into cDNA. Next relative gene expression of GTAp63, TNFRSF10B LTR transcript 2 (upper

panel) as well as the different subunits (lower panel) was assessed by qRT-PCR. mRNA levels were normalized to *RPLP0* and are shown as a fold change compared to control cells which were transfected with scrambled control siRNAs. Depletion of all three subunits resulted in a slight induction of LTR12 transcription. The induction varied between 4- and 35-fold for GTAp63 and 2- and 11-fold for TNFRSF10B LTR transcript 2. Transcriptional silencing was only efficient for NF-YC and NF-YB in combination with NF-YA#2. Error bars represent SD (n=3). * = p<0.05, ** = p<0.01, *** = p<0.001.

5.11 LTR12-binding pattern of nuclear transcription factor Y changes upon treatment with HDAC inhibitor

5.11.1 Identification of genomic regions with strong NF-Y binding

Since NF-Y was shown to bind to LTR12 in different cell lines, we sought to determine if this was also true for testicular cancer cells. Moreover, we were interested in determining whether binding of NF-Y to LTR12 changes upon treatment with HDAC inhibitors. With the help of Prof. Roberto Mantovani (Department of Biomolecular Sciences and Biotechnology, Milan, Italy), we retrieved the coordinates of NF-Y peaks within LTR12 sequences (Table 5-III). According to these peaks, we designed primers for the subsequent analysis of chromatin immunoprecipitation of NF-Y in GH cells. Primers for LTR12 adjacent to *DHRS2, PGPEP1L, TNFRSF10B* and *TP63* gave rise to the expected PCR products when tested on genomic DNA.

Gene	NF-Y	Cell type	CCAAT	Peak coordinates
PTPN13	YB	K	Yes	chr4:87.469.060-87.469.160
TMOD1	YB	K, G	Yes	chr9:100,336,900-100,337,400
CSF3	YB	K, G, H	Yes	chr17:38.168.300-38.168.650
	YB	K	No	chr17:38.167.750-38.168.050
CCR4	YB	K	Yes	chr3:32.982.100-32.982.200
SLC36A2	YB	K	Yes	chr5:150.786.750-150.787.000
KCNN2	YB	G	Yes	chr5:113,768,850-113,769,450
TNFRSF10B	YA/YB	K, G, H	Yes	chr8:22,927,750-22,928,100
PGPEP1L	YB	K, G, H	Yes	chr15:99,550,850-99,551,200
DHRS2	YB	K, G	Yes	chr14:24,105,350-24,105,700
	YB	K, G	Yes	chr14:24,106,900-24,107,250
GBP5	YB	G	Yes	chr1:89.738.550-89.738.900
C9orf53	No		No	
TENM1	No		No	

Table 5-III. Location of NF-Y bound to LTR12 in the human genome

The coordinates of NF-Y peaks within LTR12 sequences upstream of cellular genes obtained by ChIP-seq analysis are presented. The names of the cellular genes adjacent to the LTR12s are given in the table. The signals were obtained either with specific antibodies for NF-Y subunit alpha „YA“ or beta „YB“. For the subsequent analysis of ChIP data from GH cells, oligonucleotide sequences were chosen within the NF-Y coordinates shown here. Cell types: K – K562; G – GM12878; H – HeLa-S3. The ChIP-seq experiment was published by Fleming J.D. *et al.* [122] and the table prepared by Prof. R. Mantovani (Department of Biomolecular Sciences and Biotechnology, Milan, Italy).

5.11.2 Increased occupancy of LTR12 with NF-Y after treatment with HDAC inhibitor

GH cells were treated with 0.5 µM Trichostatin A 18 hours prior to chromatin harvesting. Next, the chromatin was immunoprecipitated with specific antibodies against NF-YA and NF-YB. As a control, chromatin was also immunoprecipitated with IgG. The maximum recovery with IgG at all target sites was at 0.02% of input (data not shown). The recovery as percentage of input of the respective target site was determined. The inactive promoter region of myoglobin was analyzed as a negative control. Thereby, unspecific binding of the antibodies to the DNA was eliminated. Cyclin B1 was analyzed as a positive control [110]. Both antibodies resulted in an efficient recovery of Cyclin B1 (Figure 5-14A+B). However, the signals at the LTR12 sites upon precipitation with the antibody against NF-YA were only slightly above background (Figure 5-14A). Signals for NF-YB were generally stronger than for NF-YA (Figure 5-14B). NF-YB interaction with the LTR12 upstream of *PGPEP1L* was significantly increased upon treatment with TSA. On average, this increase was about 2.4-fold. The same tendency was also observed at the LTR12 upstream of *DHRS2* (p-value 0.236), *TNFRSF10B* (p-value 0.081) and *TP63* (p-value 0.118). Binding of NF-YB at these promoter regions was increased by an average of 2.8-fold at the LTR12 upstream of *DHRS2*, 3.2-fold upstream of *TNFRSF10B* and 2.2-fold upstream of *TP63*. These data indicate that NF-Y is not only present at the endogenous retroviral promoter elements, but its binding pattern also changes in response to treatment with TSA.

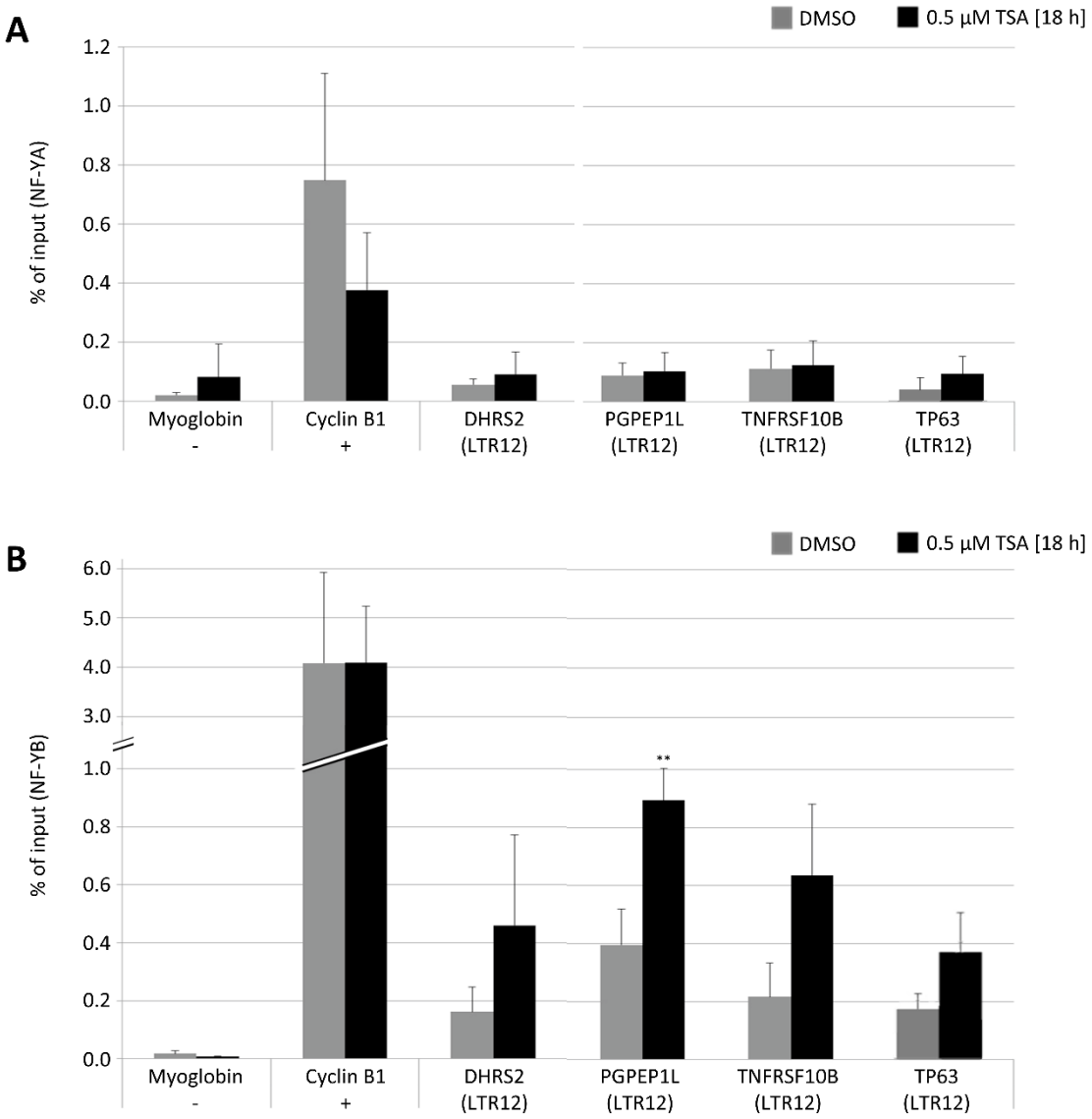

Figure 5-14. Chromatin immunoprecipitation reveals increasing occupancy of LTR12 with NF-YB after HDAC inhibitor treatment

GH cells were treated with 0.5 µM Trichostatin A (TSA) 18 hours prior to chromatin harvesting. Next chromatin was immunoprecipitated with specific antibodies against **[A]** NF-YA or **[B]** NF-YB. The recovery (% of input) for each subunit at different LTR12 locations is depicted. Signals for NF-YB were generally stronger than for NF-YA. As a positive control, Cyclin B1 was analyzed. The inactive promoter region of myoglobin served as an internal negative control. NF-YB interaction with the LTR12 upstream of *PGPEP1L* was significantly increased upon treatment with TSA. The same tendency was also observed at the LTR12 regions upstream of *DHRS2*, *TNFRSF10B* and *TP63*. As a control, an immunoprecipitation with IgG was performed. IgG recovery rates were under 0.02% for all tested target sites. Error bars represent SD (n=3). * = $p<0.05$, ** = $p<0.01$, *** = $p<0.001$.

6 Discussion

6.1 Identification of *TNFRSF10B* as a novel gene driven by LTR12 and re-activatable mediator of testicular cancer cell death

TNFRSF10B is well known for its involvement in programmed cell death. The protein encoded by this gene contains an intracellular death domain and is activated by TRAIL to transduce apoptosis signals. Transcription of *TNFRSF10B* is enhanced upon DNA damage in a p53-dependent manner [128] and contributes majorly to germ cell death in humans as well as rodents [129, 130]. Sensitization of human cancer cell lines to TRAIL-mediated apoptosis by treatment with HDAC inhibitors was first observed over a decade ago [131-134]. Nakata *et al.* and others suggested, that the upregulation of TNFRSF10B/DR5 by histone deacetylase inhibitors was causing the enhancement of apoptosis [135, 136]. Since observed in leukemia cells with inactive p53, this induction was most likely p53-independent [136] and may instead have been driven by LTR12 activity.

Since *TNFRSF10B* was among the candidate genes whose transcripts contained an LTR12 and that were induced by HDAC inhibitor treatment (Table 2-I), we sought to determine if the upstream located LTR12 was indeed acting as an alternative promoter for *TNFRSF10B* transcription and whether this contributed to cell death in germ cells.

6.1.1 A transcript encoding death receptor 5 originates from an LTR12

We confirmed the presence of a solitary LTR of the endogenous retrovirus family 9 (ERV9) upstream of *TNFRSF10B* in the human genome (Figure 5-2A). Since the LTR12 upstream *TNFRSF10B* was only present in the genomes of humans, chimpanzees, gorillas, orangutans and gibbons, the transposition occurred roughly 18 million years ago in a common ancestor (Figure 5-2 and Figure 5-3). We identified three distinct transcripts of *TNFRSF10B* originating from the LTR12 (Figure 5-1A). Transcription of all three transcripts was significantly enhanced by treatment with the HDAC inhibitor TSA (Figure 5-1B). Interestingly, LTR12 promoter activity was only observed in the small intestine and testis (Figure 5-4B). This indicates that the LTR12 serves as tissue-specific promoter for *TNFRSF10B*. These data fit with previous results obtained for an LTR12 that drives transcription of the *TP63* gene in a tissue-specific manner [90]. Transcription of the LTR12-driven transcript of *TP63*, GTAp63, was found to be largely confined to the human testis [90]. However, no GTAp63 expression was detected in the small intestine. The reasons for differing results regarding transcription of *TNFRSF10B* and *TP63* in the small intestine might be due to sequence variations in the two LTR12s. Mutations accumulated in the LTR12 upstream of *TNFRSF10B* might have given rise to binding sites for intestine specific transcription factors. While no such factors were identified by *in-silico* predictions (data not shown), their binding *in vivo* cannot necessarily be excluded.

6.1.2 HDAC inhibitor treatment sensitizes testicular cancer cells to TRAIL-mediated apoptosis

We observed enhanced cell death upon combinatorial treatment of testicular cancer cells with HDAC inhibitor TSA and DR5 ligand TRAIL (Figure 5-5). These synergistic effects depended on *TNFRSF10B* expression as demonstrated by its siRNA-mediated depletion (Figure 5-5B). These results are in line with previous findings of enhanced apoptosis upon combinatorial treatment with TSA and TRAIL in other cancer cell lines, thus providing further evidence that HDAC inhibitors are important in the regulation of TNFRSF10B-dependent cell death.

6.1.3 Promoter activity of LTR12 is enhanced in a range of human cancer cell lines

Interestingly, transcription of LTR12-driven *TNFRSF10B* was enhanced by HDAC inhibitors not only in testicular cancer cells, but also in various other cancer cell lines (Figure 5-7B). These results demonstrate that LTR12 promoter activity can be specifically modulated in a wide range of human cancer cells. This observation fits with previous reports of increased TNFRSF10B expression upon treatment with HDAC inhibitors in various human leukemia, colon adenocarcinoma and other cell lines [135-137]. The strong increase in LTR12 promoter activity might markedly contribute to the observed increase in TNFRSF10B protein levels. Moreover, LTR12 promoter activity seems to be p53-independent, since the cell lines tested included cell lines lacking p53 such as H1299 cells. Thus, these findings add to the growing body of data indicating that upregulation of TNFRSF10B can occur in a p53-independent manner [136] and provide evidence for an alternative pro-apoptotic pathway.

6.2 Global TE silencing factors have little influence on LTR12 transcription

As described above (see 2.1.1), mobilization of transposable elements helps to drive evolution but can also be harmful to the host [14, 43, 138]. Therefore, the spreading of TEs has to be controlled tightly [43]. In depth studies have identified various mechanisms for TE silencing in the genome (see 2.2). These include DNA methylation, histone modifications and post-transcriptional silencing by small inhibitory RNAs [31, 32, 52]. DNA methylation is a well-established method of TE silencing and it has been suggested that this process originally evolved primarily for this purpose [139]. Paternal and maternal DNA undergo de-methylation in early stages of embryonic development [42, 140]. This implies the necessity of additional TE silencing strategies to avoid their uncontrolled spreading [43, 52]. Accordingly, numerous studies to identify TE silencing factors were carried out in stem cells and embryos, predominantly from mice. Among the identified silencing factors were the scaffold protein KAP1 and the histone demethylase KDM1A [62, 63]. KAP1 is recruited to TE sequences by KRAB-ZFP

transcription factors, where it functions to recruit additional TE silencing factors. For example, KAP1 directs the NuRD (nucleosome remodeling and histone deacetylase) complex, as well as KDM1A, to chromatin [43, 58, 62]. The NuRD complex consists of six core subunits, including ATPases MI-2 alpha and Mi-2 beta as well as HDACs 1 and 2 [141, 142]. It couples chromatin remodeling ATPase and deacetylase activity, providing the ability to render chromatin inactive [143]. KDM1A functions to remove methyl groups from H3K4, resulting in gene silencing. Interestingly, KDM1A was shown to associate with the NuRD subunits HDAC1 and HDAC2 in mESC [144]. Moreover, acetylated histones were reported to repress its H3K4 demethylase activity [145, 146].

Promoter activity for the different solitary LTR12s in the human genome seems to be regulated in a tissue-specific manner [10]. Moreover, it can be repressed upon transformation [90]. To identify silencing mechanisms involved in LTR12 regulation in human cells, we depleted various TE silencing factors and monitored transcription originating from LTR12s in their absence. Since LTR12 promoter activity can be restored by treatment with HDAC inhibitors (Figure 5-7), we initially focused on factors that were previously linked to histone acetylation and deacetylation.

Depletion of the histone demethylase KDM1A resulted in a slight induction of LTR12 transcription in testicular cancer cells (Figure 5-11) and did not interfere with the induction of LTR12 by HDAC inhibition. Thus, removal of the activating histone 3 lysine residue 4 methylation might contribute to LTR12 silencing, but is not a predominant factor required for its repression. Moreover, KDM1A does not seem to be an essential factor in the directed activation of LTR12 upon HDACi treatment. However, KDM1A knock-down efficiency, though significant at the mRNA level, could not be verified at the protein level and might therefore have been incomplete.

Furthermore, no changes in LTR12 promoter activity were observed upon depletion of KAP1, TET1 and PIWIL1 (data not shown). However, given that LTR12s are not present upstream *TP63* and *TNFRSF10B* in mice, the previous observations of ERV de-repression upon depletion of the respective factors do not necessarily contradict our findings, since previous studies were mostly carried out in mice and accordingly did not focus on HERV-9 LTRs. Initial experiments with the DNA de-methylating agent 5'Azacytidine did not result in alterations in GTAp63 transcription (personal communication from Dr. Ulrike Beyer). Therefore, we focused on mechanisms other than DNA methylation. Additionally, MeDIP with methyl-DNA-antibody resulted in no signal for LTR12s upstream of *TP63* and *TNFRSF10B* in testicular cancer cells (data not shown), indicating the absence of DNA methylation at these LTR12s. While these preliminary findings do not exclude the possibility that alterations in DNA methylation are responsible for the changes observed in LTR12 activity upon HDAC inhibitor treatment, they do argue

strongly against it. Studies with genome wide bisulfite sequencing of untreated and TSA-treated cancer cells might shed light on putative DNA methylation changes at LTR12 promoter sites.

Overall, analysis of the effects of HDAC inhibition on various LTR-driven cellular genes revealed a rather specific induction of genes controlled by TEs of the LTR12 family (Figure 5-8, Figure 5-9). Therefore, while the orchestrated activation of LTR12s may in part be regulated by the aforementioned silencing mechanisms, such as KDM1A-confered histone demethylation, our data indicated the involvement of LTR12-specific factors. Based on this evidence, we decided to focus on TE silencing factors with putative affinity for specific binding sites within LTR12 promoter sequences.

6.3 NF-Y binding to LTR12 increases in TSA-treated cells

In-silico prediction of potential transcription factor binding sites shared by all LTR12s, whose promoter activity was increased in TSA-treated cells (Table 2-I, Figure 5-8, Figure 5-9), identified NF-Y as a putative regulator (Table 5-II). NF-Y is a trimeric transcription factor (TF) that consists of three subunits - alpha appears to confer sequence-specificity for the DNA motif CCAAT while beta and gamma exert histone-like structural features [80, 81]. Binding of NF-Y was observed both in core promoters and enhancer elements [147]. Various studies identified NF-Y to be crucial in the regulation of cell growth, promoting transcription of various cell cycle genes [148-150]. Moreover, NF-Y binding in the promoter region of various cellular genes was shown to be essential for their transcriptional activation by HDAC inhibitors [151-153]. However, NF-Y might not only enhance gene transcription but also repress it [154, 155]. The mechanisms underlying these contradictory outcomes are not fully understood yet. Apart from transactivating gene transcription, NF-Y might also serve as a promoter organizer – e.g. cooperating with neighboring TFs and recruiting histone-modifying enzymes [147, 155]. In line with these hypotheses, NF-Y was found to be associated with histone acetyl transferases as well as deacetylases [149, 151, 154, 156, 157]. Apart from the recruitment of acetyltransferases and deacetylases, NF-Y may also be post-translationally modified itself by ubiquitination, phosphorylation and acetylation [81, 158, 159]. These modifications might further alter the functional implications of NF-Y bound to a genomic region [155]. In one study, acetylation of NF-Y subunit alpha was shown to increase its stability and transactivation activity [158]. Recently, a genome-wide study of NF-Y binding sites in three human cell lines revealed, that a bulk of these sites overlapped with endogenous retroviral LTRs [122].

We thus sought to determine if NF-Y was indeed present at these LTR12s and elucidate the impact of its binding on LTR12 promoter activity. We observed the presence of NF-Y at all 4 genomic LTR12s that we tested in GH cells. These LTR12s were located upstream of the cellular genes *DHRS2*, *PGPEP1L*, *TNFRSF10B* and *TP63* (Figure 5-14). We noted marked differences in the binding intensities of the alpha and beta subunit. This corresponds to previous observations by Fleming *et al*. in K562 cells, GM12878 cells and HeLa-S3 cells. This difference could be due to target loci bound exclusively by NF-YB. However, Fleming *et al.* hypothesized that, in comparison to the NF-YA antibody, the NF-YB antibody was more "immune-efficient", rendering some NF-YA peaks below the detection limit rather than reflecting an actual abundancy of exclusive NF-YB sites [122]. Binding of NF-YA and NF-YB to the different LTR12s was increased in TSA-treated GH cells (Figure 5-14). Preliminary data showed the same increase in NF-YB binding in HeLa and U2OS cells (data not shown). The increase in LTR12 promoter activity upon HDAC inhibitor treatment might therefore be accompanied by a general increase in NF-Y binding. Thus, NF-Y might positively regulate LTR12 promoter activity.

However, experimental assessment of NF-Ys role in regulating the promoter activities of LTR12s has produced contradictory results. For example, lentiviral depletion of NF-Y subunit alpha with shRNAs in H322 cells resulted in a slight transcriptional repression of *TP63*, an effect not observed in HeLa-S3 cells, providing evidence that NF-Y positively regulates LTR12 promoter activity (personal communication from Prof. Roberto Mantovani). On the contrary, our preliminary results showed that depletion of NF-Y by siRNAs, while not as efficient as depletion by lentivirally delivered shRNAs, resulted in an increase in LTR12 transcription (Figure 5-13) which rather points towards a repressive function for NF-Y present at the retroviral promoter elements.

These seemingly contradictory findings can be reconciled by the fact that NF-Y has already been described to exert dual functions at promoters. Peng *et al.* observed cell-specific interactions of NF-Y with promoter elements and other proteins that modulate its transcriptional activity [154, 160].

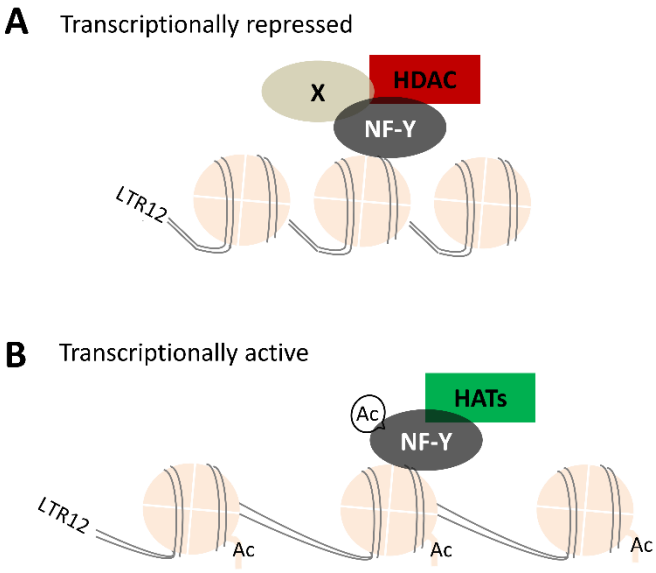

Figure 6-1. Possible influence of NF-Y on LTR12 promoter activity

Depending on their genomic locations LTR12s seem to be transcriptionally active in specific tissues. NF-Y is present at LTR12s regardless of their activity. Additional factors as well as post-translational modifications might alter complex formation and thereby chromatin activity. **[A]** In most tissues a factor X might be present, strengthening interaction of NF-Y with HDACs, thus leading to transcriptional repression. Upon transformation, factor X might be upregulated in testicular cancer cells. **[B]** Upon absence of factor X or treatment with HDAC inhibitors, NF-Y associates with HATs, resulting in an upregulation of LTR12 promoter activity in various human cell lines. Herein, acetylation of NF-Y itself might alter its interaction with factor X.

Thus, one could speculate that NF-Y present at LTR12 promoter elements might recruit HDACs resulting in transcriptional repression (Figure 6-1). This interaction could be strengthened by another "factor X", which might be absent or altered in germ cells. Upon treatment with HDAC inhibitors, acetylation of NF-Y itself might enhance its affinity for LTR12 and abolish the interaction with the repressive factor X. Moreover, upon release from HDAC complexes, the available NF-Y might interact with HATs instead [160]. These changes might be quite dynamic, fitting to the observation that interactions of HDACs with transcription factors exist in "rapid equilibrium" [161]. Thus, NF-Y may have a dual function as activator or repressor of LTR12 promoter activity, depending on the cellular context.

In the present study, we only analyzed the binding pattern of NF-Y at four LTR12 genomic loci. Thus, further studies are required to clarify the role of NF-Y in HDACi-mediated activation of a broader range of LTR12 promoters. ChIP-seq analysis of TSA-treated cancer cells could on the one hand reveal if all LTR12s, that drive the expression of adjacent cellular genes in a HDACi-responsive manner, show increased NF-Y binding. On the other hand, genomic loci of HERV elements that were shown to be non-responsive to treatment with HDACi (Figure 5-8, Figure 5-9) could be analyzed as controls.

To identify cofactors in LTR12-regulation, the proteome of normal testis could be compared to testicular cancer cells. Since LTR12 promoter activity is markedly reduced in the latter, a possible

repressive “factor X” might be exclusively present in transformed cells. Moreover, Co-IP experiments with NF-Y in untreated versus TSA-treated cancer cells followed by mass spectrometry could help to identify binding partners and shed light on a possible interaction of NF-Y with a repressive cofactor.

6.4 New perspectives for anti-cancer effects of HDAC inhibitors

Histone acetylation and deacetlyation is a well-established epigenetic mechanism involved in transcriptional regulation [54, 60, 103]. Promoter regions of active genes usually display high levels of histone acetylation [60]. The maintenance of adequate acetylation levels at active and low acetylation levels at inactive gene promoters might be quite dynamic [162]. The enzymes involved in the addition and removal of acetyl groups to and from histones are histone acetyltransferases and deacetlyases respectively [98]. However, the molecular targets of HDACs also include nonhistone substrates [100]. The latter include transcription factors, HATs themselves, alpha-tubulin and chaperone proteins – influencing the stability, interactions or, for example, localization of the acetylated proteins [100, 163]. The molecular responses to HDAC activity range from apoptosis, migration and differentiation to angiogenesis [163, 164]. Since cancer cells are characterized by six principle hallmarks, including the induction of angiogenesis and active invasion and metastasis [165, 166], a link between HDAC activity and cancer treatment is not farfetched. Although the data is still rudimentary, certain HDAC isoforms were found to be overexpressed in many cancers supporting this potential link [164]. The anticancer effects of HDAC inhibitors are well documented, which is exemplified by the abundance of HDAC inhibitors in clinical trials as well as the approval of SAHA and romidepsin by the US Food and Drug Administration for the treatment of cutaneous T-cell lymphoma (CTCL) [102, 163]. SAHA is a hydroxamic acid HDACi, binding to zinc ions in the active site of HDACs [102]. While Panobinostat is in phase III clinical trials for CTCL, ongoing phase II are being conducted for Belinostat, Entinostat, Mocetinostat, Givinostat, Pactinostat, Chidamide, Quisinostat and Abexinostat for different cancer types, including lymphomas and solid tumors [163].

Given that we observed strong upregulation of LTR12 promoter activity upon treatment with HDAC inhibitors, we sought to determine the molecular grounds of this HDAC-dependent regulation and how the LTR12-driven upregulation of anti-tumor proteins might be exploited.

Interestingly, treatment with HDAC inhibitors did not only induce LTR12-driven gene expression in testicular cancer cells as reported previously [90], but also in a set of human cancer cells derived from different tissues (Figure 5-7). Moreover, we observed an increase in LTR12 promoter activity upon

treatment with HDAC inhibitors from different chemical classes (Figure 5-6). Thus, the possibility of these changes arising as a mere off-target effect of TSA is rather unlikely. The strongest LTR12 induction was observed upon treatment with TSA, Entinostat and Mocetinostat. In a recent reclassification of inhibitor-specificities, these three inhibitors were shown to exert high specificity for HDAC1, HDAC2, HDAC3 as well as the CoREST, NuRD and NCoR complexes [163, 167, 168]. However, they were shown to have little affinity for Sin3 as well as HDAC isoforms 8, 6 and 10. This fits with the observation that depletion of HDAC8 had little effect on LTR12 activity (Figure 5-10). Since depletion of HDAC1, 2 and 3 also resulted in only minor changes (Figure 5-10), the regulation is most likely to be mediated by HDAC-containing protein complexes rather than single HDAC proteins. HDACs in these complexes might be harder to deplete by siRNAs as most HDAC interactions in complexes such as NuRD are highly stable [161, 169]. Moreover, effects on gene expression upon depletion of HDACs versus inhibitor treatment were reported to show only about 4% overlap [170]. Dejligbjerg *et al.* hypothesized that depleting HDACs might alter rather than disrupt multi-protein complexes and therefore result in aberrant cellular responses [170]. Accordingly, the minor changes in LTR12 transcription we observed upon depletion of HDAC1, 2 and 3 might not necessarily indicate that these isoforms are not primarily involved in LTR12 silencing.

The identification of multiple LTR12-driven cellular genes that are involved in the apoptotic response and can be upregulated by HDAC inhibitor treatment is an exciting finding. The strong upregulation of LTR12s in a variety of cancer cell lines might result in cancer cell death by upregulation of anti-apoptotic proteins as observed for TNFRSF10B. This provides another explanation as to how HDACis might exert their anticancer effects and also argue for combinatorial treatment of cancer with, for example, TRAIL, as previously suggested [136].

6.5 Conclusions and future perspectives

In this work, we characterized an additional LTR12-driven pro-apoptotic gene besides *TP63*. LTR12-driven transcripts of *TNFRSF10B* were detected in the human testis and small intestine and we observed a dramatic increase in LTR12 promoter activity upon treatment with HDAC inhibitors. This induction was not limited to one specific inhibitor, but was observed upon the application of inhibitors of different chemical classes. Interestingly, among these inhibitors were the FDA-approved SAHA as well as Entinostat and Mocetinostat, which are currently undergoing phase II clinical trials. Though upregulation of TNFRSF10B protein levels after treatment with HDACi was previously reported in a range of tumor cells, their mechanistic basis – LTR12-driven transcription – has been unknown. We

show for the first time, that LTR12 promoter activity is linked to TNFRSF10B expression. Aside from linking this activation to LTR12 promoter activity, we also provide further evidence that combinatorial treatment with TSA and TRAIL additively augments cell death as shown here for testicular cancer cells. Since the increase in LTR12 promoter activity upon treatment with HDACi was not limited to testicular cancer cells, one may speculate that the specific upregulation of LTR12 largely contributes to mediating the observed apoptotic effects.

Regarding the underlying mechanisms of LTR12 regulation of TNFRSF10B, we showed that NF-Y is abundantly present at LTR12 genomic loci and its binding increases upon application of HDACi. Therefore, we propose a crucial role for NF-Y in the orchestrated repression and activation of LTR12 promoter elements in the human genome.

The specific activation of LTR12-driven transcription of putative tumor suppressor genes like *TP63* and *TNFRSF10B* suggests a novel mechanism of how inhibition of HDACs can exert anti-cancer effects. Further analysis of NF-Y and identification of potential cofactors in LTR12-regulation might enable us to understand resistance to HDACi treatment and overcome it in a variety of tumors. Moreover, the contribution of LTR12 activation implies that biological effects of HDAC inhibitors, as observed in mouse models, might not necessarily reflect the situation in humans, since the distribution of retroviral elements differs greatly between these two species. Furthermore, we present yet another example of how co-evolution of TE with the host might have been beneficial for the host and therefore be rendered active in the human genome instead of being eliminated as “junk DNA”.

7 References

1. Weiss, R.A., *The discovery of endogenous retroviruses.* Retrovirology, 2006. **3**: p. 67.
2. Payne, L.N. and R.C. Chubb, *Studies on the nature and genetic control of an antigen in normal chick embryos which reacts in the COFAL test.* J Gen Virol, 1968. **3**(3): p. 379-91.
3. Boeke, J.D. and J.P. Stoye, *Retrotransposons, Endogenous Retroviruses, and the Evolution of Retroelements*, in *Retroviruses*, J.M. Coffin, S.H. Hughes, and H.E. Varmus, Editors. 1997: Cold Spring Harbor (NY).
4. Temin, H.M. and S. Mizutani, *RNA-dependent DNA polymerase in virions of Rous sarcoma virus.* Nature, 1970. **226**(5252): p. 1211-3.
5. Baltimore, D., *RNA-dependent DNA polymerase in virions of RNA tumour viruses.* Nature, 1970. **226**(5252): p. 1209-11.
6. Lander, E.S., et al., *Initial sequencing and analysis of the human genome.* Nature, 2001. **409**(6822): p. 860-921.
7. Consortium, E.P., *An integrated encyclopedia of DNA elements in the human genome.* Nature, 2012. **489**(7414): p. 57-74.
8. Pray, L., *Transposons, or jumping genes: Not junk DNA.* Nature Education, 2008. **1**(1): p. 32.
9. de Koning, A.P., et al., *Repetitive elements may comprise over two-thirds of the human genome.* PLoS Genet, 2011. **7**(12): p. e1002384.
10. Rebollo, R., M.T. Romanish, and D.L. Mager, *Transposable elements: an abundant and natural source of regulatory sequences for host genes.* Annu Rev Genet, 2012. **46**: p. 21-42.
11. Kapitonov, V.V. and J. Jurka, *A universal classification of eukaryotic transposable elements implemented in Repbase.* Nat Rev Genet, 2008. **9**(5): p. 411-2; author reply 414.
12. Gifford, W.D., S.L. Pfaff, and T.S. Macfarlan, *Transposable elements as genetic regulatory substrates in early development.* Trends Cell Biol, 2013. **23**(5): p. 218-26.
13. Chen, J.M., et al., *Meta-analysis of gross insertions causing human genetic disease: novel mutational mechanisms and the role of replication slippage.* Hum Mutat, 2005. **25**(2): p. 207-21.
14. Iskow, R.C., et al., *Natural mutagenesis of human genomes by endogenous retrotransposons.* Cell, 2010. **141**(7): p. 1253-61.
15. Ostertag, E.M. and H.H. Kazazian, Jr., *Biology of mammalian L1 retrotransposons.* Annu Rev Genet, 2001. **35**: p. 501-38.
16. Mills, R.E., et al., *Recently mobilized transposons in the human and chimpanzee genomes.* Am J Hum Genet, 2006. **78**(4): p. 671-9.
17. Mills, R.E., et al., *Which transposable elements are active in the human genome?* Trends Genet, 2007. **23**(4): p. 183-91.

18. Stoye, J.P., *Studies of endogenous retroviruses reveal a continuing evolutionary saga.* Nat Rev Microbiol, 2012. **10**(6): p. 395-406.
19. Jern, P. and J.M. Coffin, *Effects of retroviruses on host genome function.* Annu Rev Genet, 2008. **42**: p. 709-32.
20. Bannert, N. and R. Kurth, *The evolutionary dynamics of human endogenous retroviral families.* Annu Rev Genomics Hum Genet, 2006. **7**: p. 149-73.
21. Larsson, E., N. Kato, and M. Cohen, *Human endogenous proviruses.* Curr Top Microbiol Immunol, 1989. **148**: p. 115-32.
22. Magiorkinis, G., et al., *Env-less endogenous retroviruses are genomic superspreaders.* Proc Natl Acad Sci U S A, 2012. **109**(19): p. 7385-90.
23. Temin, H.M., *Structure, variation and synthesis of retrovirus long terminal repeat.* Cell, 1981. **27**(1 Pt 2): p. 1-3.
24. Dupressoir, A., C. Lavialle, and T. Heidmann, *From ancestral infectious retroviruses to bona fide cellular genes: role of the captured syncytins in placentation.* Placenta, 2012. **33**(9): p. 663-71.
25. Boller, K., et al., *Human endogenous retrovirus HERV-K113 is capable of producing intact viral particles.* J Gen Virol, 2008. **89**(Pt 2): p. 567-72.
26. Stoye, J.P., *Endogenous retroviruses: still active after all these years?* Curr Biol, 2001. **11**(22): p. R914-6.
27. Cohen, C.J., W.M. Lock, and D.L. Mager, *Endogenous retroviral LTRs as promoters for human genes: a critical assessment.* Gene, 2009. **448**(2): p. 105-14.
28. Weiss, R.A. and J.P. Stoye, *Virology. Our viral inheritance.* Science, 2013. **340**(6134): p. 820-1.
29. Gifford, R. and M. Tristem, *The evolution, distribution and diversity of endogenous retroviruses.* Virus Genes, 2003. **26**(3): p. 291-315.
30. Jurka, J., J. Walichiewicz, and A. Milosavljevic, *Prototypic sequences for human repetitive DNA.* J Mol Evol, 1992. **35**(4): p. 286-91.
31. Levin, H.L. and J.V. Moran, *Dynamic interactions between transposable elements and their hosts.* Nat Rev Genet, 2011. **12**(9): p. 615-27.
32. Crichton, J.H., et al., *Defending the genome from the enemy within: mechanisms of retrotransposon suppression in the mouse germline.* Cell Mol Life Sci, 2014. **71**(9): p. 1581-605.
33. Bird, A., *DNA methylation patterns and epigenetic memory.* Genes Dev, 2002. **16**(1): p. 6-21.
34. Bestor, T.H., *The DNA methyltransferases of mammals.* Hum Mol Genet, 2000. **9**(16): p. 2395-402.
35. Goll, M.G. and T.H. Bestor, *Eukaryotic cytosine methyltransferases.* Annu Rev Biochem, 2005. **74**: p. 481-514.

36. Lewis, J.D., et al., *Purification, sequence, and cellular localization of a novel chromosomal protein that binds to methylated DNA.* Cell, 1992. **69**(6): p. 905-14.
37. Nan, X., F.J. Campoy, and A. Bird, *MeCP2 is a transcriptional repressor with abundant binding sites in genomic chromatin.* Cell, 1997. **88**(4): p. 471-81.
38. Klose, R.J. and A.P. Bird, *Genomic DNA methylation: the mark and its mediators.* Trends Biochem Sci, 2006. **31**(2): p. 89-97.
39. Iguchi-Ariga, S.M. and W. Schaffner, *CpG methylation of the cAMP-responsive enhancer/promoter sequence TGACGTCA abolishes specific factor binding as well as transcriptional activation.* Genes Dev, 1989. **3**(5): p. 612-9.
40. Okano, M., S. Xie, and E. Li, *Cloning and characterization of a family of novel mammalian DNA (cytosine-5) methyltransferases.* Nat Genet, 1998. **19**(3): p. 219-20.
41. Okano, M., et al., *DNA methyltransferases Dnmt3a and Dnmt3b are essential for de novo methylation and mammalian development.* Cell, 1999. **99**(3): p. 247-57.
42. Wu, S.C. and Y. Zhang, *Active DNA demethylation: many roads lead to Rome.* Nat Rev Mol Cell Biol, 2010. **11**(9): p. 607-20.
43. Rowe, H.M. and D. Trono, *Dynamic control of endogenous retroviruses during development.* Virology, 2011. **411**(2): p. 273-87.
44. Tahiliani, M., et al., *Conversion of 5-methylcytosine to 5-hydroxymethylcytosine in mammalian DNA by MLL partner TET1.* Science, 2009. **324**(5929): p. 930-5.
45. Ito, S., et al., *Tet proteins can convert 5-methylcytosine to 5-formylcytosine and 5-carboxylcytosine.* Science, 2011. **333**(6047): p. 1300-3.
46. Ficz, G., et al., *Dynamic regulation of 5-hydroxymethylcytosine in mouse ES cells and during differentiation.* Nature, 2011. **473**(7347): p. 398-402.
47. He, Y.F., et al., *Tet-mediated formation of 5-carboxylcytosine and its excision by TDG in mammalian DNA.* Science, 2011. **333**(6047): p. 1303-7.
48. Williams, K., et al., *TET1 and hydroxymethylcytosine in transcription and DNA methylation fidelity.* Nature, 2011. **473**(7347): p. 343-8.
49. Valinluck, V., et al., *Oxidative damage to methyl-CpG sequences inhibits the binding of the methyl-CpG binding domain (MBD) of methyl-CpG binding protein 2 (MeCP2).* Nucleic Acids Res, 2004. **32**(14): p. 4100-8.
50. Lavie, L., et al., *CpG methylation directly regulates transcriptional activity of the human endogenous retrovirus family HERV-K(HML-2).* J Virol, 2005. **79**(2): p. 876-83.
51. Smiraglia, D.J., et al., *Distinct epigenetic phenotypes in seminomatous and nonseminomatous testicular germ cell tumors.* Oncogene, 2002. **21**(24): p. 3909-16.

52. Leung, D.C. and M.C. Lorincz, *Silencing of endogenous retroviruses: when and why do histone marks predominate?* Trends Biochem Sci, 2012. **37**(4): p. 127-33.

53. Hutnick, L.K., et al., *Repression of retrotransposal elements in mouse embryonic stem cells is primarily mediated by a DNA methylation-independent mechanism.* J Biol Chem, 2010. **285**(27): p. 21082-91.

54. Tessarz, P. and T. Kouzarides, *Histone core modifications regulating nucleosome structure and dynamics.* Nat Rev Mol Cell Biol, 2014. **15**(11): p. 703-8.

55. Kooistra, S.M. and K. Helin, *Molecular mechanisms and potential functions of histone demethylases.* Nat Rev Mol Cell Biol, 2012. **13**(5): p. 297-311.

56. Jaenisch, R. and A. Bird, *Epigenetic regulation of gene expression: how the genome integrates intrinsic and environmental signals.* Nat Genet, 2003. **33 Suppl**: p. 245-54.

57. Friedman, J.R., et al., *KAP-1, a novel corepressor for the highly conserved KRAB repression domain.* Genes Dev, 1996. **10**(16): p. 2067-78.

58. Cheng, C.T., C.Y. Kuo, and D.K. Ann, *KAPtain in charge of multiple missions: Emerging roles of KAP1.* World J Biol Chem, 2014. **5**(3): p. 308-20.

59. Schultz, D.C., et al., *SETDB1: a novel KAP-1-associated histone H3, lysine 9-specific methyltransferase that contributes to HP1-mediated silencing of euchromatic genes by KRAB zinc-finger proteins.* Genes Dev, 2002. **16**(8): p. 919-32.

60. Barski, A., et al., *High-resolution profiling of histone methylations in the human genome.* Cell, 2007. **129**(4): p. 823-37.

61. Matsui, T., et al., *Proviral silencing in embryonic stem cells requires the histone methyltransferase ESET.* Nature, 2010. **464**(7290): p. 927-31.

62. Macfarlan, T.S., et al., *Endogenous retroviruses and neighboring genes are coordinately repressed by LSD1/KDM1A.* Genes Dev, 2011. **25**(6): p. 594-607.

63. Rowe, H.M., et al., *KAP1 controls endogenous retroviruses in embryonic stem cells.* Nature, 2010. **463**(7278): p. 237-40.

64. Turelli, P., et al., *Interplay of TRIM28 and DNA methylation in controlling human endogenous retroelements.* Genome Res, 2014. **24**(8): p. 1260-70.

65. Law, J.A. and S.E. Jacobsen, *Establishing, maintaining and modifying DNA methylation patterns in plants and animals.* Nat Rev Genet, 2010. **11**(3): p. 204-20.

66. Ghildiyal, M. and P.D. Zamore, *Small silencing RNAs: an expanding universe.* Nat Rev Genet, 2009. **10**(2): p. 94-108.

67. Hamilton, A., et al., *Two classes of short interfering RNA in RNA silencing.* EMBO J, 2002. **21**(17): p. 4671-9.

68. Ambros, V., et al., *MicroRNAs and other tiny endogenous RNAs in C. elegans.* Curr Biol, 2003. **13**(10): p. 807-18.
69. Cox, D.N., et al., *A novel class of evolutionarily conserved genes defined by piwi are essential for stem cell self-renewal.* Genes Dev, 1998. **12**(23): p. 3715-27.
70. Luteijn, M.J. and R.F. Ketting, *PIWI-interacting RNAs: from generation to transgenerational epigenetics.* Nat Rev Genet, 2013. **14**(8): p. 523-34.
71. Peng, J.C. and H. Lin, *Beyond transposons: the epigenetic and somatic functions of the Piwi-piRNA mechanism.* Curr Opin Cell Biol, 2013. **25**(2): p. 190-4.
72. Aravin, A.A., et al., *Developmentally regulated piRNA clusters implicate MILI in transposon control.* Science, 2007. **316**(5825): p. 744-7.
73. Kuramochi-Miyagawa, S., et al., *DNA methylation of retrotransposon genes is regulated by Piwi family members MILI and MIWI2 in murine fetal testes.* Genes Dev, 2008. **22**(7): p. 908-17.
74. Sigurdsson, M.I., et al., *The distribution of a germline methylation marker suggests a regional mechanism of LINE-1 silencing by the piRNA-PIWI system.* BMC Genet, 2012. **13**: p. 31.
75. Chiu, Y.L. and W.C. Greene, *The APOBEC3 cytidine deaminases: an innate defensive network opposing exogenous retroviruses and endogenous retroelements.* Annu Rev Immunol, 2008. **26**: p. 317-53.
76. Esnault, C., et al., *APOBEC3G cytidine deaminase inhibits retrotransposition of endogenous retroviruses.* Nature, 2005. **433**(7024): p. 430-3.
77. Stetson, D.B., et al., *Trex1 prevents cell-intrinsic initiation of autoimmunity.* Cell, 2008. **134**(4): p. 587-98.
78. Isbel, L. and E. Whitelaw, *Endogenous retroviruses in mammals: an emerging picture of how ERVs modify expression of adjacent genes.* Bioessays, 2012. **34**(9): p. 734-8.
79. Faulkner, G.J., et al., *The regulated retrotransposon transcriptome of mammalian cells.* Nat Genet, 2009. **41**(5): p. 563-71.
80. Romier, C., et al., *The NF-YB/NF-YC structure gives insight into DNA binding and transcription regulation by CCAAT factor NF-Y.* J Biol Chem, 2003. **278**(2): p. 1336-45.
81. Nardini, M., et al., *Sequence-specific transcription factor NF-Y displays histone-like DNA binding and H2B-like ubiquitination.* Cell, 2013. **152**(1-2): p. 132-43.
82. Long, Q., et al., *A long terminal repeat of the human endogenous retrovirus ERV-9 is located in the 5' boundary area of the human beta-globin locus control region.* Genomics, 1998. **54**(3): p. 542-55.
83. Yu, X., et al., *The long terminal repeat (LTR) of ERV-9 human endogenous retrovirus binds to NF-Y in the assembly of an active LTR enhancer complex NF-Y/MZF1/GATA-2.* J Biol Chem, 2005. **280**(42): p. 35184-94.

84. Medstrand, P., J.R. Landry, and D.L. Mager, *Long terminal repeats are used as alternative promoters for the endothelin B receptor and apolipoprotein C-I genes in humans.* J Biol Chem, 2001. **276**(3): p. 1896-903.

85. Fellenberg, F., et al., *GBP-5 splicing variants: New guanylate-binding proteins with tumor-associated expression and antigenicity.* J Invest Dermatol, 2004. **122**(6): p. 1510-7.

86. La Mantia, G., et al., *Identification of new human repetitive sequences: characterization of the corresponding cDNAs and their expression in embryonal carcinoma cells.* Nucleic Acids Res, 1989. **17**(15): p. 5913-22.

87. La Mantia, G., et al., *Identification and characterization of novel human endogenous retroviral sequences prefentially expressed in undifferentiated embryonal carcinoma cells.* Nucleic Acids Res, 1991. **19**(7): p. 1513-20.

88. Lania, L., et al., *Structural and functional organization of the human endogenous retroviral ERV9 sequences.* Virology, 1992. **191**(1): p. 464-8.

89. Chen, H.J., et al., *A retroviral repetitive element confers tissue-specificity to the human alcohol dehydrogenase 1C (ADH1C) gene.* DNA Cell Biol, 2002. **21**(11): p. 793-801.

90. Beyer, U., et al., *Endogenous retrovirus drives hitherto unknown proapoptotic p63 isoforms in the male germ line of humans and great apes.* Proc Natl Acad Sci U S A, 2011. **108**(9): p. 3624-9.

91. Gabrielli, F., et al., *A nuclear protein, synthesized in growth-arrested human hepatoblastoma cells, is a novel member of the short-chain alcohol dehydrogenase family.* Eur J Biochem, 1995. **232**(2): p. 473-7.

92. Heinz, S., et al., *Genomic organization of the human gene HEP27: alternative promoter usage in HepG2 cells and monocyte-derived dendritic cells.* Genomics, 2002. **79**(4): p. 608-15.

93. Westfall, M.D. and J.A. Pietenpol, *p63: Molecular complexity in development and cancer.* Carcinogenesis, 2004. **25**(6): p. 857-64.

94. Mills, A.A., *p63: oncogene or tumor suppressor?* Curr Opin Genet Dev, 2006. **16**(1): p. 38-44.

95. Yang, A., et al., *p63 is essential for regenerative proliferation in limb, craniofacial and epithelial development.* Nature, 1999. **398**(6729): p. 714-8.

96. Candi, E., et al., *TAp63 and DeltaNp63 in cancer and epidermal development.* Cell Cycle, 2007. **6**(3): p. 274-85.

97. Suh, E.K., et al., *p63 protects the female germ line during meiotic arrest.* Nature, 2006. **444**(7119): p. 624-8.

98. Yang, X.J. and E. Seto, *The Rpd3/Hda1 family of lysine deacetylases: from bacteria and yeast to mice and men.* Nat Rev Mol Cell Biol, 2008. **9**(3): p. 206-18.

99. Walkinshaw, D.R., et al., *Histone deacetylases as transducers and targets of nuclear signaling.* J Cell Biochem, 2008. **104**(5): p. 1541-52.

100. Spange, S., et al., *Acetylation of non-histone proteins modulates cellular signalling at multiple levels.* Int J Biochem Cell Biol, 2009. **41**(1): p. 185-98.

101. Bertrand, P., *Inside HDAC with HDAC inhibitors.* Eur J Med Chem, 2010. **45**(6): p. 2095-116.

102. Martinet, N. and P. Bertrand, *Interpreting clinical assays for histone deacetylase inhibitors.* Cancer Manag Res, 2011. **3**: p. 117-41.

103. Johnstone, R.W., *Histone-deacetylase inhibitors: novel drugs for the treatment of cancer.* Nat Rev Drug Discov, 2002. **1**(4): p. 287-99.

104. Fulda, S. and D. Vucic, *Targeting IAP proteins for therapeutic intervention in cancer.* Nat Rev Drug Discov, 2012. **11**(2): p. 109-24.

105. Mahalingam, D., et al., *TRAIL receptor signalling and modulation: Are we on the right TRAIL?* Cancer Treat Rev, 2009. **35**(3): p. 280-8.

106. Reis, C.R., et al., *Rapid and efficient cancer cell killing mediated by high-affinity death receptor homotrimerizing TRAIL variants.* Cell Death Dis, 2010. **1**: p. e83.

107. van Roosmalen, I.A., W.J. Quax, and F.A. Kruyt, *Two death-inducing human TRAIL receptors to target in cancer: similar or distinct regulation and function?* Biochem Pharmacol, 2014. **91**(4): p. 447-56.

108. Wang-Johanning, F., et al., *Quantitation of HERV-K env gene expression and splicing in human breast cancer.* Oncogene, 2003. **22**(10): p. 1528-35.

109. Ruebner, M., et al., *Reduced syncytin-1 expression levels in placental syndromes correlates with epigenetic hypermethylation of the ERVW-1 promoter region.* PLoS One, 2013. **8**(2): p. e56145.

110. Benatti, P., et al., *Specific inhibition of NF-Y subunits triggers different cell proliferation defects.* Nucleic Acids Res, 2011. **39**(13): p. 5356-68.

111. Kohany, O., et al., *Annotation, submission and screening of repetitive elements in Repbase: RepbaseSubmitter and Censor.* BMC Bioinformatics, 2006. **7**: p. 474.

112. Jurka, J., et al., *Repbase Update, a database of eukaryotic repetitive elements.* Cytogenet Genome Res, 2005. **110**(1-4): p. 462-7.

113. Messeguer, X., et al., *PROMO: detection of known transcription regulatory elements using species-tailored searches.* Bioinformatics, 2002. **18**(2): p. 333-4.

114. Farre, D., et al., *Identification of patterns in biological sequences at the ALGGEN server: PROMO and MALGEN.* Nucleic Acids Res, 2003. **31**(13): p. 3651-3.

115. Ishiguro, T., et al., *Homogeneous quantitative assay of hepatitis C virus RNA by polymerase chain reaction in the presence of a fluorescent intercalater.* Anal Biochem, 1995. **229**(2): p. 207-13.

116. Livak, K.J. and T.D. Schmittgen, *Analysis of relative gene expression data using real-time quantitative PCR and the 2(-Delta Delta C(T)) Method.* Methods, 2001. **25**(4): p. 402-8.

117. Shapiro, A.L., E. Vinuela, and J.V. Maizel, Jr., *Molecular weight estimation of polypeptide chains by electrophoresis in SDS-polyacrylamide gels.* Biochem Biophys Res Commun, 1967. **28**(5): p. 815-20.

118. Laemmli, U.K., *Cleavage of structural proteins during the assembly of the head of bacteriophage T4.* Nature, 1970. **227**(5259): p. 680-5.

119. Bittner, M., P. Kupferer, and C.F. Morris, *Electrophoretic transfer of proteins and nucleic acids from slab gels to diazobenzyloxymethyl cellulose or nitrocellulose sheets.* Anal Biochem, 1980. **102**(2): p. 459-71.

120. Thorpe, G.H., et al., *Phenols as enhancers of the chemiluminescent horseradish peroxidase-luminol-hydrogen peroxide reaction: application in luminescence-monitored enzyme immunoassays.* Clin Chem, 1985. **31**(8): p. 1335-41.

121. Denissov, S., et al., *Identification of novel functional TBP-binding sites and general factor repertoires.* EMBO J, 2007. **26**(4): p. 944-54.

122. Fleming, J.D., et al., *NF-Y coassociates with FOS at promoters, enhancers, repetitive elements, and inactive chromatin regions, and is stereo-positioned with growth-controlling transcription factors.* Genome Res, 2013. **23**(8): p. 1195-209.

123. Edgar, R., M. Domrachev, and A.E. Lash, *Gene Expression Omnibus: NCBI gene expression and hybridization array data repository.* Nucleic Acids Res, 2002. **30**(1): p. 207-10.

124. Liu, T., et al., *Cistrome: an integrative platform for transcriptional regulation studies.* Genome Biol, 2011. **12**(8): p. R83.

125. Goodman, M., *The genomic record of Humankind's evolutionary roots.* Am J Hum Genet, 1999. **64**(1): p. 31-9.

126. Kaufmann, S.H., et al., *Specific proteolytic cleavage of poly(ADP-ribose) polymerase: an early marker of chemotherapy-induced apoptosis.* Cancer Res, 1993. **53**(17): p. 3976-85.

127. Chaitanya, G.V., A.J. Steven, and P.P. Babu, *PARP-1 cleavage fragments: signatures of cell-death proteases in neurodegeneration.* Cell Commun Signal, 2010. **8**: p. 31.

128. Wu, G.S., et al., *KILLER/DR5 is a DNA damage-inducible p53-regulated death receptor gene.* Nat Genet, 1997. **17**(2): p. 141-3.

129. Coureuil, M., et al., *Puma and Trail/Dr5 pathways control radiation-induced apoptosis in distinct populations of testicular progenitors.* PLoS One, 2010. **5**(8): p. e12134.

130. McKee, C.M., Y. Ye, and J.H. Richburg, *Testicular germ cell sensitivity to TRAIL-induced apoptosis is dependent upon p53 expression and is synergistically enhanced by DR5 agonistic antibody treatment.* Apoptosis, 2006. **11**(12): p. 2237-50.

131. Inoue, H., et al., *Histone deacetylase inhibitors sensitize human colonic adenocarcinoma cell lines to TNF-related apoptosis inducing ligand-mediated apoptosis.* Int J Mol Med, 2002. **9**(5): p. 521-5.

132. Rosato, R.R., et al., *Simultaneous activation of the intrinsic and extrinsic pathways by histone deacetylase (HDAC) inhibitors and tumor necrosis factor-related apoptosis-inducing ligand (TRAIL) synergistically induces mitochondrial damage and apoptosis in human leukemia cells.* Mol Cancer Ther, 2003. **2**(12): p. 1273-84.

133. Zhang, X.D., et al., *The histone deacetylase inhibitor suberic bishydroxamate: a potential sensitizer of melanoma to TNF-related apoptosis-inducing ligand (TRAIL) induced apoptosis.* Biochem Pharmacol, 2003. **66**(8): p. 1537-45.

134. Neuzil, J., E. Swettenham, and N. Gellert, *Sensitization of mesothelioma to TRAIL apoptosis by inhibition of histone deacetylase: role of Bcl-xL down-regulation.* Biochem Biophys Res Commun, 2004. **314**(1): p. 186-91.

135. Kim, Y.H., et al., *Sodium butyrate sensitizes TRAIL-mediated apoptosis by induction of transcription from the DR5 gene promoter through Sp1 sites in colon cancer cells.* Carcinogenesis, 2004. **25**(10): p. 1813-20.

136. Nakata, S., et al., *Histone deacetylase inhibitors upregulate death receptor 5/TRAIL-R2 and sensitize apoptosis induced by TRAIL/APO2-L in human malignant tumor cells.* Oncogene, 2004. **23**(37): p. 6261-71.

137. Yeh, C.C., et al., *Suberoylanilide hydroxamic acid sensitizes human oral cancer cells to TRAIL-induced apoptosis through increase DR5 expression.* Mol Cancer Ther, 2009. **8**(9): p. 2718-25.

138. Bourque, G., et al., *Evolution of the mammalian transcription factor binding repertoire via transposable elements.* Genome Res, 2008. **18**(11): p. 1752-62.

139. Yoder, J.A., C.P. Walsh, and T.H. Bestor, *Cytosine methylation and the ecology of intragenomic parasites.* Trends Genet, 1997. **13**(8): p. 335-40.

140. Feng, S., S.E. Jacobsen, and W. Reik, *Epigenetic reprogramming in plant and animal development.* Science, 2010. **330**(6004): p. 622-7.

141. Allen, H.F., P.A. Wade, and T.G. Kutateladze, *The NuRD architecture.* Cell Mol Life Sci, 2013. **70**(19): p. 3513-24.

142. Ramirez, J. and J. Hagman, *The Mi-2/NuRD complex: a critical epigenetic regulator of hematopoietic development, differentiation and cancer.* Epigenetics, 2009. **4**(8): p. 532-6.

143. Denslow, S.A. and P.A. Wade, *The human Mi-2/NuRD complex and gene regulation.* Oncogene, 2007. **26**(37): p. 5433-8.

144. Whyte, W.A., et al., *Enhancer decommissioning by LSD1 during embryonic stem cell differentiation.* Nature, 2012. **482**(7384): p. 221-5.

145. Forneris, F., et al., *Human histone demethylase LSD1 reads the histone code.* J Biol Chem, 2005. **280**(50): p. 41360-5.

146. Lee, M.G., et al., *Functional interplay between histone demethylase and deacetylase enzymes.* Mol Cell Biol, 2006. **26**(17): p. 6395-402.

147. Oldfield, A.J., et al., *Histone-fold domain protein NF-Y promotes chromatin accessibility for cell type-specific master transcription factors.* Mol Cell, 2014. **55**(5): p. 708-22.

148. Wasner, M., et al., *Three CCAAT-boxes and a single cell cycle genes homology region (CHR) are the major regulating sites for transcription from the human cyclin B2 promoter.* Gene, 2003. **312**: p. 225-37.

149. Salsi, V., et al., *Interactions between p300 and multiple NF-Y trimers govern cyclin B2 promoter function.* J Biol Chem, 2003. **278**(9): p. 6642-50.

150. Kabe, Y., et al., *NF-Y is essential for the recruitment of RNA polymerase II and inducible transcription of several CCAAT box-containing genes.* Mol Cell Biol, 2005. **25**(1): p. 512-22.

151. Jin, S. and K.W. Scotto, *Transcriptional regulation of the MDR1 gene by histone acetyltransferase and deacetylase is mediated by NF-Y.* Mol Cell Biol, 1998. **18**(7): p. 4377-84.

152. Park, S.H., et al., *Transcriptional regulation of the transforming growth factor beta type II receptor gene by histone acetyltransferase and deacetylase is mediated by NF-Y in human breast cancer cells.* J Biol Chem, 2002. **277**(7): p. 5168-74.

153. Hirose, T., et al., *p53-independent induction of Gadd45 by histone deacetylase inhibitor: coordinate regulation by transcription factors Oct-1 and NF-Y.* Oncogene, 2003. **22**(49): p. 7762-73.

154. Peng, Y. and N. Jahroudi, *The NFY transcription factor functions as a repressor and activator of the von Willebrand factor promoter.* Blood, 2002. **99**(7): p. 2408-17.

155. Ceribelli, M., et al., *The histone-like NF-Y is a bifunctional transcription factor.* Mol Cell Biol, 2008. **28**(6): p. 2047-58.

156. Currie, R.A., *NF-Y is associated with the histone acetyltransferases GCN5 and P/CAF.* J Biol Chem, 1998. **273**(3): p. 1430-4.

157. Peng, Y., et al., *Irradiation modulates association of NF-Y with histone-modifying cofactors PCAF and HDAC.* Oncogene, 2007. **26**(54): p. 7576-83.

158. Manni, I., et al., *Posttranslational regulation of NF-YA modulates NF-Y transcriptional activity.* Mol Biol Cell, 2008. **19**(12): p. 5203-13.

159. Yun, J., et al., *Cdk2-dependent phosphorylation of the NF-Y transcription factor and its involvement in the p53-p21 signaling pathway.* J Biol Chem, 2003. **278**(38): p. 36966-72.

160. Peng, Y. and N. Jahroudi, *The NFY transcription factor inhibits von Willebrand factor promoter activation in non-endothelial cells through recruitment of histone deacetylases.* J Biol Chem, 2003. **278**(10): p. 8385-94.

161. Joshi, P., et al., *The functional interactome landscape of the human histone deacetylase family.* Mol Syst Biol, 2013. **9**: p. 672.

162. Wang, Z., et al., *Genome-wide mapping of HATs and HDACs reveals distinct functions in active and inactive genes.* Cell, 2009. **138**(5): p. 1019-31.

163. West, A.C. and R.W. Johnstone, *New and emerging HDAC inhibitors for cancer treatment.* J Clin Invest, 2014. **124**(1): p. 30-9.

164. Witt, O., et al., *HDAC family: What are the cancer relevant targets?* Cancer Lett, 2009. **277**(1): p. 8-21.

165. Hanahan, D. and R.A. Weinberg, *The hallmarks of cancer.* Cell, 2000. **100**(1): p. 57-70.

166. Hanahan, D. and R.A. Weinberg, *Hallmarks of cancer: the next generation.* Cell, 2011. **144**(5): p. 646-74.

167. Bradner, J.E., et al., *Chemical phylogenetics of histone deacetylases.* Nat Chem Biol, 2010. **6**(3): p. 238-243.

168. Bantscheff, M., et al., *Chemoproteomics profiling of HDAC inhibitors reveals selective targeting of HDAC complexes.* Nat Biotechnol, 2011. **29**(3): p. 255-65.

169. Kloet, S.L., et al., *Towards elucidating the stability, dynamics and architecture of the nucleosome remodeling and deacetylase complex by using quantitative interaction proteomics.* FEBS J, 2014.

170. Dejligbjerg, M., et al., *Differential effects of class I isoform histone deacetylase depletion and enzymatic inhibition by belinostat or valproic acid in HeLa cells.* Mol Cancer, 2008. **7**: p. 70.

8 Appendix

Detailed summary of the LTR12 locations which were found to be bound by NF-Y subunit alpha and/or beta in three human cell lines. The overlapping sites are also visualized in Figure 5-12.

Cell line	**NF-Y subunit**	**LTR12 location (hg19)**			**Adjacent cellular gene**
		chromosome	*start*	*end*	
HeLa-S3	NF-Y alpha	chr8	22927451	22928865	*TNFRSF10B*
		chr6	30774508	30775782	*IER3*
	NF-Y beta	chr8	22927451	22928865	*TNFRSF10B*
		chr17	38167005	38169009	*CSF3*
		chr6	30774508	30775782	*IER3*
		chr5	12796289	12796978	*CT49*
K562	NF-Y alpha	chr8	22927451	22928865	*TNFRSF10B*
		chr1	89738137	89739573	*GBP5*
		chr14	24104837	24105861	*DHRS2*
		chr3	32980994	32982647	*CCR4*
		chr6	30774508	30775782	*IER3*
		chr4	87468293	87469596	*PTPN13*
	NF-Y beta	chr3	189313733	189314949	*GTAp63*
		chr8	22927451	22928865	*TNFRSF10B*
		chr4	100274696	100275434	*ADH1C*
		chr1	89738137	89739573	*GBP5*
		chr9	92094404	92095897	*SEMA4D*
		chr14	24104837	24105861	*DHRS2*
		chr14	24106921	24107605	
		chr12	100823898	100825322	*NR1H4*
		chr7	120699844	120701243	*CPED1*
		chr9	74578275	74579651	*C9orf85*
		chr3	32980994	32982647	*CCR4*
		chr15	78537615	78539044	*ACSBG1*
		chr1	154650332	154651788	*KCNN3*
		chr17	38167005	38169009	*CSF3*

		chr9	100336320	100337735	*TMOD1*
		chr5	150786356	150787204	*SLC36A2*
		chr6	30774508	30775782	*IER3*
		chr12	18652900	18654112	*PIK3C2G*
		chr5	12661848	12663161	*CT49*
		chr5	12796289	12796978	
		chr4	87468293	87469596	*PTPN13*
		chr7	4832980	4834366	*RADIL*
GM12878	NF-Y alpha	chr1	89738137	89739573	*GBP5*
	NF-Y beta	chr3	189313733	189314949	*GTAp63*
		chr8	22927451	22928865	*TNFRSF10B*
		chr1	89738137	89739573	*GBP5*
		chr14	24104837	24105861	*DHRS2*
		chr14	24106921	24107605	
		chr7	120699844	120701243	*CPED1*
		chr3	32980994	32982647	*CCR4*
		chr15	78537615	78539044	*ACSBG1*
		chr17	38167005	38169009	*CSF3*
		chr9	100336320	100337735	*TMOD1*
		chr5	150786356	150787204	*SLC36A2*
		chr6	30774508	30775782	*IER3*
		chr5	12796289	12796978	*CT49*
		chr4	87468293	87469596	*PTPN13*
		chr7	4832980	4834366	*RADIL*

Table 8-I. Binding of NF-Y subunits to LTR12 in three human cell lines

ACKNOWLEDGMENTS

First of all, I want to thank my supervisor Prof. Matthias Dobbelstein for giving me the opportunity to study endogenous retroviruses in his lab. His willingness to discuss work in progress, new ideas and his passion for science in general greatly contributed to this project. Moreover, I want to thank him for his trust and hence the freedom that he gave me to develop and follow my own ideas.

Further, I would like to thank my thesis committee members Prof. Holger Reichardt and Prof. Michael Zeisberg for their genuine interest in my project and the very fruitful discussions in our annual meetings. I would also like to thank the members of my extended committee for their time and consideration.

Additionally, I would like to thank everybody who contributed to this project in one way or another: Dr. Ulrike Beyer for her excellent work preceding my studies and for passing on a great deal of her profound methodological knowledge. Kamila Sabagh for her efforts to obtain stable clones and establishing a luciferase assay. Prof. Steven Johnsen for his interest and support regarding the understanding of ChIP-seq data. Prof. Lutz Walter and Dr. Jens Gruber for their help with trying to establish a knock-down in Jurkat cells. Prof. Roberto Mantovani for his great expertise and sharing of data regarding NF-Y. Moreover, thanks to Dr. Ulrike Keitel, Nadine Stark, Dr. Daniela Kramer and Magdalena Wienken for their time and extensive help with methodological questions.

I would also like to thank the Göttingen Graduate School for Neurosciences, Biophysics and Molecular Biosciences (GGNB) for organizing interesting workshops and excursions and their extraordinary competent and friendly staff.

Many thanks to the Dobbelstein and Moll group and the nice work environment that I was lucky enough to work in. Thanks to the permanent and visiting friendly faces in the small lab and my office and all the scientific discussions, support and laughter shared. Thanks to our team assistant Karola Metze who was of great help with every question. Special thanks also to my fellow colleagues who suffered through the Mensa food with me on a daily basis, making it bearable with many nice conversations; especially Franzi - thanks for all the (funny) investigations of life’s bigger and smaller mysteries.

I want to thank my friends in- and outside Göttingen. And I want to thank my family, particularly my parents Conny and Ewald for continuously encouraging me to ask all the important w-questions, their support and love. Thanks also to my brothers Lutz, Felix and Till and their significant others. Last but not least, I want to thank my wonderful husband and best friend Jaffer.